DOCTOR OF PHILOSOPHY IN
INDUSTRIAL ENGINEERING

XXX CYCLE

PhD COURSE COORDINATOR
Prof. Maurizio DE LUCIA

Advanced numerical modeling of reciprocating compressors

Scientific Sector ING-IND/09

PhD Student
Dr. Andrea Tanganelli

Tutor
Prof. Giovanni Ferrara

Co-tutor
Ing. Federico Sorgonà

PhD Course Coordinator
Prof. Maurizio De Lucia

2014/2017

ISBN XXX–XX–XXXX–XXX–X
D/XXXX/XXXX/XX

Declaration

I hereby declare that this submission is my own work and, to the best of my knowledge and belief. It contains no material previously published or written by another person, nor material which to a substantial extent has been accepted for the award of any other degree or diploma at University of Florence or any other educational institution, except where due references are provided in the thesis itself.

Furthermore, all data here reported are intellectual property of *Baker Hughes, a GE company*, and cannot be divulged to third parties.

Any contribution made to the research by others, with whom I have been working, is explicitly acknowledged in the thesis.

_____

Andrea Tanganelli

October 2017

Ringraziamenti

A conclusione di questo mio percorso, penso sia doveroso ringraziare i Prof. Ennio Carnevale e Giovanni Ferrara per avermi concesso l'opportunità di intraprendere e seguire questo dottorato di ricerca.

In particolare, ringrazio il Prof. Giovanni Ferrara nella figura di tutor, sempre disponibile e pronto a consigliarmi nonostante i numerosi impegni.

Un particolare ringraziamento a tutti gli amici del gruppo di ricerca REASE che mi sono stati vicini durante questi tre anni contribuendo a rendere piacevoli e costruttive le giornate trascorse in Facoltà: Alessandro, Alfonso, Andrea F., Domenico, Fabio E., Fabio T., Francesco, Giulia, Giulio, Giovanni G., Giovanni V., Isacco, Luca, Lorenzo B., Lorenzo F., Michele, Niccolò e Simone.

Non posso non rivolgere un ringraziamento speciale a Francesco per avermi sempre aiutato e supportato in tutte le attività svolte insieme, condividendo le sue conoscenze e competenze e permettendomi di crescere durante questo percorso formativo.

Infine, un forte ringraziamento ai miei genitori e a tutta la mia famiglia per aver sempre creduto in me e per avermi supportato in tutti questi anni.

Abstract

The quantification of pressure losses generated during the suction and discharge phases is essential to predict the working cycle of a reciprocating compressor. Beyond automatic valves, which are the main sources of fluid-dynamic losses, a relevant contribution is provided by all of the other components along the cylinder suction and discharge paths.

Low-order numerical models for the simulation of the working cycle account for pressure losses through the imposition of global flow coefficients, which must be known from either experiments or three-dimensional CFD simulations. Therefore, the accuracy of the prediction of the absorbed power is strongly related to the methodology for the evaluation of the flow coefficients for all of the components. The geometrical features of the gas path have a great impact on the flow coefficient, which also depends on the piston motion during the cycle: indeed, the compression chamber shape, the pocket section and the flow pattern vary as a function of the piston position. Moreover, the valve and the working fluid used, as well as the operating conditions have a strong influence on the flow coefficient evaluation. For this reason, the number of configurations that should be simulated is extremely high and the evaluation of the pressure losses in the suction and discharge gas path with a 3D CFD steady state simulation is impossible without a substantial reduction of the set-up times and of the number of simulations.

Within this scenario, the aim of this thesis is the introduction of a new methodology for the evaluation of the pressure losses occurring along the overall gas path in order to obtain a strong reduction of both the set-up and computational times for the realization of steady state CFD simulations.

In more detail, the proposed approach starts by the idea to obtain the computational domain by means of parametric CAD models of the fluid domain directly without the need of starting from the more complex 3D drawings of the solid metal components and assemblies. This solution requires a greater initial effort for the realization of a parametric CAD model but allows an important reduction of the set-up times when simulating more cylinders starting from the same parametric model. The idea of the CFD routine described in this thesis is then to use parametric CAD models for the simulations of a large number of cylinders in order to reduce the global computational times. Indeed, the parameterization comprises also the mesh definition and the simulation setup phases, thus leading to a fully automatable approach.

Nevertheless, even in case of exploiting the use of parametric models, the number of simulation cases that should be analyzed for each machine is still too high. For this reason, a detailed analysis was carried out to define the minimum number of simulations needed to obtain accurate results with the minimal computational times. Different solutions are then proposed in order to reduce the number of configurations to simulate; the evaluation of all the possible operating conditions of the large size reciprocating compressors analyzed in this thesis was obtained by means of 48 simulations for each machine. Moreover, the results obtained by the application of the defined approach to an industrial case are shown.

In the second part, the utility of the simplified parametric routine to enhance the predictability in reciprocating compressors is highlighted by applying the results achieved to different numerical approaches.

In particular, the effect of the approximations introduced in the flow coefficient evaluation on the performance prediction of large size reciprocating compressors is investigated. The numerical model used for the analysis is an in-house one-dimensional model based on the finite volume method (FVM). The study is carried out for three different compressor sizes and three different working gases, showing that the requirements in terms of flow coefficient accuracy depend on the specific case. The comparison between the numerical results using different flow coefficients and the measurements collected on a dedicated test bench allowed highlighting the importance to accurately predict the flow coefficient along the overall suction and discharge gas path.

Moreover, a methodology to perform a 2D CFD simulation of the working cycle of a reciprocating compressor is developed in order to provide more accurate results than low-order models and, at the same time, to guarantee the reduction of the computational effort with respect to unsteady 3D CFD simulations. In more detail, the analysis presented in this work is carried out for a double-acting large bore cast iron cylinder. The simplifications required to allow the reduction of the three-dimensional fluid domain to an equivalent two-dimensional configuration are shown. In particular, the importance to use the flow coefficients obtained by means of the simplified CFD parametric routine for the pressure losses evaluation in the suction and discharge gas-path is highlighted.

Finally, the possibility to use the parametric CFD routine to increase the predictability of the heat transfer process in a reciprocating compressor is shown. A brief description of a conjugate heat transfer (CHT) approach is given and the suitability to use the parametric routine for the forced convection modeling inside suction and discharge gas ducts is underlined.

Furthermore, the utility of the parametric routine as well as the accuracy of both 2D and CHT models is highlighted by means of the comparison between the numerical results and the measurements collected during experimental campaigns.

Table of contents

List of figures

List of tables

List of symbols and acronyms

A	Square matrix
A_{eff}	Valve effective area
A_{lift}	Area under the lift
A_{por}	Transversal section of porous medium
A_{ref}	Reference area
A_t	Throat area
B	Source vector
B	Cylinder bore
B_S	Body sizing
B^*	Dimensionless bore diameter
C	Clearance
C	Volumetric capacity
CE	Crank End
C_f	Skin friction
CFD	Computational Fluid Dynamics
C_H	Chamber height
CHT	Conjugate heat transfer
CPU	Central Processing Unit
CS	Cast steel
C_{tr}	Transversal porosity multiplier coefficient
C_μ	Eddy viscosity model coefficient
D	Darcy coefficient/Diameter
D_v	Valve diameter

DNS	Direct Numerical Simulation
E	Energy
E_{int}	Energy introduced into the gas
E_{sub}	Energy subtracted by cooling
f	Flux function
F	Forcheimer coefficient (Resistance loss coefficient)
FVM	Finite volume method
GGI	General Grid Interface
h	Valve lift
H_C	Cylinder height
HE	Head End
H_P	Pocket height
HTC	Heat transfer coefficient
*HTC**	Dimensionless heat transfer coefficient
k	Turbulence kinetic energy/Thermal conductivity
Ks	Flow coefficient
Ks_p	Plenum flow coefficient
Ks_{TOT}	Global flow coefficient
Ks_v	Valve flow coefficient
*Ks**	Scaled flow coefficient
i	Internal energy
l_0	Turbulence length scale
L	Characteristic length
L_P	Pocket length/Plenum lenght
L_s	Machining length on the cylinder head
L_v	Valve length
m	Mass flow rate
*M**	Dimensionless mass flow rate
m_{id}	Ideal mass flow rate
m_{real}	Real mass flow rate
n	Polytropic compression index
NCI	Nodular cast iron

Nu	Nusselt number
P	Pressure
p^*	Dimensionless pressure
p_{AVE}	Average pressure
p_{EXP}	Experimental pressure
p_0	Upstream total pressure
p_{crit}	Critical pressure
p_{01}	Total inlet pressure
p_2	Static outlet pressure
p_d	Discharge pressure
p_s	Suction pressure
p_t	Throat pressure
P	Absorbed power
P_{disch}	Absorbed power by discharge valve
PF	Pocket Factor
Pk	Production of turbulent kinetic energy
P_{suct}	Power absorbed by suction valve
Q	State vector/Heat flux
Q	Energy dissipation function/Cell average value of q
R	Compression ratio
R	Universal constant of gas
Ra	Rayleight number
$RANS$	Reynolds-Averaged Navier-Stokes
Re	Reynolds number
$R\text{-}sq$	Coefficient of determination
S	Entropy
S	Source term/Piston stroke
SI_{ES}	Sphere of influence element sizing
T	Time/Throat section
T	Temperature/Time interval
T^*	Dimensionless temperature
T_{bulk}	Bulk temperature

TDC	Top Dead Center
T_{disch}	Discharge temperature
T_{AVE}	Average temperature
T_{EXP}	Experimental temperature
T_{NUM}	Numerical approach temperature
T_{suct}	Suction temperature
T_w	Wall temperature
T^+	Boundary layer dimensionless temperature
u	Mean fluid velocity along the wall
u^*	Friction velocity/Dimensionless fluid velocity
u^+	Boundary layer dimensionless fluid velocity
$U_{freestream}$	Free-stream velocity
v	Velocity
v_p	Average piston velocity
v_x	Axial velocity
V	Volume
V_{cyl}	Cylinder displacement
V_d	Discharge Volume
V_{suct}	Volume of the sucked gas
x	Vector of dependent variable/Piston position
y	Wall distance
y^+	Dimensionless wall distance
Z	F-Wave numerical flux increments

A	Thermal diffusivity
β^*	k-ω model constant
β_s	Pocket angle
Γ	Diffusivity
γ	Specific heats ratio
Δp	Pressure loss
Δp^*	Dimensinless pressure loss
Δp_{tot}	Global pressure loss
Δp_v	Valve pressure loss
ΔT	Global heating
ΔT^*	Dimensionless global heating
E	Turbulent dissipation rate
η_v	Volumetric efficiency
Λ	Filling coefficient
M	Dynamic viscosity
μ_t	Eddy viscosity
N	Kinematic viscosity
Ξ	Local pressure loss coefficient
P	Density
Σ	Clearance volume ratio
T	Viscous stress tensor
τ_R	Reynolds tensor stress
τ_w	Wall shear stress
Φ	Generic flow quantity
Φ	Diameter of the valve ring circumference
Ψ	Capacity total loss coefficient
ψ_H	Gas heating corrective factor
ψ_L	Gas leakage corrective factor
ψ_v	Valve losses corrective factor
Ω	Specific turbulence dissipation rate
Ω_{cyl}	Useful area of cylinder

Introduction

Reciprocating compressors are currently based on a mature and consolidated technology. These machines are used for multiple applications and with different size: for example, it is possible to find small machines (100 W) for the refrigeration and others having a power capability above 10 MW for the natural gas liquefaction. In the past, the complexity and unsteadiness of the flow discouraged high level fluid-dynamic studies and research activities was therefore focused on reliability and maintenance issues. On the other hand, the increasing interest in every energy conversion process, invested in the recent past also the reciprocating compressors and new studies were done with the goal to evaluate the performance and to reduce the global losses.

It is possible to divide the main losses that affect the global system efficiency in four groups [1]:

- friction losses;
- electrical losses;
- working cycle losses (compression and expansion);
- thermodynamic losses.

For the last group, the most critical problems are related both to the pressure losses along the suction and discharge gas flow path and to the heat losses between the working fluid and the solid walls of the machine. The research in the technical literature is focused on different aspects regarding the analysis of the compressor performance. Different models were proposed for the prediction of the working cycle with the goal to increase the predictability and others were defined to evaluate the thermal state of the cylinder in order to consider the possibility to optimize the refrigeration system, usually used for large size reciprocating compressors.

For an accurate prediction of the global performance, three-dimensional CFD transient simulations should be used: however, the computational cost of these simulations is too high and not compatible with any industrial process. For this reason the thermodynamic cycle of a reciprocating compressor is often calculated by means of low order (0D-1D) numerical models, with a substantial reduction of the calculation time.

Both 0D and 1D models require the knowledge of the flow coefficient (*Ks*) to account for the global pressure losses along the suction and discharge flow path [2]. The evaluation of this coefficient is one of the key aspects to consider for the performance prediction of these machines. In fact, although the valves are commonly thought to provide the most relevant contribution to the global pressure losses in a reciprocating compressor, a key role is also played by other components along the cylinder suction and discharge paths.

Focusing on automatic ring valves, the standard approach to estimate the pressure losses is based on the determination of flow coefficients derived from experimental data obtained in a dedicated test bench. A large number of studies were done for this component and databases realized by means of experimental tests from the valve manufacturers are available. Conversely, there is a lack of information concerning the flow behavior in the other components along the gas path and their losses are often taken into account by correcting the valve's flow coefficient by means of empirical correlations.

In this context, the use of CFD (Computational Fluid Dynamics) for the simulation of the whole gas passage throughout the inner paths of cylinders represent a viable solution for the prediction of the global pressure losses. However, these simulations are very demanding both in terms of computational resources and in man work for the set-up. In recent studies, steady state simulations were used to evaluate the global pressure losses in the suction and discharge gas path of a large size reciprocating compressor thus obtaining a substantial reduction of the computational resource and a good estimation of the overall pressure losses along the gas path [3].

However, the complexity of the geometry is still unaltered in particular for the geometrical feature of the valves. Since the size of the valve channels and the overall domain dimensions differ by more than three orders of magnitude, the meshing process requires noticeable man work for set-up and the grid density should still be fine enough to capture the flow structures at the smallest scales.

A possible approach that allows reducing both the computational and set-up times maintaining the accuracy of the results was proposed by Balduzzi [3]. This approach is based on a simplification of the computational domain by substituting the valve geometry with an equivalent porous medium that generates localized pressure drop equivalent to the actual valve. The CFD domain is therefore split into three different regions: the two zones, upstream and downstream the valves, are modeled as simple fluid regions (analogous to the simulation with the valve) and are in communication with a new cylindrical zone where the equations of the porous model are applied. The approach proposed by Balduzzi allows an important reduction of the computational and set-up times: however, the use of these kind of simulations in industrial applications for the pressure losses evaluation remains difficult for the dependence of the pressure losses on a large number of geometrical and thermodynamic variables. In fact, in a common industrial application, it is possible to find a large number of machines that differ for multiple geometrical features that have a direct impact on the global pressure losses. Indeed, large-size machines are custom-made and each produced unit has a unique design (indicated in this thesis as 'cylinder code'). Moreover, a single machine could be used with different valves and in different operating conditions. The number of configurations that should be simulated is extremely high and the evaluation of the pressure losses in the suction and discharge gas path with a 3D CFD steady state simulation is impossible without a substantial reduction of the set-up times and of the number of simulations.

In this context, it is useful to remember that the pre-processing phase of a steady state CFD simulation of a reciprocating compressor starts from the manipulation and defeaturing of the solid CAD models to extract the fluid domains of the compression chamber and of the suction and discharge ducts. The obtained fluid domains are then simplified and meshed; this approach is extremely time consuming and requires a very high effort for setting up the CFD simulation. Moreover, it is not automatable and the routine has to be repeated for each configuration. For this reason, such approach could be used for the simulation of a small set of cylinders but it is not suitable for a reliable database in a common industrial application.

Within this scenario, the Industrial Department of the University of Florence jointly with Baker Hughes, a GE company, developed an original simplified CFD routine, with the purpose of introducing a new methodology for the evaluation of the pressure losses

occurring along the overall gas path. The objective of this routine, is the definition of a solution that allows a strong reduction of both the set-up and computational times with respect to the common approach described above for the realization of steady state CFD simulations.

In more detail, the proposed approach starts by the idea to obtain the computational domain by means of parametric CAD models of the fluid domain directly without the need of starting from the more complex 3D drawings of the solid metal components and assemblies. The advantage of such approach is related to the fact that many machines have common geometrical features (e.g. number of valves or cylinders materials) and it is possible to gather these machines in a smaller number of cylinder "families". Therefore, each parametric CAD model of the cylinder could be used for a large number of cases. This solution requires a greater initial effort for the realization of a parametric CAD model but allows an important reduction of the set-up times when simulating more cylinders codes starting from the same parametric model. The idea of the CFD routine described in this thesis is then to use parametric CAD models for the simulations of a large number of cylinders in order to reduce the global computational times. Indeed, the parameterization comprises also the mesh definition and the simulation setup phases, thus leading to a fully automatable approach.

Nevertheless, even in case of exploiting the use of parametric models, the number of simulation cases that should be analyzed for each machine is still too high. For this reason, a detailed analysis was carried out to define the minimum number of simulations needed to obtain accurate results with the minimal computational times. Different solutions are then proposed in order to reduce the number of configurations to simulate; the evaluation of all the possible operating conditions of the large size reciprocating compressors analyzed in this thesis was obtained by means of 48 simulations for each machine.

The described approach was then used in an industrial application; in fact, the whole fleet of cylinders of Baker Hughes was simulated making use of the simplified CFD parametric routine.

Moreover, the utility of the simplified parametric routine to enhance the predictability is shown by applying the results obtained to different numerical approaches. In more detail, the possibility to use the flow coefficients calculated with the parametric

routine for the pressure losses evaluation in low order models is highlighted. The flow coefficients calculated were then used as input in 1D-2D models developed by the REASE GROUP of the Industrial Department of the University of Florence.

The development of the 1D model is not the main objective of this thesis; however, a brief description of the model and a comparison between the numerical results using different flow coefficients and the measurements collected on a dedicated test bench during experimental campaigns carried out by Baker Hughes are shown. In particular, the importance to accurately predict the flow coefficient along the overall suction and discharge gas path, as well as the dependence of the requirements in terms of the accuracy of this parameter by the specific case are underlined.

Moreover, a methodology to perform a 2D CFD simulation of the working cycle of a reciprocating compressor was developed in order to provide more accurate results than low-order models and, at the same time, to guarantee the reduction of the computational effort with respect to unsteady 3D CFD simulations. The analyses presented in this work were carried out for a double-acting large bore cast iron cylinder; the simplifications required to allow the reduction of the three-dimensional fluid domain to an equivalent two-dimensional configuration are shown. In particular, the importance to use the flow coefficients obtained by means of the simplified CFD parametric routine for the pressure losses evaluation in the suction and discharge gas-path is highlighted.

Finally, the suitability to use the parametric CFD routine to increase the predictability of the heat transfer process in a reciprocating compressor is shown. A brief description of a conjugate heat transfer (CHT) approach developed in previous works of the REASE GROUP of the Industrial Department of the University of Florence [4] is given. Once again, the utility of the parametric CFD routine for the forced convection modeling inside suction and discharge gas ducts is underlined.

Starting from all these considerations, in this thesis, the main outcomes of the research are presented by means of seven chapters.

In particular, Chapter 1 contains some information on the thermodynamics and mechanics of reciprocating compressors; specific attention is paid to the definition of the flow coefficient and to the description of the cooling system in a reciprocating compressor.

Chapter 2 shows the basics of CFD analysis, focusing the interest on the treatment of steady-state Navier-Stokes equation and the boundary layer modelling.

The simplified CFD parametric routine is shown in Chapter 3 and Chapter 4. In more detail, the definition and validation of the parametric routine, as well as the solutions adopted for the evaluation of all the possible operating conditions of each machine by means of 48 simulations are described Chapter 3. The results of the application of the parametric approach to the actual database are analyzed and discussed in Chapter 4.

Finally, some applications of the obtained results are shown in Chapter 5, Chapter 6 and Chapter 7 .

In particular, in Chapter 5 reports a brief description of the 1D model and a comparison between the numerical results using different flow coefficients with the experimental measurements, showing the increased predictability achieved thanks to a more accurate evaluation of flow coefficients.

Analogously, the 2D and the CHT models are described in Chapter 6 and Chapter 7, respectively. In both chapters, the utility of the simplified CFD parametric routine as well as the accuracy of these models is highlighted by means of the comparison between the numerical results and the measurements collected during experimental campaigns.

1 The reciprocating compressor

1.1 History of reciprocating compressor

The reciprocating compressor is an operative machine, acted by a driver unit, dedicated to the compression of gas. The practice of applying mechanical work for pressure increasing of air has been realized in early times. In fact, operated bellows were used in metal foundries till the Middle ages (Figure 1.1).

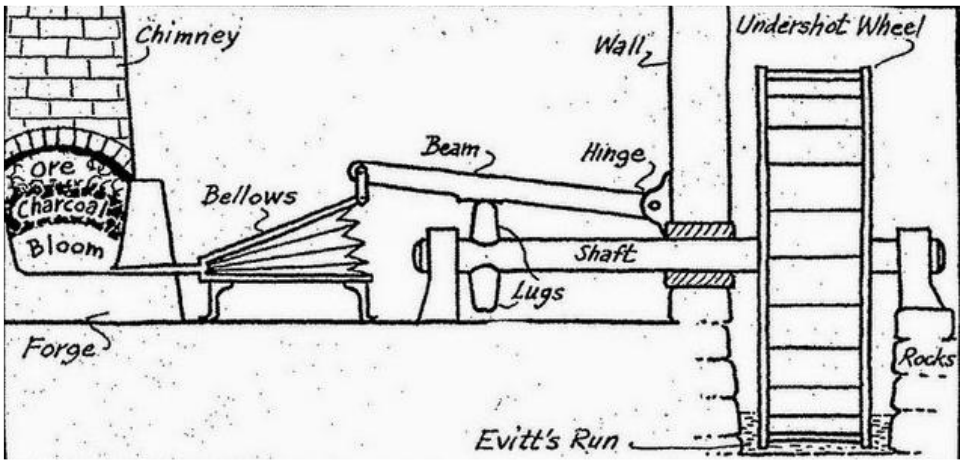

Figure 1.1 – Operated bellows used in metal foundries in the Middle ages

In 1641 Otto von Guericke developed an air pump to create vacuum. On the 8th of May 1654, in Magdeburg, he performed the experiment called "Magdeburg semi-spheres experiment". This experiment can be considered as the forerunner of today's piston compressors [5].

Later, the development of reciprocating compressors has been supported by the born of the steam engine. The conceptual analogies of the two machines (the former

transfers work to the fluid, the latter receives work from the fluid) allowed to couple them in the working conditions (Figure 1.2).

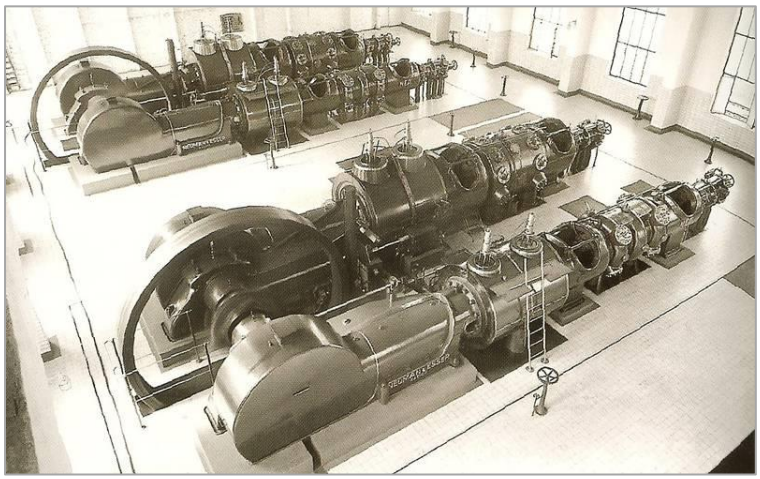

Figure 1.2 – A reciprocating compressor acted by a steam engine

The first industrial single stage reciprocating compressor worked between 3 and 7 bar. At the end of the 19th century multistage compressors were developed (technical gas processing); in particular, the process development in the chemical industry required compressors with ever increasing throughputs and delivery pressures. However, the mass production of small compressors began with the use of compressed air as energy supply and as a part of refrigeration plant.

Nowadays reciprocating compressors are widely employed: in fact, they are a fundamental component both for industrial plants and civil applications. They are involved in a high number of processes which differs both for typology and machinery size required: gas transportation and storage, oil&gas industry applications, refrigeration plants (both industry and civil) and high pressure applications such the LPDE (Low density polyethylene) production. It follows that they are the most diffused type of compressors: in fact, the worldwide installed reciprocating compressors horsepower is approximately three times that of centrifugal compressors [6].

Reciprocating compressors are usually used for high pressure ratio and low volumetric flow rate. In Figure 1.3 the specific field of application of the main typologies of compressors (reciprocating, centrifugal and screw compressors) are shown.

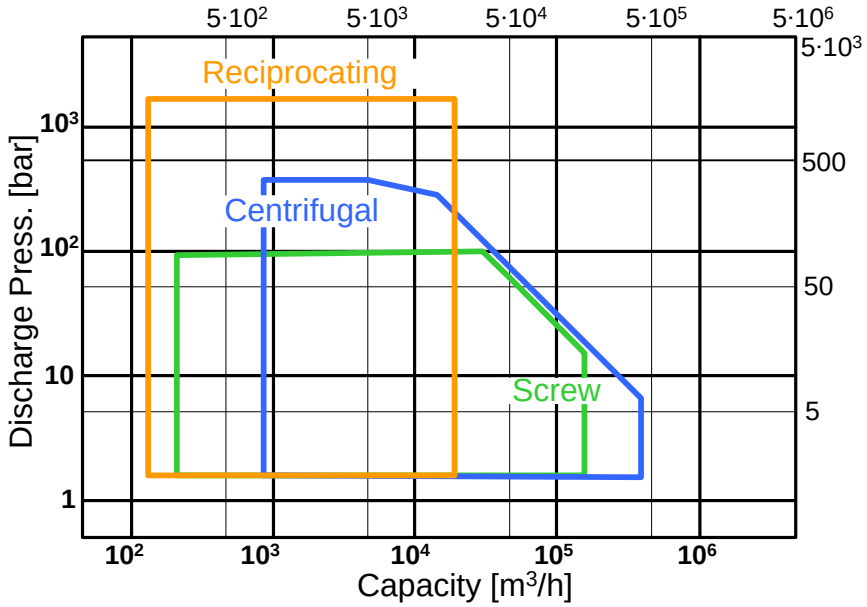

Figure 1.3 – Application fields of compressors

The main advantages following by the use of reciprocating compressors can be summarized as follows [5]:

- high compression efficiency respect to centrifugal compressor for the same opearting conditions (flow rate and pressure ratio), in particular for pressure ratio higher than 2;
- high pressure ratios reached with few stage of compression;
- low opearating condition sensitive respect to gas properties change;
- good adaptability to flow rate variations.

On the other hand reciprocating compressors show the following disadvantages respect to centrifugal compressors:

- high installation plot area for a given flow rate;
- higher installation and maintenance costs (approximatively three and half times greater than centrifugal compressors);
- pressure pulsations generation that need to be controlled in order to avoid structural vibrations, structural breaks and high operating conditions noise;
- contamination of processed gas with lube oil, necessary for crank thrust lubrication.

1.2 Structure and working principles

The reciprocating compressor (Figure 1.4) is an operative machine dedicated to the compression of gas. The main parts of a reciprocating compressors are the cylinder, the driven piston and the self-acting valves. During the reciprocating compressor working, the compressor shaft receives a rotating movement that, through a system composed by connecting-rod and crank is converted in reciprocating motion, to be so transferred to crosshead, rod and piston [3]. This last component slides into a cylinder and produces the compression of the gas between the piston surface and the compressor head. In most applications the piston compresses the gas inside the two cylinder ends: forward (cylinder head side) and backward (crank-mechanism side). This is the so called double acting arrangement (Figure 1.5). Sometimes the piston movement allows the gas compression into only one of the cylinder ends: a cylinder having such an arrangement is named single end.

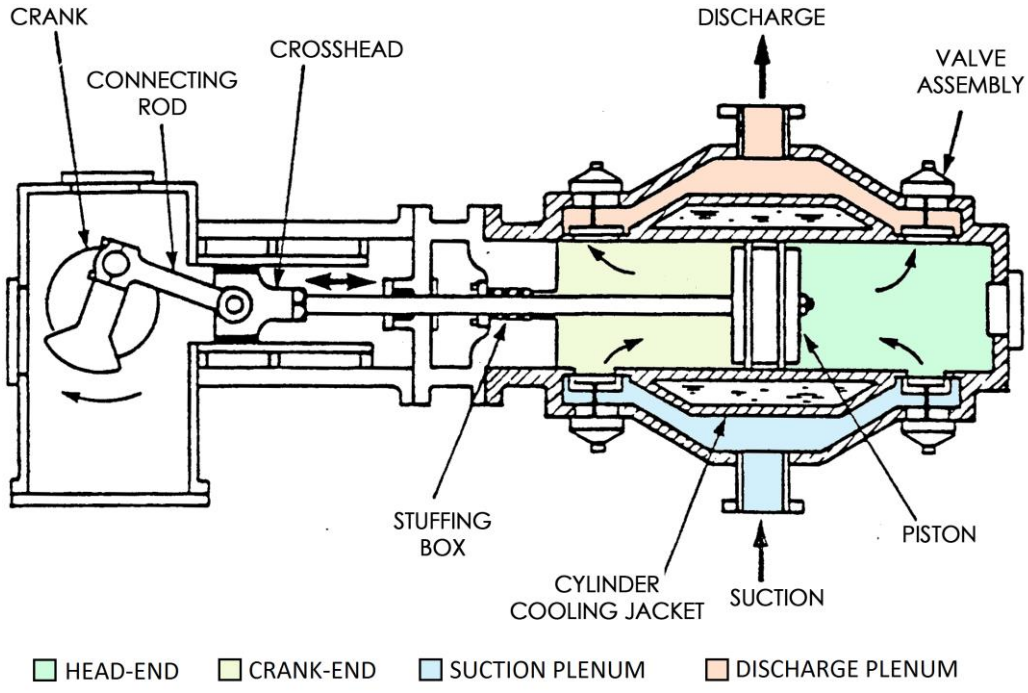

Figure 1.4 – Schematic representation of a reciprocating compressor section

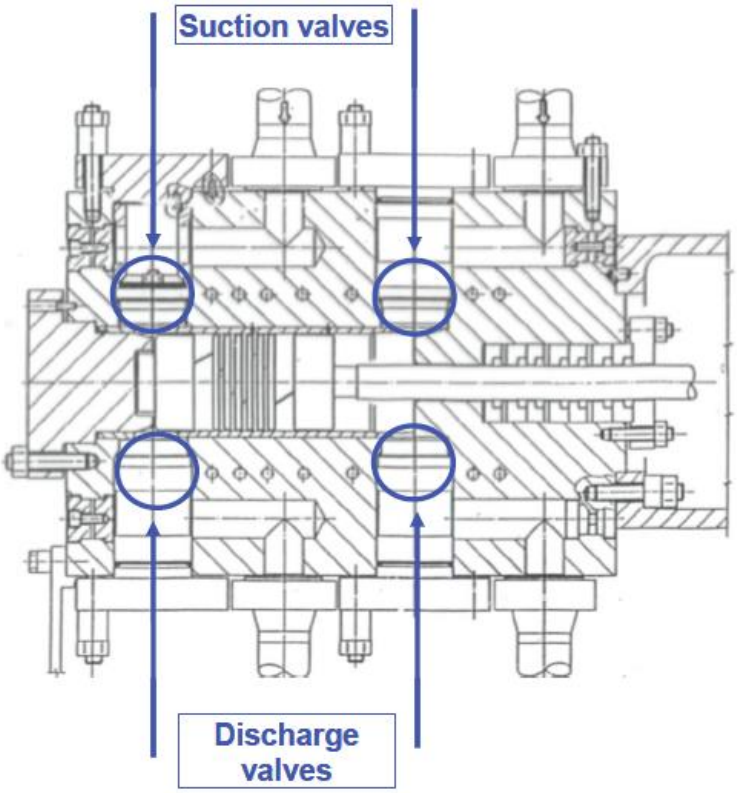

Figure 1.5 - Double acting arrangement

The inlet and the outlet of the gas from the cylinder usually take place through automatic valves that open due to the action of a differential pressure (upstream and downstream themselves) and close due to the work of dedicated springs, whose loads are opposed to the direct gas flow, housed into the same valves (Figure 1.6).

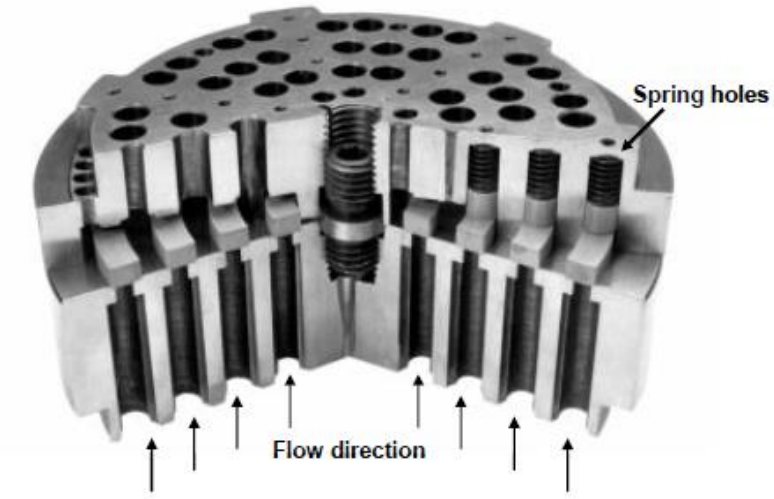

Figure 1.6 - Reciprocating compressor automatic valves

1.3 Ideal cycle

A reciprocating compressor is a machine that transfers the power received at the shaft to the handled gas by increasing its pressure from the suction value to the discharge one. The necessity to predict its performance in terms of adsorbed power, volumetric efficiency, maximum discharge temperature, real mass flow rate etc., imposes a rigorous analysis of the thermodynamics cycle characterizing such a kind of machine.

The ideal cycle of a reciprocating compressor is shown in Figure 1.7 (*p*-*V* diagram).

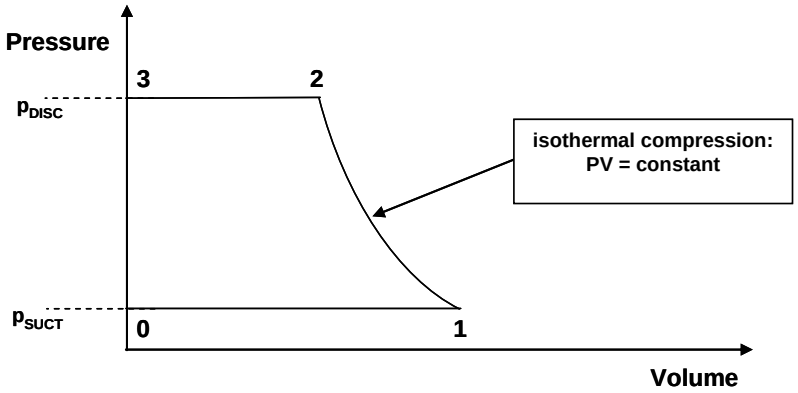

Figure 1.7 – *p*-*V* diagram for the ideal cycle

In this cycle it is possible to define the following phases:

- 0 – 1: suction phase at constant pressure p_s. During this phase the cylinder is filled with the gas at the suction conditions (pressure and temperature); for an ideal cycle the in-cylinder pressure is equal to the suction ambient pressure for the whole phase.
- 1 – 2: compression phase at constant temperature (minimum absorbed power).
- 2 – 3: discharge phase at constant pressure p_d. For an ideal cycle the in-cylinder pressure is equal to the discharge ambient pressure for the whole phase.
- 3 – 0: pressure drop due to the complete delivery of the gas at the end of the discharge phase and to the reversal piston motion.

The power spent for the gas compression is directly represented by the closed area of the cycle.

1.4 Theoretical cycle

The actual gas compression cycle does not correspond to the aforementioned processes. The behavior is indeed different because of the influence of particular phenomena occurring in the real machine. The theoretical cycle can be often considered a good approximation of the real one, whereby it takes into account the main aspects of the real physical processes. However, some secondary effects are neglected, as, for example, the presence of the lubricant oil and the increase of certain losses due to the wear of the components [3].

A typical theoretical cycle is shown in Figure 1.8 where blue dashed lines indicate an ideal cycle which operates between the same discharge and suction pressures. It is possible to notice that the work (equal to the internal area of the corresponding cycle) spent for the ideal cycle is sensibly lower than the theoretical one.

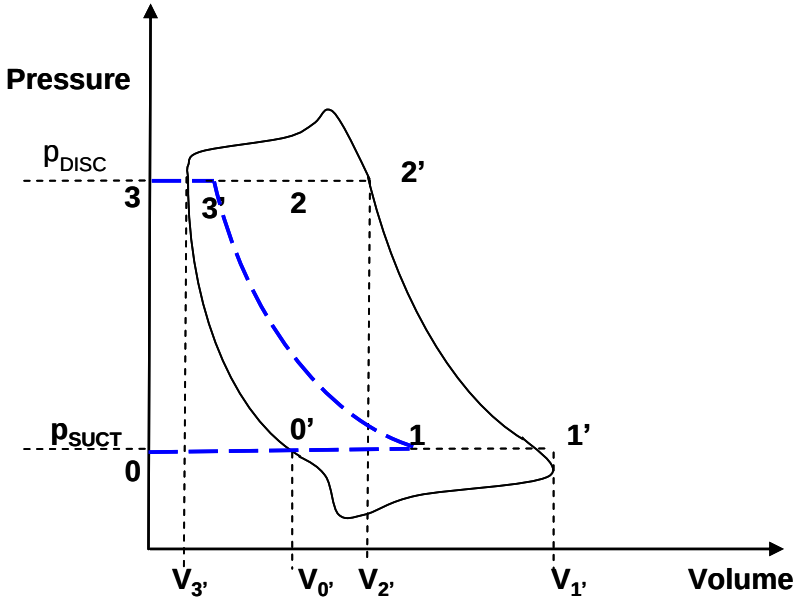

Figure 1.8 – Theoretical cycle vs Ideal cycle

The phases of the ideal cycle are consequently modified:

- 0' – 1': suction phase that starts from point 0' for the expansion of the fluid trapped in the dead volume from the discharge pressure p_d to the suction pressure p_s. The suction pressure is lower than the ideal cycle for the opposition of the

valves to their opening and to the pressure losses occurring along the suction components.

- 1' – 2': compression phase from the suction pressure p_s to the discharge pressure p_d. In the theoretical cycle this phase can be described by a polythropic law.
- 2' – 3': discharge phase that ends at the point 3' for the dead volume $V_{3'}$. This volume is due both for the constructive tolerances and for the volumes of the automatic valves [7]. Similarly to the suction phase, the discharge pressure inside the cylinder is different from the ideal constant discharge pressure. In particular in this case it is higher, thus increasing the compression work.
- 3' – 0': the pressure drop is not instantaneous but occupies a share of the piston stroke, from point 3' to point 0', which in the ideal cycle belonged to the gas intake. The net part of the suction stroke dedicated to the intake is then reduced and the working fluid capacity of the real machine is decreased.

1.5 Pressure losses in a reciprocating compressor

The ideal compression cycle is modified due to two main effects derived from the presence of valves. The first one is caused by the preload of the springs and the other is due to the gas pressure drop during its passage through the valves. The two influences of springs preload and valve pressure drop on the theoretical cycle are examined separately for a better clarification, even if, actually, they occur simultaneously [3].

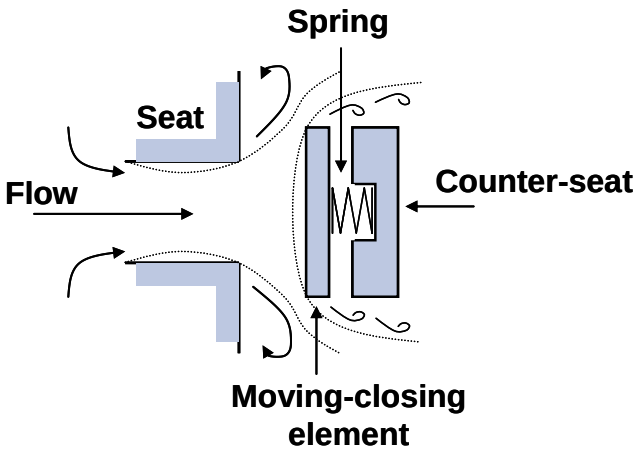

Figure 1.9 – Schematic of a valve

A schematic of a valve is given in Figure 1.9: in this figure is showed how an automatic valve is equipped with antagonist springs, used to assure the closure of the valve. Because of the preload, the valve offers a certain opposition to its opening causing a lower initial suction pressure and an higher initial discharge pressure inside the cylinder with reference to the pressures considered in the ideal cycle. Therefore, this effect results in a higher compression ratio (with the same nominal suction and discharge pressures) developed only to overcome the described springs opposition.

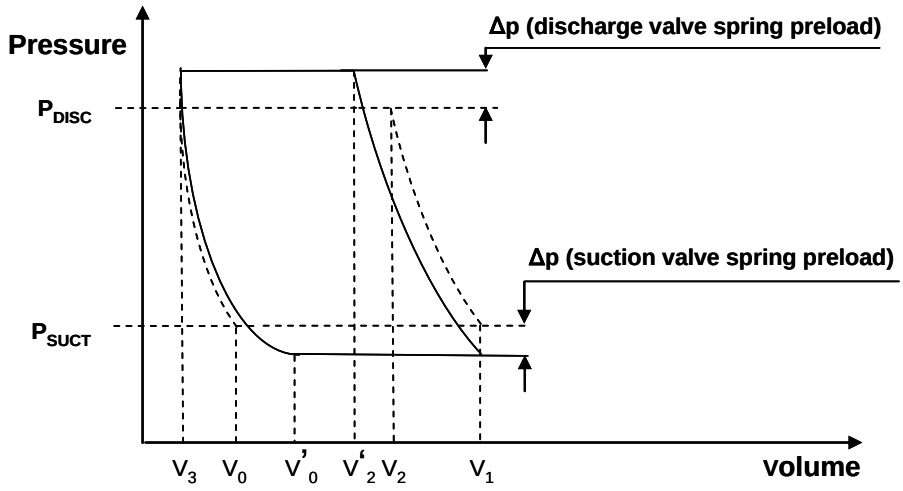

Figure 1.10 – Effect of springs preloads on the theoretical cycle

With reference to Figure 1.10, it is possible to say that the higher compression ratio produces a capacity reduction for two main effects:

- the overpressure at the end of the discharge phase establishes a sucked capacity reduction because the re-expansion, starting at a higher pressure, is completed at a bigger volume;
- the reduction of the intake pressure determines a proportional reduction of the gas density, thus reducing the mass flow rate.

Globally, the valve preload increases the work absorbed for gas compression at each cycle, even if the work is partially reduced by a reduction in handled gas quantity.

The second effect that must be taken into account is the increase of the absorbed power for the gas flowing through the valve. In fact, the opening of the valves allows the fluid passage across the valves passage area, causing no negligible pressure drop.

The compression cycle is consequently modified as shown in Figure 1.11.

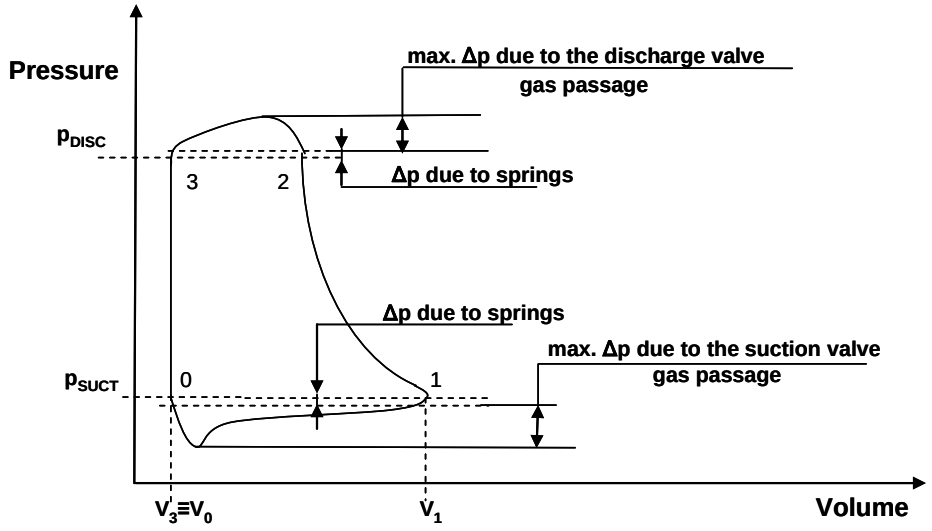

Figure 1.11 – Effect of the springs and of the valves pressure drop on the theoretical cycle

These pressure drops are proportional to the square of gas passage instantaneous velocities, which are variable during one revolution of the compressor shaft, being directly proportional to the piston instantaneous velocity. The opposition of the valves to the gas passage establishes further pressure drops acting to reduce the cylinder inner pressure at the suction phase and to increase the cylinder inner pressure during the discharge phase. It results in a greater compression ratio (at the same nominal suction and discharge pressures) developed only to overcome the further pressure drops due to the flow motion. Consequence of the greater compression ratio is that the gas discharge temperature and the power spent for the compression are both increased. The effect of the valves losses can be taken into account by introducing a corrective factor ($\psi_v < 1$) that reduces the nominal gas flow [8].

Due to these influence of the valves on the thermodynamic cycle, it follows the importance to define valve performance indicators in order to evaluate the valve pressure drop and the valve absorbed power. The valve pressure drop due to the gas flowing through the valve can be evaluated as follow:

$$\Delta p_v = \rho \xi \frac{v_f^2}{2}$$

where ξ is the loss coefficient of the valve (depending on its fluid dynamics features and its geometrical size), ρ is the gas flow density at the valve passage thermodynamic conditions and v_f is the gas flow velocity through the valve.

This formula allows calculating, in first approximation, both the maximum valve pressure drop and the average pressure drop depending only on the values of the valve gas velocities (maximum or average). The valve absorbed power, corresponding to the energy dissipated by the gas passage through the valve during suction and discharge phases, can be evaluated using the following formulas [8]:

$$P_{suct} = \bar{v}_{suct}{}^2 C \xi_{suct} \lambda (3 - 2\lambda)$$

$$P_{disch} = \bar{v}_{disch}{}^2 C \xi_{disch} \frac{\lambda}{r^{\frac{1}{\gamma}}} \left(3 - 2\frac{\lambda}{r^{\frac{1}{\gamma}}} \right)$$

where P_{suct} and P_{disch} are respectively the suction and discharge valve absorbed power, $\bar{v}_{suct}$ and $\bar{v}_{disch}$ are the gas flow average velocities through the valves, C is the volumetric capacity of gas passing through the valve; r is the compression ratio, γ is the specific heats ratio and λ is a parameter called filling coefficient.

The other source of losses in a reciprocating compressor are [3]:

- gas heating losses in the suction side;
- deviation from isohermal compression;
- cylinder clearence;
- gas leakages.

The work spent for the compression establishes an increase in temperature of the compressed gas; for this reason a part of the received heat is transferred by the gas to the cylinder, both to its mechanical components and to its cooling medium (if provided). Therefore the gas sucked at the intake side at cycle by cycle increases its temperature while is approaching the cylinder; at the end of the suction phase, the cylinder is effectively filled with a gas warmer than that coming from the suction line. For this reason the gas density is lower than the suction nominal density, and consequently the capacity is reduced. This effect can be taken into account by introducing a corrective factor ($\psi_H < 1$) in order to reduce the nominal sucked gas capacity.

Another important loss is represented by the deviation from isothermal compression during the compression stage. The phenomenon of gas heating during the compression, as a consequence of friction between gas molecules and mechanical parts, implies that the isothermal curve is replaced by a polytrophic compression curve. Generally, the compression polytrophic curve can be considered adiabatic (without heat exchange) with sufficient approximation, according to the following law:

$$pV^{\gamma} = const.$$

where p is the in-cylinder gas pressure, and V is the volume of the gas inside the cylinder.

However, it is possible to notice that the assumption of adiabatic compression is in contrast with what explained before. In other words, the phenomenon of gas heating at the suction side implies the presence of heat release during the compression process. This is obviously in conflict with the just made approximation of adiabatic compression. This contrast is common in the reference literature and it is going to be neglected in the next exposure: to put it better, the compression work is calculated assuming an adiabatic transformation and the heat transfer is calculated apart, making the two phenomena disconnected, at least in first approximation [3].

The new cycle is shown Figure 1.12.

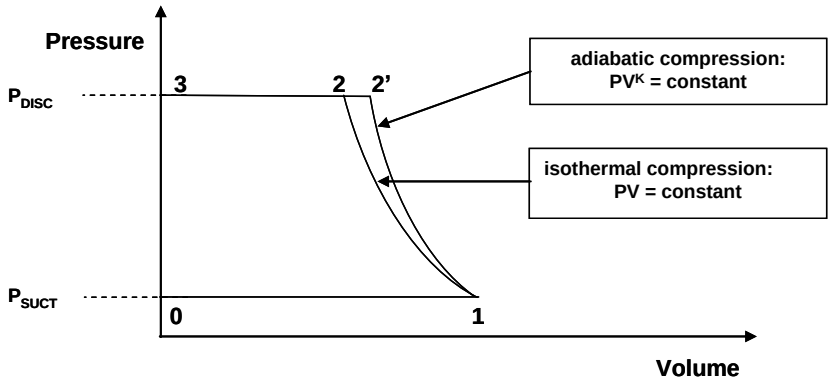

Figure 1.12 - Isothermal and adiabatic compression comparison in the ideal cycle

Another significant influence is due to the presence of the cylinder clearance that affects the amount of total volume where the gas is compressed. When the piston arrives at the TDC at the end of the discharge phase, the cylinder inner volume left at the gas disposal is not null for the following physical residual volumes:

- volumes between piston circular base surfaces and front surfaces of the head (forward end) and of the cylinder (backward end), necessary to avoid mechanical impacts;
- inner volumes own of the valves;
- volumes between valves and cylinder bore;
- volumes between the outer profile of the piston and the cylinder bore.

Therefore a certain amount of residual gas still remains to fill all the volume at its disposal at the discharge pressure. During the expansion phase the piston reverts the motion direction resulting in both a re-expansion of residual gas entrapped into the cylinder and a temperature reduction (contrarily to what happens during the polytrophic compression). Also this re-expansion curve can be considered adiabatic in first approximation but with a different exponent respect to the one used for the adiabatic compression. It's possible to define the new factor γ' (lower than the one relative to the adiabatic compression) as:

$$\gamma' = \gamma - 1$$

The re-expansion is completed when the cylinder inner pressure is reduced to the value of the suction pressure, allowing the opening of the suction valve. It follows that the piston stroke dedicated to the gas suction is reduced.

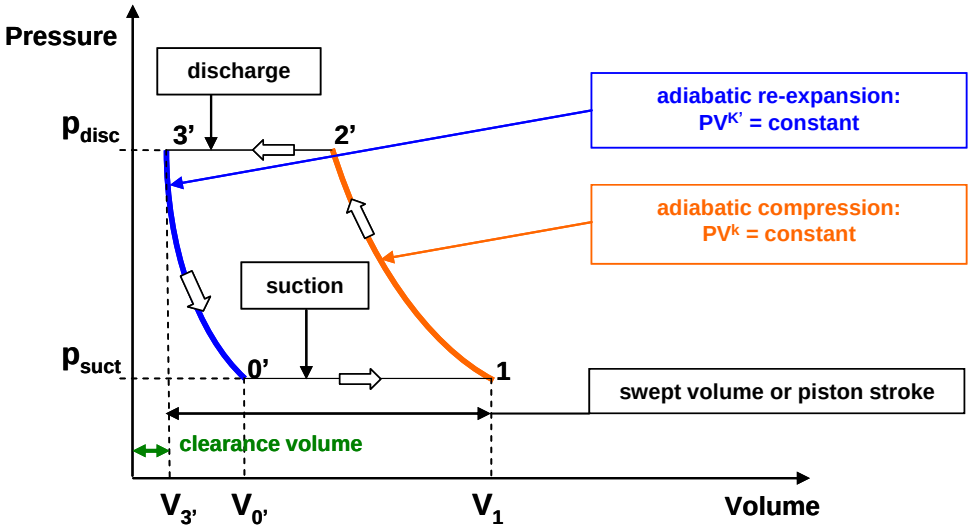

Figure 1.13 - Theoretical compression cycle with clearance effect

The effect of the clearance volume $V_{3'}$ on the reduction of the handled capacity is higher as higher are both the clearance itself and the compression ratio.

The main parameters that fix the effect of the clearance volume on the capacity, from an analytical standpoint, are the following two [8];

- filling coefficient λ;
- clearence volume ratio σ.

The first one gives an indication about how much of the cylinder volume is effectively used during the suction phase and is defined as:

$$\lambda = \frac{V_1 - V_{0'}}{V_1 - V_{3'}}$$

The second is indicative of how much of the cylinder volume is corresponding to the gas residual volume inside the cylinder at the end of the discharge phase and is expressed as:

$$\sigma = \frac{V_{3'}}{V_1 - V_{3'}}$$

These two parameters are connected together by the following law:

$$\lambda = 1 - \sigma \left[\left(\frac{p_d}{p_s} \right)^{\frac{1}{\gamma'}} - 1 \right]$$

that, knowing the clearance volume σ, allows having an indication about the capacity that can be got from the particular selected cylinder as a function of the compression ratio. Moreover, this relation can be used to compare cylinders involved in the same application, assuming that all the other sources of losses are not taken into account in the comparison.

The last effect that influences the thermodynamic cycle is the gas leakages. This phenomenon occurs when the seals (mechanical, with or without dedicated gaskets) cannot assure perfect gas tight. More in details the gas leakage can be addressed to the valves (imperfect sealing between the valve moving elements and the valve seats and between the valve seats and the cylinder seats) and to the piston rings. In fact, considering a double-acting cylinder, when on one side of the piston the pressure reaches its maximum value, on the other side it approaches its minimum. Therefore, the pressure difference equals the design pressure ratio and the rings sealing can bring to gas flowing from one side to another.

The amount of the gas leakages depends on some parameters such as [3]:

- molecular weight of the gas (greater leakages occur with lower molecular weight);
- compression ratio (greater leakages occur with greater *r*);
- rotational speed (greater leakages occur with lower speeds);

- cylinders arrangement (greater leakages occur for dry lube cylinders and lower for the lubricated ones);
- operating hours after the last maintenance (greater leakages occur when the wear rate of the employed components is at the maximum level, close to the next scheduled routine maintenance of the cylinders).

The effect of the gas leakages can be taken into account by introducing a corrective factor ($\psi_L < 1$) that reduces the nominal sucked gas capacity.

1.6 Performance indicators

The cycle area enclosed among the two suction and discharge isobar transformations and the compression and expansion curves represents the work spent in a thermodynamic cycle to compress the gas. Therefore, knowing this area and the compressor rotational speed, it is possible to calculate the power used for the gas compression.

In order to optimize the general performance of the compression system, each compression stage should have compression ratios within a restricted range.

In general, it is recommended [3]:

- to avoid very low compression ratios (indicatively not lower than 1.5). In fact, compression ratios lower than 1.5 result in a rather low compression efficiency due to the very high power dissipated at the cylinder valves, compared to the adiabatic power necessary for the gas compression;
- to avoid very high compression ratios (indicatively not higher than 4). Compression ratios higher than 4 will result both in a rather low volumetric efficiency (low efficiency of the cylinder in terms of capacity) and an excessive discharge gas temperature.

One of the most important parameter for the performance characterization of a reciprocating compressor is the volumetric efficiency η_v defined as follow:

$$\eta_v = \frac{V_{suct}}{V_{cyl}} = \frac{C_{suct}}{C_{cyl}}$$

where:

- V_{suct} is the volume of the sucked gas by the compressor;
- V_{cyl} is the cylinder displacement (the volume swept by the piston);
- C_{suct} is the medium volumetric capacity of sucked gas during the intake phase (generally not known);
- C_{cyl} is the volumetric capacity corresponding to the volume of the cylinder, calculated as a function of geometrical and operational parameters (like bore diameter, rod diameter, stroke, rotational speed):

$$C_{cyl} = \Omega_{cyl} v_p$$

where:

- Ω_{cyl} is the useful area of the cylinder;
- v_p is the medium velocity of the piston.

The volumetric efficiency can be expressed as a product of the filling coefficient λ and of the capacity total loss factor ψ, which takes into account the previously described phenomena that bring to losses (gas heating, effects of the valves, gas leakages).

It results:

$$\eta_v = \psi\lambda$$

$$\psi = \psi_v \psi_H \psi_L$$

From the previous formula, it is possible to calculate the sucked gas capacity as:

$$C_{suct} = \eta_v C_{cyl} = (\psi\lambda)(\Omega_{cyl} v_p)$$

The gas capacity is one of the fundamental parameters for the reciprocating compressor sizing. Another important parameter is the gas discharge adiabatic temperature that is connected to the suction temperature by means of the following formula:

$$T_{disch} = T_{suct} r^{\frac{\gamma-1}{\gamma}}$$

where:

- r is te compression ratio;
- γ is the specific heats ratio.

This temperature must be restricted within a certain limit in order to not have a negative effect on the efficiency and on the life of all cylinder components (e.g. piston seals, valves and packing).

The design of compressor with a too high compressor ratio leads to a low volumetric efficiency or to an excessive discharge gas temperature; it should be taken into account the possibility to divide the compression ratio in several compression stages, having all the same compression ratio. This solution allows minimizing the total power spent for the gas compression. Nevertheless, it is important to consider that the multistage arrangement will involve a more complex and more expensive compressor [3].

1.7 The valves

The valves of reciprocating compressor cylinders are automatic valves, that open due to the differential pressure and close due to the action of dedicated springs located into the same valves, whose loads are opposed to the direction of the gas flow.

The common scheme of an automatic valve is shown in Figure 1.14. The valve elements are:

- seat;
- counter seat;
- moving element;
- spring.

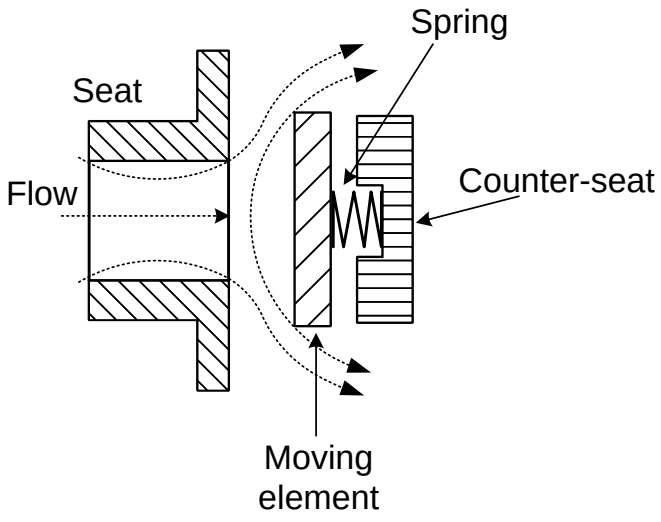

Figure 1.14 – Scheme of an automatic valve

The most used models of valves in reciprocating compressors are substantially of four types [3]:

- feathers or channels valves;
- rings valves and double rings valves;
- disk valves;
- poppet valves.

The scheme and the working principle of these types of valves is the same; the only difference is due to the geometry of the shutters. Currently, the most common valves used for reciprocating compressors are the rings valves; for this reason, in this paragraph, is shown a detailed description of this type of valve. On the contrary the details of the other three types are not discussed in this thesis.

A ring valve has one or more rings as shutters (Figure 1.15). Each of them is independent from the others, so its displacement at opening and closure is not directly influenced by other elements that, otherwise, could introduce overstresses.

The general configuration of the valve is a very robust one, suitable to be used from low/medium pressures (10 bar) up to very high ones (700 bar and more).

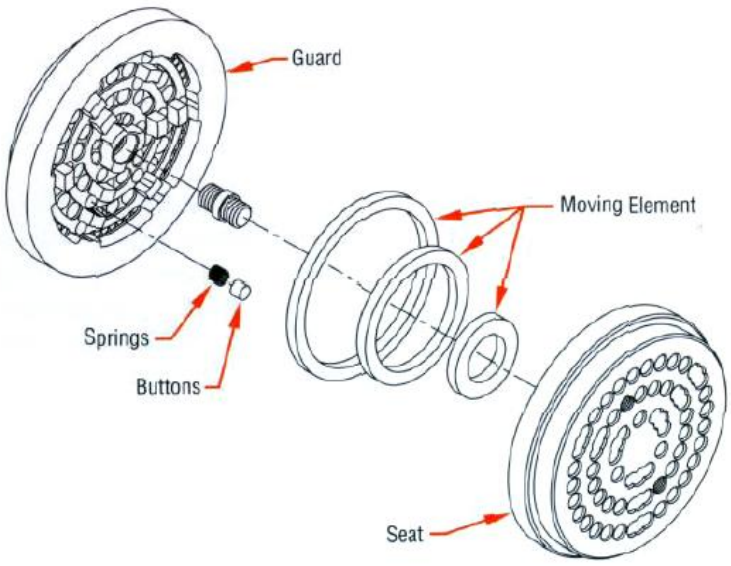

Figure 1.15 – Typical rings valve

The most important features are the rings thickness and the seat thickness; these features have to be sized to support the differential pressures (between discharge and suction) that are expected to occur into the cylinders.

In Figure 1.16, it is represented a typical suction valve with its main four components in closed position. A suction valve is easily recognizable because the gas, during the suction phase, enters in contact with the stud bolt and the nut before entering the valve itself. In fact, in this case the nut is forced on the seat upstream surface.

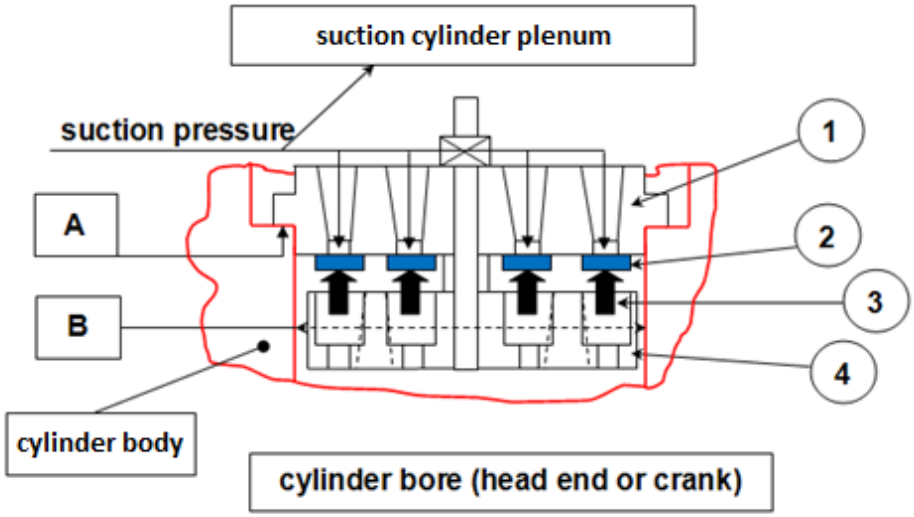

Figure 1.16 - Schematic illustration of a rings valve in closed position

When the valve is closed (Figure 1.16), the valve seat contains the gas at the suction pressure. The closure of the valve is allowed by means of the moving closing elements or shutters that are pushed against the valve seat by the springs and by the gas inside the cylinder. The springs (represented as black arrows in Figure 1.16) are fitted into dedicated housings and transfer the preload pushing the rings against the valve seat. The valve counter-seat (or valve guard) contains the springs, always exposed at the pressure of the gas inside the cylinder bore.

A suction valve in fully open position is shown in Figure 1.17 (the green arrows represent the gas flow path through the valve).

In this case, the gas entering in the cylinder pushes the rings against the valve counter-seat opening the valve and allowing the gas to enter into the cylinder during the suction phase. The springs are pushed inside their housings while the valve counter-seat allows arresting the rings movement.

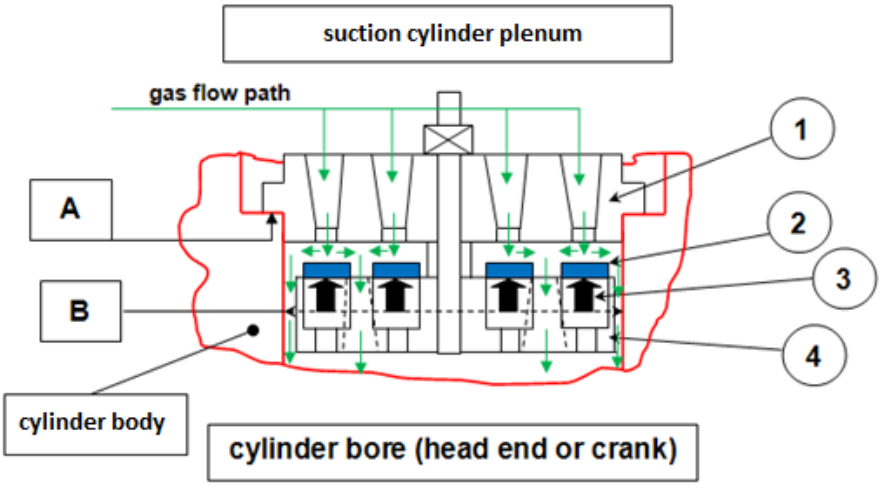

Figure 1.17 - Ring valve in fully open position

Similar considerations can be done for discharge valves, taking into account that, in this case, the valve arrangement is reverted: the valve seat is not located on the cylinder plenum chamber (discharge side) but on the cylinder bore, while the valve counter-seat is not located on the cylinder bore side, but on the cylinder plenum chamber. Besides the nut is in contact with the counter-seat downstream surface.

The main parameters of a rings valve are highlighted in Figure 1.18.

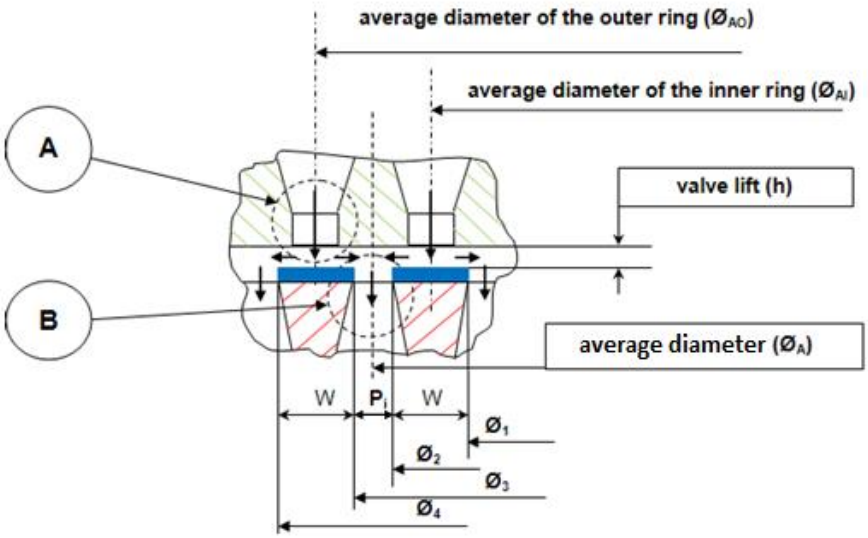

Figure 1.18 - Main parameters of the geometry of a rings valve

For a rings valve having two rings (like the valve in Figure 1.18) the gas passage area under the lift (A_{lift}) that usually corresponds also to the minimum gas passage area (or throat area) is expressed as:

$$A_{lift} = \pi(\Phi_1 + \Phi_2 + \Phi_3 + \Phi_4)h = 2\pi(\Phi_{ai} + \Phi_{ao}) = 4\pi\Phi_a h$$

where:

- $\phi_1 ... \phi_4$ are the diameters corresponding to the rings circumferences
- h is the value of the lift
- ϕ_{ai} and ϕ_{ao} are the average diameters for inner and outer rings
- ϕ_a is the average diameter of all rings circumferences expressed as:

$$\Phi_a = \frac{\sum_{i=1}^{4} \Phi_i}{4}$$

Another possible typology of valves is represented by the double rings valves. These kind of valves are mechanically arranged as the rings valves but with the moving-closing elements made in couple (two rings are effectively manufactured in only one piece), obtaining a compromise between the disks valves and the independent rings valves. The reason of their use is based on fluid dynamics considerations; with reference to Figure 1.18 it is evident that by reducing the width of the rings and their pitch it is possible to fit more rings within the same valve diameter. Therefore it is possible to get valves having a rather big geometrical lift area, compared to the lift area of valves having wider rings. A typical double rings valve is shown in Figure 1.19, where are evidenced the inner and outer diameters, the gas passages and the profiles of the springs.

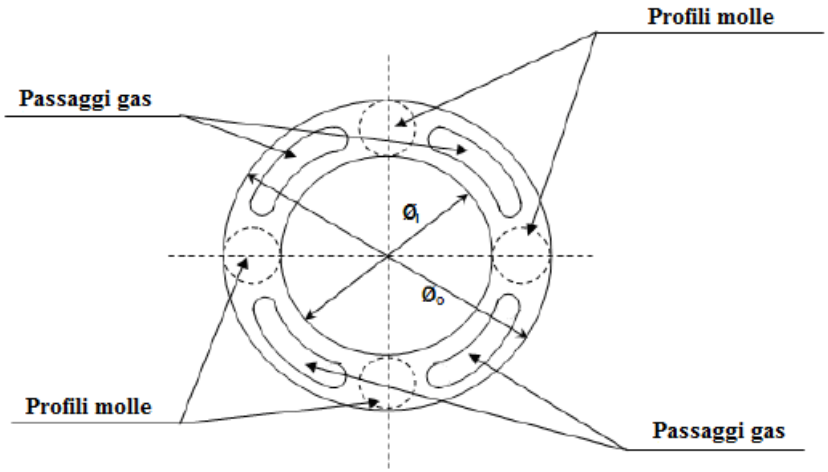

Figure 1.19 - Typical double rings valve

A double rings valve can have a A_{lift} up to 60% higher than a conventional rings valve, thanks to the increased number of rings and therefore of useful gas passages, with consequent lower valve pressure drop during the gas passage [3].

1.8 Flow coefficient

The main issue in the design of a valve is related to the pressure losses that are generated on the working fluid while the gas is flowing through the passages. As already stated in Paragraph 1.5, a pressure drop is indeed always occurring as a non-zero velocity flow is present.

This waste of energy is really relevant in such a complex geometry and therefore its evaluation is a critical aspect for the valve analysis for two main reasons [3]:

- the pressure drop given by the valve is an index of the effectiveness of the valve, being crucial for the amount of work necessary for the gas compression;
- the relationship between the pressure drop and the mass flow rate is required to be known during the complete cylinder design process, since the standard approach for the performance prediction is the use of mathematical model for the calculation of the *p-V* cycle. In order to compute the history of pressures inside the cylinder, mass flow rates and pressure drops along the suction and discharge lines must be known or evaluated.

It is then of common practice to define a mathematical formulation that relates the pressure drop and the mass flow rate of the gas passage through valve. The standard approach for describing real fluid flows through a restriction or a reduction in the flow area is to relate it to an equivalent ideal flow. The equivalent ideal flow is the steady adiabatic reversible (frictionless) flow of a perfect gas through an orifice (simplified geometry) having the same throat area. As far as the passage channels and sections are complex, it is always possible to detect a minimum passage area (generally considered the lift area A_{lift}) so that a valve can be presented schematically as a nozzle.

According to [9], [10] and [11] the expression of the ideal mass flow rate m_{id} for a nozzle (*De Laval nozzle*), considering the upstream total pressure p_0 and the throat pressure p_t, of an ideal perfect gas undergoing an isentropic transformation through an orifice of minimum area A_t is the following:

$$m_{id} = \frac{p_0 A_t}{\sqrt{\gamma R T_0}} \sqrt{\frac{2\gamma}{\gamma - 1} \left(\frac{p_t}{p_0}\right)^{\frac{2}{\gamma}}} \sqrt{1 - \left(\frac{p_t}{p_0}\right)^{\frac{\gamma-1}{\gamma}}}$$

For a real fluid flow the departures from the aforementioned ideal assumptions are taken into account by introducing a flow coefficient *Ks* (or discharge coefficient) as:

$$Ks = \frac{m_{real}}{m_{id}}$$

It expresses the multiplication factor to reduce an ideal mass flow rate of a perfect gas crossing a certain valve, so that it would match the value of the real mass flow rate of the issued gas through the same valve, once pressure drop across it has been fixed. Thus it measures the fluid dynamic efficiency of the valve.

The resulting definition of the *Ks* is then:

$$Ks = \frac{m_{real}}{\frac{p_0 A_t}{\sqrt{\gamma R T_0}} \sqrt{\frac{2\gamma}{\gamma - 1} \left(\frac{p_t}{p_0}\right)^{\frac{2}{\gamma}}} \sqrt{1 - \left(\frac{p_t}{p_0}\right)^{\frac{\gamma-1}{\gamma}}}}$$

Thanks to the previous assumption let's consider a valve having the geometrical gas passage area A_t, which is assumed, by definition, to be the area under the lift. Reducing A_t by multiplication with the *Ks* factor, it would become equal to a particular area that, if crossed by a mass flow rate of a perfect gas subjected to ideal motion, would provide the same pressure drop of the real motion. In other words, assuming the same valve geometry and the same mass flow rate between real and ideal cases, the passage area that provides the same valve pressure drop in the ideal case, respect to the real valve pressure drop, is a particular equivalent area, called effective area, A_{eff}. This assumption is just a different way to define the flow coefficient that therefore can be expressed as:

$$Ks = \frac{A_{eff}}{A_t}$$

The valve flow coefficients are generally variable with the lift and can highly change between series of valves having different basic geometries. For some of them can be slightly dependent also on the velocity, especially at low mass flow rates.

A typical range of values is between 0.3 and 0.6.

This calculation methodology is useful to measure the fluid dynamic efficiency of a valve but not taken into account for the effects of the rest of the flow system in a cylinder.

The global loss is then commonly evaluated by considering a Pocket Factor (*PF)*, that accounts for the increase in losses due to the pocket and all other components and is defined as [12], [13] and [14]:

$$PF = \frac{\xi_{valve+pocket}}{\xi_{valve}}$$

where ξ is the coefficient for a localized pressure drop Δp (Paragraph 1.5).

The Pocket Factor can be obtained either from experimental measurements or from the internal know-how accumulated over years of experience [15]. In both cases, the large variability in the geometrical shape of each element prevents the development of a reliable database for loss prediction, and most of the time, the Pocket Factor must be tuned for the specific case. In some cases, this fixed coefficient is not adequate for correctly estimating all the losses and leads to incorrect results that can affect the operation of the machine in the field or to an overestimation of the losses that may cause a less competitive machine to be selected.

The use of steady-state numerical simulations would be a viable alternative; however, this method is still limited by the extreme computational resources required.

Starting from these considerations, a new simplified CFD routine for the evaluation of the pressure losses occurring along the overall gas path is developed in this thesis. This approach, seeks to promote a standardized method that would require a smaller quantity of input information and would output more general results.

1.9 Cylinder cooling system

As revealed in Paragraph 1.5, in a reciprocating compressor, part of the energy supplied by the motor is transformed into heat, for the following phenomena [16]:

- compression of the gas;
- friction in the cylinders;
- friction in the bearings and crosshead shoes.

The most important effect is a reduction of the volumetric efficiency and an increase of the gas discharge temperature; for this reason, a cylinder cooling system is needed.
The cylinder cooling project is not simple: in fact, this system has to guarantee a compromise between the refrigeration potential and the suction capacity of the

reciprocating compressor. Without an adequate refrigeration system the machine can exhibit the following problems [16];

- less effective lubrication;
- deposits on valves;
- shorter valve life;
- higher cylinder maintenance costs;
- increased risk of fires in discharge piping.

The presence of a cooling system allows a more uniform temperature in the cylinder and lower distortion due to thermal expansions.

The quantity of heat that can be removed varies greatly as a function of numerous factors such as [17]:

- temperatures involved;
- cylinder diameter;
- compressor speed;
- type of gas;
- thickness of the walls;
- extension of the wet surface.

The evaluation of the quantity of the heat removed is very complex for the continuous variation in the pressure and temperature of the gas and therefore in the heat transmission. Moreover, also the internal surfaces that take part in the heat transmission have a not negligible effect.

However, an indirect estimation can be accomplished on the basis of thermodynamic considerations, which tell us that the relationship between the energy subtracted by cooling (E_{sub}) and the energy introduced into the gas (E_{int}) is equal to [17]:

$$\frac{E_{sub}}{E_{int}} = \frac{\gamma - n}{n(\gamma - 1)}$$

where n is the index of the polytropic compression.

Since from experience it turns out that the index of the polytropic transformation is very close to γ, the formula above takes on values equal to about 0.1. This means that the most power that can be removed by the cooling system is equal to 10% of the global expended power in the cylinder.

Most accurate results can be obtained by means of numerical techniques that, nowadays, represent the most favorable approach to quantify the heat removed in a reciprocating compressor by means of the cooling system. In this scenario, 3D CFD analyses show a great potential, regardless the high number of phenomena that have to be taken into account for an accurate modelling of the cooling system.

Different kind of refrigeration systems are available; in fact, a common reciprocating compressor can work in different operating conditions.

Some of them are described below:

- cylinders for cryogenic services where it is impossible to cool;
- cylinders with very low compression ratio and recycle pumps (or circulators) where temperatures are low and cooling is useless;
- reciprocating compressors with compression temperatures limited to 70-80° (refrigerating compressors, gases that "do not heat up"). In these cases, it is sufficient to fill the jackets with liquid, generally water-glycol solution, to equalize the temperature.
- When the temperatures at end of the compression stay below 90-100°C a thermosiphon system may be sufficient. In this case, it is used an individual loop for each cylinder, where the thermosiphon effect and the slight circulation deriving from it are exploited to pass the cooling liquid into an air or water cooled exchanger.
- When the temperature exceed the limits defined in the previous points, it is necessary to use forced circulation of the cooling liquid.

In order to avoid problems due to the condensation, it would be useful to use a cooling temperature from 5° to 20° higher than the suction cylinder temperature when saturated or wet fluid are used. In the other cases, it is possible to have cooling temperature lower than the suction temperature of the working gas.

Multiple fluids are used for the refrigeration of reciprocating compressors; the most common are demineralized water, water-oil emulsion or water glycols. In special cases, where the presence of water is absolutely unacceptable due to the nature of the gas being treated, oil, gasoline or other liquid hydrocarbons have been used [17].

2 CFD modeling

2.1 Governing Equations

In this chapter, the governing equations of the CFD method are introduced and the finite volume method (FVM) is described.

Computational Fluid Dynamics or CFD is the analysis of systems involving fluid flow, heat transfer and associated phenomena such as chemical reactions by means of computer-based simulations [18]. The objective of a CFD analysis is to define an algebraic problem equivalent to the original analytic one in order to obtain an approximate solution with a sufficient accuracy for the purpose of the analysis.

Although the physical equations that describes the dynamics of fluids are known from the second half of the 19th century, principally thanks to the work of Claude Louis Navier and George Gabriel Stokes, the computational fluid dynamics is a matter, at least as regard industrial applications, of the last thirty years. In fact, in the 1980s the solution of fluid flow problems by means of CFD was the domain of the academic field. Gradually, the widespread availability of engineering workstations, together with efficient solution algorithms and sophisticated pre- and post- processing facilities enabled the diffusion of CFD codes also for industrial applications.

Fluid flow is mathematically described by the conservation of mass, momentum and energy [18], [19], [20] and [21].

The general form of a conservation equation for a generic flow quantity φ is:

$$\frac{\partial \rho \varphi}{\partial t} + \nabla \cdot (\rho \vec{v} \varphi) - \nabla \cdot \left(\rho \Gamma_{\varphi} \nabla \varphi\right) = S_{\varphi}$$

where:

- ρ is the density;
- t is time;
- $\vec{v}$ is the velocity vector;
- Γ is the diffusivity;
- S_φ is the source term.

The Navier-Stokes (N-S) equations are a set of non-linear partial differential equations, whose analytical resolution has not yet been found.

The motion of a fluid is completely described by the previous conservation law of the three basic physic properties: mass, linear momentum and energy [3].

The first equation is then the transport equation for the conservation of mass, or continuity equation, derived by setting $\varphi = 1$ and not having mass source terms:

$$\frac{\partial \rho}{\partial t} + \nabla \cdot (\rho \vec{v}) = 0$$

Then the momentum equation, neglecting gravitational effects, is:

$$\frac{\partial \rho \vec{v}}{\partial t} + \nabla \cdot (\rho \vec{v} \vec{v}) - \nabla \cdot \tau = -\nabla p$$

where τ is viscous stress tensor given by:

$$\tau = -\mu(\nabla \vec{v} + (\nabla \vec{v})^T) + \mu \frac{2}{3} I \nabla \cdot \vec{v}$$

where μ is the viscosity of a Newtonian fluid.

Finally, the energy equation may be expressed in terms of internal energy i and is given by:

$$\frac{\partial \rho i}{\partial t} + \nabla \cdot (\rho \vec{v} i) = -p \nabla \cdot \vec{v} + \nabla \cdot (k \nabla T) + Q + S_i$$

where k is the thermal conductivity and Q is the dissipation function that accounts for all the effects due to viscous stresses in the internal energy.

The additional equation, which is essential to the resolution of a fluid dynamic model, is the equation of state of the fluid, which provides the fundamental specification of the nature of the fluid itself.

In particular, the two equations of state most commonly used are the incompressible hypothesis or the perfect gas assumption [3].

Mathematically they can be respectively expressed by means of the following formulations:

$$\rho = constant$$

$$p = \rho RT$$

Some important remarks can be made about the properties of the Navier-Stokes equations [22]:

- The term related to the shear stress tensor is a second order derivative term, as it is the diffusion flux. In particular for incompressible flows it perfectly reduces to the Laplacian operator: this confirms that the viscous terms behaves as a diffusion phenomenon.
- The nonlinearity of the systems of N-S equations is mainly related to the convective term of the equation of motion. This term is responsible for the appearance of turbulence, which is a spontaneous instability of the flow, whereby all quantities take up a statistical (chaotic) behavior.

The three equations of conservation, along with the equation of state of the substance, which are all together five scalar equations, constitute the basic laws that fully describe the behavior of a fluid.

However, for the most part of the industrials turbulence flows, the time scales and the turbulence length scales have such a wide range that they don't allow the direct solution of these equations for the total amount of the computational resources required (Direct numerical simulation DNS). For this reason, al large number of approximated models are developed in the recent past in order to predict the turbulence effect in the flow evolution and to obtain a compromise between the accuracy of the solution and the calculation times.

2.2 Finite Volume Method

In this paragraph, it is given a brief overview on the FVM method [18] and [19].

The FVM subdivides the flow domain into a finite number of smaller non-overlapping control volume. The transport equations are then integrated over each these control volumes by approximating the variation of flow properties between mesh points with differencing schemes.

The desired solution domain is subdivided (discretized) into a number of cells, or control volumes. These are contiguous, meaning that they do not overlap one another and they completely fill the domain. Generally, variables are stored at the cell centroid,

although they may be stored on faces or vertices. A cell is bounded by a set of flat faces with no limitation on the number of faces or their alignment, which can be called "arbitrarily unstructured". Two neighboring cells must only share one face, which is then called an "internal face". A face belonging only to one cell is called a "boundary face".

Using the FVM method the partial differential equation defined in Paragraph 2.1 is transformed into an algebraic expression, which can be expressed as:

$$\boldsymbol{A}\vec{x} = \vec{b}$$

where $\boldsymbol{A}$ is a square matrix, $\vec{x}$ is the vector of the dependent variable and $\vec{b}$ is the source vector. Finite Volume (FV) discretization of each term is formulated by first integrating the term over a cell volume *V*.

The spatial derivatives are converted to integrals over the cell surface *S* bounding the volume using Gauss's theorem [3]:

$$\int_V \nabla \varphi dV = \int_S d(\vec{S}\varphi)$$

where $\vec{S}$ is the surface area vector.

The diffusion term is then integrated over a control volume and linearized as follows:

$$\int_V \nabla \cdot (\Gamma \nabla \varphi)\, dV = \int_S d\left(\vec{S} \cdot (\Gamma \nabla \varphi)\right) = \sum_f \Gamma_f \vec{S}_f \cdot (\nabla \varphi)_f$$

For the convection term it's obtained:

$$\int_V \nabla \cdot (\rho \vec{v} \varphi)\, dV = \int_S d\left(\vec{S} \cdot (\rho \vec{v} \varphi)\right) = \sum_f \vec{S}_f \cdot (\rho \vec{v})_f \varphi_f = \sum_f F \varphi_f$$

The evaluation of φ_f could be done using multiple schemes. The most simple and famous are:

- the central differencing schemes;
- the up-wind schemes.

The first one is a second-order accurate scheme but it is unbounded, meaning that the error of discretization reduces with the square of the grid spacing and that the limits of φ are not necessarily preserved.

The second one is a first-order accurate scheme, it is bounded and determines φ_f from the direction of flow.

Those two schemes can be blended in order to preserve boundedness with reasonable accuracy. Many other schemes are presented by [18], [19] and [23].

The gradient term described here is an explicit term. Usually it is evaluated using the Gauss integration by applying the Gauss theorem to the volume integral:

$$\int_V \nabla \varphi dV = \int_S d\left(\vec{S}\varphi\right) = \sum_f \vec{S}_f \varphi_f$$

but there are other ways to evaluate this term.

The time derivative is integrated over a control volume as follows:

$$\frac{\partial}{\partial t}\int_V \rho\varphi dV$$

and is discretized by using "new values" φ^n at the time step being solved for and "old values" φ^o that were stored from the previous time step.

The classic first order scheme used for solving is the Euler implicit, that is discretized as follows [3]:

$$\frac{\partial}{\partial t}\int_V \rho\varphi dV = \frac{(\rho\varphi V)^n - (\rho\varphi V)^0}{\Delta t}$$

2.3 Turbulence modeling

A laminar flow is characterized by fluid layers that slide smoothly past each other and by the molecular viscosity dampens any sort of instability at high frequency and small scale. This fluid regime occurs for low Reynolds numbers, defined as:

$$Re = \frac{\rho v L}{\mu}$$

where *L* is a characteristic length that describes the size of the problem.

At high Reynolds number the character of the flow changes with a transition to a turbulent state. Turbulent flows are irregular in the sense that they contain structures which show rapid fluctuation in time and space, leading to increase mixing friction, heat transfer ratio and spreading rate [3]. In fact, in a turbulent flow, the fluid moves in a disorganized manner and its particles show not regular trajectories also when their movement proceed in a defined direction. This movement is characterized by an high mixing with the diffusion of every physical quantity.

The turbulence is the natural state of the fluids motion and for this reason its study is extremely important. The most important characteristics of a turbulent flow are:

- three-dimensional flow;
- unsteady flow with high temporal fluctuations of every phisical quantity in a wide band of frequencies, also for steady state boundary conditions;
- vorticity;
- high mixing;
- at first glance, the flow movement looks like random.

A key process that spreads the motion over a wide range of structure scales is called vortex stretching. Turbulent structures gain energy if the vortex are oriented in a direction which allows the mean velocity gradients to stretch them. This mechanism is called production of turbulence. The kinetic energy of the turbulent structures is then convected, diffused and dissipated.

Most of the energy is carried by the large scale structures. The stretching phenomenon causes an energy cascade from large eddies to the smaller ones. For the shortest wave-lengths then energy is finally dissipated by the action of viscosity.

If the unsteady N-S equations are used to solve a flow, a vast range of length and time scales has to be computed. This would require a very fine grid and very high resolution times. This approach is called Direct Numerical Simulation (DNS) and it is applicable only for very simple problems. An averaging process of the equation is then needed to generate a simplified set of equation that give an approximate solution of the real flow [18], [21] and [23]. The averaging process leads to a number of unknown being greater than the number of scalar equations, so the problem of closure of equation arises. A turbulence model is therefore needed to account for some part of the fluctuating motion and must be defined accordingly to the level of the performed averaging of the equation.

Two techniques are commonly used [3]:

- Large Eddy Simulation (LES) in which the equations are filtered in order to separate the velocity field in an explicitly resolved part, related to the large-scale structures (“large eddies”), and in a modeled part (called “sub-grid” part) where the small-scale structures are implicitly included in a subgrid-scale model.
- Reynolds-Averaged Navier-Stokes (RANS) in which the entire fluctuating part of the solved quantities is modeled and only the mean flow value is solved.

2.3.1 RANS models

The procedure that, starting from a three-dimensional unsteady flow, bring to the average equations is realized by Osborne Reynolds. The Reynolds averaging approach involves separating the flow quantities into stationary and random parts, by defining a mean flow value and a fluctuating part. For a generic variable φ this separation it is expressed as:

$$\varphi = \bar{\varphi} + \varphi'$$

where φ' is the fluctuating component and $\bar{\varphi}$ is the mean one defined as:

$$\bar{\varphi} = \frac{1}{T}\int_{t}^{t+T} \varphi(t)dt$$

where *T* is the time interval on which the time-averaged estimation is executed. It has to be chosen large enough respect to the turbulence time scale, but also small enough compared to the time scale of all other unsteady physical phenomena. For this reason, these models are not able to treat unsteady events characterized by time scales comparable with the time scale own of the turbulence [3].

The averaging process is driven by the substitution of the time-averaged quantities in the Navier-Stokes set of equations. Substituting for the averaged properties in the continuity equation and in the momentum one it is obtained:

$$\frac{\partial \bar{\rho}}{\partial t} + \nabla \cdot \left(\bar{\rho}\vec{\bar{v}}\right) = 0$$

$$\frac{\partial \bar{\rho}\vec{\bar{v}}}{\partial t} + \nabla \cdot \left(\bar{\rho}\vec{\bar{v}}\vec{\bar{v}}\right) = \nabla \cdot (-\bar{p}\vec{I} + \bar{\tau}_{av} + \bar{\tau}_{R})$$

where the continuity equation has still the same structure while in the momentum equation a new term ($\bar{\tau}_R$) is added to the averaged viscous shear stresses tensor ($\bar{\tau}_{av}$).

This term is called Reynolds tensor stress and arises from the nonlinear convective term in the un-averaged original equation. It is important to note that the Reynolds stresses not exist; they appear in the N-S equations only for the process of decomposition and average of these equations. However, once that the mean quantities are separated by the fluctuating ones, these terms can be seen as transport of momentum between the fluid elements generated by the turbulent fluctuations. This process is similar to the one that, following the kinetic theory, causes the viscous stresses generation starting from the thermal molecular movement.

In cartesian coordinates the Reynolds tensor stress has the following general mathematical representation:

$$\tau_{R,ij} = -\rho\overline{v'_i v'_j}$$

Its presence is the reason for the existence of the turbulence models; in fact, the fluctuating parts of the local velocities cannot be computed because they are new unknowns. Therefore, the application of the averaging process drives to the necessity to establish new relations for these unknown Reynolds-stresses. Many turbulence models have been developed to approximate such terms and to obtain the so-called "closure of the problem".

The Boussinesq approximation is based on the analogy between viscous and Reynolds stresses that are then supposed to be proportional to the mean velocity gradients by means of the introduction of a proper term: the eddy viscosity or turbulent viscosity μ_t: Therefore, it is obtained:

$$-\rho\overline{v'_i v'_j} = \mu_t\left[\left(\frac{\partial v_i}{\partial x_j}+\frac{\partial v_j}{\partial x_i}\right)-\frac{2}{3}\delta_{ij}\frac{\partial v_k}{\partial x_k}\right]-\frac{2}{3}\delta_{ij}k$$

where *k* represents the specific kinetic energy of the fluctuation and is given by:

$$k \equiv \frac{v'_i v'_j}{2}$$

To compute μ_t further modeling is required; turbulence models are classified into categories based on the numbers of transport equations required to calculate μ_t. The most popular type of turbulence model used is of the two-equation type [3]. Two transport equations are used for the calculation of the turbulent kinetic energy *k* and the turbulent length scale (l_0) or a function of it. The choice of the second variable is arbitrary and many proposals have been presented. The most popular involves using:

- the dissipation rate of turbulence (ε);
- the specific dissipation of turbulence kinetic energy (ω).

The *k*-ε model, developed by Jones and Launder [24], is one of the most used; for this model the turbulent scale is calculated using a second transport equation for the turbulent dissipation rate ε.

The eddy viscosity is typically derived from:

$$\mu_t = c_\mu \rho \frac{k^2}{\varepsilon}$$

where c_μ is a model coefficient.

The transport equations are the following:

$$\frac{\partial \rho k}{\partial t} + \nabla \cdot (\rho \vec{v} k) = \nabla \cdot \left[\left(\mu + \frac{\mu_t}{\sigma_k} \right) \nabla k \right] + P_k - \rho \varepsilon$$

$$\frac{\partial \rho \varepsilon}{\partial t} + \nabla \cdot (\rho \vec{v} \varepsilon) = \nabla \cdot \left[\left(\mu + \frac{\mu_t}{\sigma_\varepsilon} \right) \nabla \varepsilon \right] + \frac{\varepsilon}{k} (c_{\varepsilon 1} P_k - c_{\varepsilon 2} \rho \varepsilon)$$

where P_k is the production of turbulent kinetic energy defined as:

$$P_k = -\frac{2}{3} \rho k \nabla \cdot \vec{v}$$

The constants of the model are:

$c_\mu = 0.09$, $c_{\varepsilon 1} = 1.44$, $c_{\varepsilon 2} = 1.92$, $\sigma_k = 1.0$ e $\sigma_\varepsilon = 1.3$.

The advantage of *k-ε* model is that it is relatively simple, robust and largely validated as it is widely used in industrial applications. It performs well for attached flows with thin shear layers and jets but fails to predict the correct flow behavior in many flows with adverse pressure gradients, extended separated flow regions, swirl, curvature, secondary flows and unsteady flows.

The *k-ω* model, developed by Wilcox [25], uses the k-specific dissipation rate as second variable to compute the turbulent length scale. The eddy viscosity is obtained by:

$$\mu_t = \rho \frac{k}{\omega}$$

The turbulence transport equations are:

$$\frac{\partial \rho k}{\partial t} + \nabla \cdot (\rho \vec{v} k) = \nabla \cdot \left[\left(\mu + \frac{\mu_t}{\sigma_k} \right) \nabla k \right] + P_k - \rho \beta^* \omega k$$

$$\frac{\partial \rho \omega}{\partial t} + \nabla \cdot (\rho \vec{v} \omega) = \nabla \cdot \left[\left(\mu + \frac{\mu_t}{\sigma_\omega} \right) \nabla \omega \right] + \alpha \rho \frac{\omega}{k} P_k - \rho \beta \omega^2$$

and the model constants are:

$\alpha = 5/9$, $\beta = 3/40$, $\beta^* = 0.09$, $\sigma_k = 0.5$ e $\sigma_\omega = 0.5$.

The *k-ω* model allows a good treatment of the flow for low Reynolds numbers, being more accurate and more robust in the analysis of the flow near the walls. For this reason, it is particular indicated in the resolution of internal flows that are usually highly influenced by the presence of the solid faces.

2.4 Boundary layer modeling

The turbulence theory and the turbulence models (Paragraph 2.3) are based on hypotheses that are verified only for high Reynolds numbers; however, near to the wall the local Reynolds number decreases for the effect of the boundary layer. In the boundary layer, there are high gradients of velocity and temperature; for this reason, particular attention is required in the mesh realization for an accurate prediction of the fluid-dynamic behavior of the flow. The characterization of this behavior near to the wall is extremely important in order to obtain an accurate evaluation of the global pressure losses in the machine. The boundary layer is generally described using dimensionless parameters [26] as the dimensionless distance from the wall y^+ (wall unit) defined as:

$$y^+ \equiv \frac{yu^*}{\nu}$$

where:

- y is the distance from the wall;
- ν is the kinematic viscosity;
- u^* is the friction velocity defined as:

$$u^* \equiv \sqrt{\frac{\tau_w}{\rho}}$$

with ρ fluid density and τ_w wall shear stress expressed as:

$$\tau_w \equiv \mu \left.\frac{\partial u}{\partial y}\right|_{y=0}$$

where μ is the dynamic viscosity and u is the mean fluid velocity along the wall.

The velocity can be described in a dimensionless form (u^+) as a function of the mean fluid velocity and of the friction velocity obtaining:

$$u^+ \equiv \frac{u}{u^*}$$

For cases with heat transfer, the dimensionless temperature may be calculated using the following equation:

$$T^+ \equiv \frac{T_w - T}{T^*}$$

where:

- T_w is the wall temperature at a certain point;
- T is the fluid temperature;
- T^* is expressed as:

$$T^* \equiv \frac{\alpha q_w}{k u^*}$$

with α thermal diffusivity, q_w wall heat flux and k thermal conductivity.

A fundamental aspect on the evaluation of the fluid near to the wall is represented by the universal behavior of the boundary layers in terms of dimensionless parameters.

For this reason, it is possible to define three different regions; the viscous sub-layer, the inertial sub-layer and the outer region [18].

The first one includes the fluid closest to the wall where the viscous effects are dominant. This layer is in practice extremely thin ($y^+ < 11$) and is characterized by the following relation between u^+ and y^+:

$$u^+ = y^+$$

Because of the linear relationship between velocity and distance from the wall, the fluid layer adjacent to the wall is often known as linear sub-layer.

Outside the viscous sublayer ($30 < y^+ < 100$) a region exists where viscous and turbulent effects are both important. In this region, the relationship between u^+ and y^+ is logarithmic and is expressed as:

$$u^+ = \frac{1}{\kappa} \ln y^+ + B = \frac{1}{\kappa} \ln(E y^+)$$

where κ and B are constants equal to $\kappa = 0.4$ and $B = 5.5$ (or $E = 9.8$) for smooth walls; wall roughness causes a decrease in the value of B. The values of κ and B are universal constants valid for all turbulent flows past smooth walls at high Reynolds number. Because of the logarithmic relationship between u^+ and y^+ the layer where y^+ takes value between 30 and 100 is often called as log-law layer.

At larger values of y, is located the zone called outer layer, where the inertial effects are dominants.

Figure 2.1 shows the close agreement between theoretical equations used for the description of the fluid behavior in the linear sub-layer and in the log-law layer in their respective areas of validity and experimental data [27].

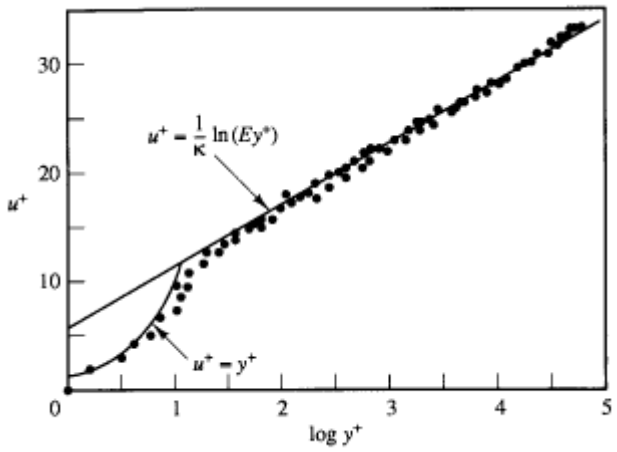

Figure 2.1 – Velocity distribution near a solid wall

There are two common near-wall modelling techniques employed in CFD: Low Reynolds number modelling and Wall function theory [26].

If the boundary layer is meshed sufficiently fine so that the first cell is placed entirely in the laminar sublayer of the boundary layer, the approach used is generally referred to as Low Reynolds modelling. In Low Reynolds modelling, the governing equations of fluid flow are solved in all regions of the boundary layer. It is more time consuming but generally more accurate than the Wall function approach.

In dimensionless units, the height of the first cell is generally taken to be approximately $y^+ = 1$, though the laminar sublayer is valid up to $y^+ < 11$.

In the range of $30 < y^+ < 100$ there exists a buffer region between the laminar sublayer and the log-law region of the boundary layer. It is generally not advisable to have meshes where the first cell lies within the buffer region, though often it is unavoidable in CFD [26].

For meshes where the first cell is located at $y^+ > 30$, Wall function theory may be applied. Wall functions allow CFD models to interpret behavior near a wall without the need for a very fine mesh that discretizes the generally quite thin laminar sublayer at the surface of the wall. The Wall function equations are based on an analytical solution of the transport equations in combination with experimental data fitting. The result is a reduction in computation time and a relatively accurate representation of what happens within the boundary layer, at least under the conditions for which the wall functions were derived.

Wall functions are recommended for cases where the domain is complex or so large that it would require an extremely elaborate mesh leading to a long computation time. On the other hand, wall functions may cease to be valid in complex situations. Nevertheless, they are often used for complex calculations, which can be responsible for considerable errors in near-wall flow [26].

2.5 Porous modeling

Porous medium is modeled by attenuating the time derivative with a term χ, whose value is between 0 and 1, and by adding a sink term $\vec{S}$ to the standard Navier-Stokes momentum equation. It is obtained:

$$\frac{\partial \chi \rho \vec{v}}{\partial t} + \nabla \cdot (\rho \vec{v} \vec{v}) - \nabla \cdot \tau = -\nabla p + \vec{S}$$

The source term, $\vec{S}$, is composed of two parts: a viscous loss term and an inertial loss term, creating a pressure drop that is proportional to the velocity and velocity squared, respectively. This equation is known as the Darcy-Forchheimer equation [28], [29] and [30]:

$$\vec{S} = -\left(\mu \boldsymbol{D} + \frac{1}{2}\rho |v| \boldsymbol{F}\right) \vec{v}$$

where $\boldsymbol{D}$ and $\boldsymbol{F}$ are matrices and the two terms are respectively the Darcy or permeability term and the Forchheimer or inertial term. In the case of simple homogeneous porous media it becomes:

$$\vec{S} = -\left(\mu D + \frac{1}{2}\rho |v| F\right) \vec{v}$$

where the matrices $\boldsymbol{D}$ and $\boldsymbol{F}$ are represented as scalars D and F. The source term can also be modeled as:

$$\vec{S} = -\rho C_0 |\vec{v}|^{\left(\frac{C_1 - 1}{2}\right)}$$

where C_0 and C_1 are user defined empirical coefficients.

3 Simplified CFD routine for the global pressure losses evaluation

3.1 Introduction

The increasing demand for high efficiency in the field of energy production has also had an impact on reciprocating compressors. For these machines the performance predictability is one of the most important challenge in order to reduce both times and costs of the design.

For an accurate prediction of the global performance, three-dimensional CFD transient simulations should be used: however, the computational costs of these simulations are too high and not compatible with any industrial process. For this reason the thermodynamic cycle of a reciprocating compressor is often calculate by means of low order (0D-1D) numerical models, with a substantial reduction of the calculation times. Both 0D and 1D models require the knowledge of the flow coefficient (*Ks*) to account of the global pressure losses along the suction and discharge flow path. In the past, most studies were focused only on the analysis of the valve pressure losses. More recently, the interest has been extended to the prediction of the losses through valve pockets and cylinder ducts. In fact, these losses are a crucial aspect for a more accurate estimation of the absorbed power. In this context, the use of CFD (Computational Fluid Dynamics) for the simulation of the whole gas passage throughout the inner paths of

cylinders could be a possible solution for the prediction of the global pressure losses. However, these simulations are very demanding both in terms of computational resources and in man work for the set-up.

Within this scenario, the Industrial Department of the University of Florence jointly by Baker Hughes, a GE company, developed an original simplified CFD routine, with the purpose of introducing a new methodology for the evaluation of the pressure losses occurring along the overall gas path. The main goal of this approach was the development of parametric CFD models of the entirety of the suction and discharge systems that allow an important reduction of the set-up and computational times.

3.2 State of the art

The main irreversibility that affect the reciprocating compressor efficiency is related to the pressure losses along the gas flow path. Although the valves are correctly thought to provide the most significant contribution to these losses, a key role is also played by other components along the cylinder suction and discharge paths. The prediction of the behavior of these components is a critical issue for the evaluation of the absorbed power but the accuracy of these estimates is affected by the complex phenomena involved in the working cycle like pulsating flow or aeromechanical interactions.

As explained in Paragraph 1.8, the standard approach for the evaluation of the pressure losses of automatic valves is based on flow coefficients derived from experimental data collected on a dedicated test bench. Conversely, there is a lack of information concerning the flow behavior of the other components, which compromises the level of confidence of the predictions. In common practice, these losses are often taken into account by correcting the valve flow coefficient by means of empirical correlations mainly based on experience [12], [13] and [14].

For an accurate prediction of the global pressure losses, three-dimensional CFD transient simulations of the entire gas passage through the inner paths of cylinders should be used [31], [32] and [33]. However, these simulations require extremely high resolution both in terms of spatial and temporal discretization, which results in unreasonably lengthy simulations and specialized hardware requirements.

A more suitable and feasible approach is the evaluation of pressure losses under steady-state conditions, neglecting the gas dynamics and focusing the attention only on the aspects related to gas friction [33]. This approach is not able to consider the global compression cycle like a transient approach but allows a substantial reduction of the computational resource and a good estimation of the overall pressure losses along the gas path maintaining a strong dependence of the results on the specific geometric and fluid-dynamic parameters selected for the calculation.

However, the complexity of the geometry remains a factor, mainly due to the geometrical features of the valve. Since the size of the valve channels and the overall domain dimensions differ by more than three orders of magnitude, the meshing process requires a significant manual set-up effort and the grid density must still be fine enough to capture the flow structures at the smallest scale.

A possible approach that allows reducing both the computational and set-up times maintaining the accuracy of the results was proposed by [34] and [35]. This approach is based on the assumption that a definable relationship between the distinct sources of losses can be established and on the replacement of the valve with an equivalent porous region that generates a localized pressure drop together with a straightening of the flow (Figure 3.1). This methodology, which is based on the "superposition principle", allows a standardized method that requires a smaller quantity of input information obtaining more general results.

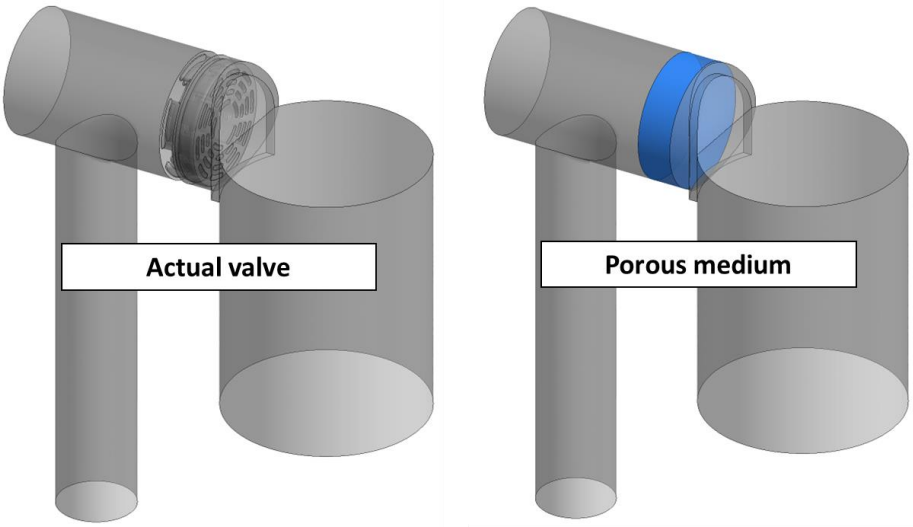

Figure 3.1 – CFD domain simplification

The substitution of the actual geometry of the valve with an equivalent cylindrical porous model allows reducing both the meshing and the global simulation times respectively of around 80% and 70% [34] and [35]. However, the use of these kind of simulations in industrial applications for the pressure losses evaluation remains difficult for the dependence of the pressure losses by a large number of geometrical and thermodynamic variables. In fact, in a common industrial application, it is possible to find a large number of machines that differ for multiple geometrical features that influence the global pressure losses. Moreover, a single machine could be used with different valves and in different operating conditions. The number of configurations that should be simulated is extremely high and the evaluation of the pressure losses in the suction and discharge gas path with a 3D CFD simulation is impossible without a substantial reduction of the set-up times and of the number of simulations.

The use of parametric models to account for the effect of the geometrical features in the global pressure losses and to reduce both the computational and set-up effort was proposed by [15]. In this work, a new methodology for the evaluation of valve pocket losses is presented. Since the pocket losses have been proven to be independent of the actual valve installed, a set of CFD simulations using a parameterized geometry of the valve pocket was performed and the relationship between the losses of the pocket and its geometrical features was obtained. However, the approach proposed by Balduzzi was applied for a very simplified geometry of the valve pocket, without taking into account the actual geometrical features, nor the suction and discharge gas path.

3.3 Modeling approach

3.3.1 Definition of the "parametric approach"

The methodology proposed in this work, aim to extend the use of parametric models to the overall suction and discharge gas path in order to obtain a compromise between the set-up and computational times and the accuracy of the results in the global pressure losses evaluation. The main objective is the realization of a routine that allows the whole fleet of cylinders of Baker Hughes to be simulated in order to obtain a reliable database of the global flow coefficients (*Ks*) to use in low order models to take the global pressure losses into account. For this reason, detailed analyses on the influence of the geometrical and thermodynamic variables in the global pressure losses along the suction and discharge gas path were carried on in order to reduce the number of configurations that should be simulated. At the same time, simplified parametric models of the overall suction and discharge gas path were developed with the goal to evaluate the global pressure losses in the machine with set-up and computational times compatible with the common industrial processes.

In fact, in order to realize a reliable database for the evaluation of the overall pressure losses in the suction and discharge gas path, it is important to take the following considerations into account:

- in a common industrial application, it is possible to find a large number of machines that differ for multiple geometrical features that have a direct impact on the global pressure losses. Indeed, large-size machines are custom-made and each produced unit has a unique design (indicated in this thesis as "cylinder code");
- dealing with double acting cylinders and using steady state simulations, at least four simulations are needed for each cylinder code; one simulation for every phase (suction and discharge) and for every effect (crank end side and head end side);
- each cylinder code could be used with different bore diameters and with different valves typologies (having different flow coefficients and different reference areas);

- the global pressure losses (and the calculated flow coefficients) change with the piston position (piston masking effect);
- each cylinder code could be used with different fluid and in different operating conditions (different pressures and temperatures).

For all these reasons, it is impossible to obtain a reliable database with acceptable calculation and set-up times with a "common" approach. Therefore, an accurate study on the effects of all of these variables on the results is necessary, along with the definition of a simplified routine that allows reducing the number of simulations and the set-up effort for the simulations pre-processing phase.

The common strategy to realize a complete CFD analysis for the evaluation of the fluid dynamic efficiency of a reciprocating compressor cylinder starts by the extraction of the fluid domains of the compression chamber and of the suction and discharge ducts from the solid CAD model (Figure 3.2).

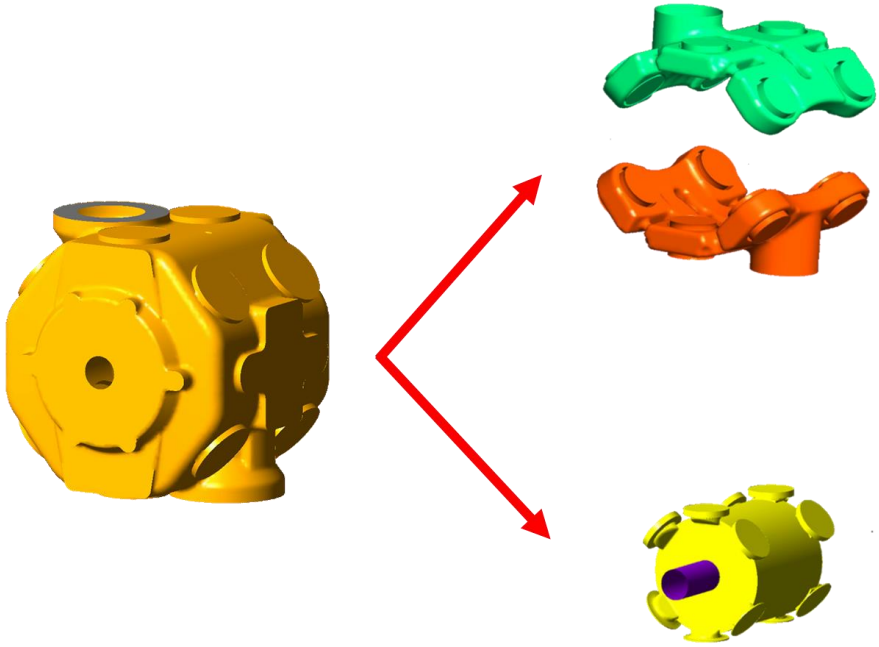

Figure 3.2 – Fluid domain extraction by a solid CAD model

The obtained fluid domain is then simplified through a defeaturing in the CAD pre-processing phase and manually meshed; this operating procedure is extremely time consuming and it has to be repeated for each simulation case considering the variation of the main parameters (i.e. suction/discharge, head-end/crank-end, piston position, etc).

Moreover, it is not automatable and the routine has to be repeated for each cylinder code. For this reason, a similar approach could be used for the simulation of a small number of cylinders but does not allow obtaining a reliable database in a common industrial application.

The proposed approach is to obtain the computational domain by means of parametric CAD models of the fluid domain directly (Figure 3.3) without the need of starting from the more complex 3D drawings of the solid metal components and assemblies. The advantage of such approach is related to the fact that many cylinder codes have common geometrical features (e.g. number of valves or cylinders materials) and it is possible to gather this codes in a smaller number of cylinder "families". Therefore, each parametric CAD model of the cylinder could be used for a large number of cases. This solution requires a greater initial effort for the realization of a parametric CAD model but allows an important reduction of the set-up times when simulating more cylinders codes starting from the same parametric model.

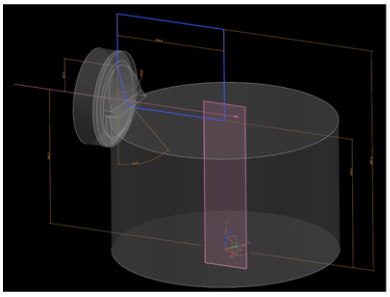

Parameters

DS_CE_BOMBEY_ANGLE	15
DS_VALVE_DIAMETER	242
DS_FLANGE_OFFSET	0
DS_GAS_CHAMBER_CUT_3_HEIGHT	300
DS_GAS_CHAMBER_BLEND_3	25
DS_MACHINING_ANGLE	0
DS_BORE_CAPOSTIPITE	510
DS_CAMPANA_SUCT_HOLE_DISTANCE	102
DS_DELTA_FLANGE_DISTANCE_BORE_CAPOSTIPITE	365
DS_CAMPANA_SUCT_LENGTH	225
DS_DELTA_CYLINDER_HEIGHT_LINER_HEIGHT	70
DS_CYLINDER_HEIGHT	340
DS_GAS_CHAMBER_CUT_1	167,5
DS_VALVE_LENGTH	54
DS_DELTA_GAS_CHAMBER_DIA_INT_BORE_CAPOSTIPITE	180
DS_GAS_CHAMBER_PROFILE_RADIUS	224,4
DS_GAS_CHAMBER_CUT_3_TOP	100
DS_CAMPANA_SUCT_DIAMETER_HOLE	60
DS_PIPE_DIAMETER	250
DS_GAS_CHAMBER_THICKNESS	110
DS_DELTA_VALVE_POSITION_2_CYLINDER_HEIGHT	15
DS_MACHINING_HEIGHT	0
DS_CAMPANA_SUCT_HOLE_ANGLE	45
DS_GAS_CHAMBER_THICKNESS_REV	175
DS_CAMPANA_SUCT_DIAMETER_EXT	262
DS_DISTANCE_PIECE_HOLE_WIDTH	170
DS_PISTON_HEAD_DISTNCE	300
DS_DELTA_CE_POCKET_SPIANATURA_BOMBEY_BORE_CAPOSTIPITE	10,5
DS_DELTA_DISTANCE_PIECE_DIA_EXT_BORE_CAPOSTIPITE	26
DS_CE_POCKET_BLEND_1	20
DS_CE_POCKET_BLEND_2	5
DS_DELTA_CHAMBER_HEIGHT_CYLINDER_HEIGHT	320
DS_DELTA_TAPPO_DISTANCE_BORE_CAPOSTIPITE	600
DS_DELTA_BORE_CAPOSTIPITE_BORE	0
DS_STROKE	360
DS_GAS_CHAMBER_CUT_3_BOT	40
DS_CE_POCKET_DIAMETER_1	195
DS_CE_POCKET_DIAMETER_2	175
DS_LINER_HOLE_DIAMETER	190
DS_LINER_THICKNESS_CAPOSTIPITE	13
DS_VALVES_ANGLE	66
DS_CAMPANA_SUCT_CHAMFER	59
DS_DISTANCE_PIECE_HEIGHT	292
DS_VALVE_NUMBER	2
DS_FONDO_HEIGHT	312
DS_CAMPANA_SUCT_HOLE_NUMBER	4
DS_FONDO_HEIGHT_INTERNAL	222
DS_CE_POCKET_ANGLE_1	15
DS_CE_POCKET_ANGLE_2	45
DS_CE_POCKET_ANGLE_3	40

Figure 3.3 – Parametric model for the fluid domain realization

The idea of the CFD routine described in this thesis is then to use parametric CAD models for the simulations of a large number of cylinders in order to reduce the global computational times. Indeed, the parameterization comprises also the mesh definition and the simulation setup phases, thus leading to a fully automatable approach.

For each "family" a *Master Model* can be created, including the parameterization of the CAD model, the mesh setup and the simulation settings; for this reason, the number of *Master Models* that has to be realized will be equal to the number of cylinder families, substantially lower than the number of cylinder codes. The procedure for the realization of a CFD steady state simulation of a large-size reciprocating compressor by means of the two approaches described in this paragraph is summarized in Figure 3.4.

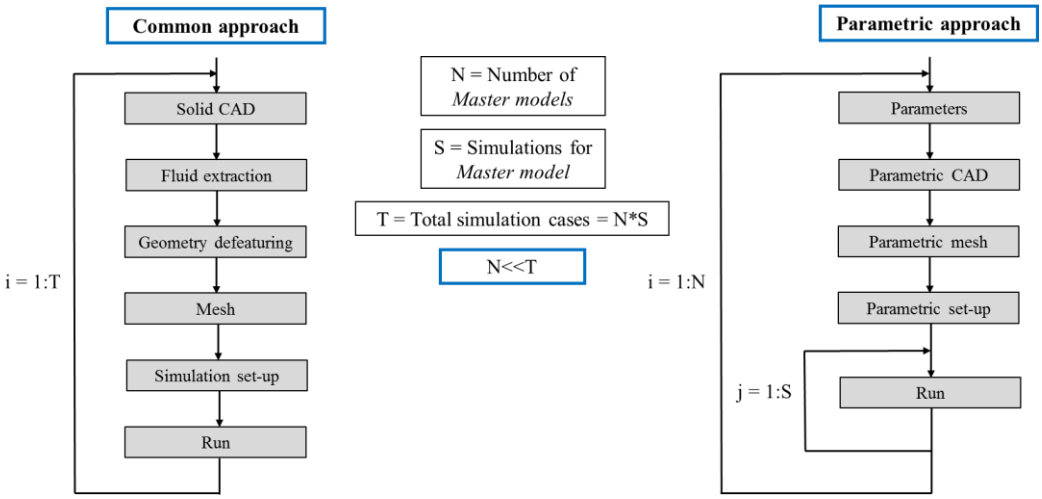

Figure 3.4 – Different strategies for the realization of a CFD steady state simulation

An estimation of the global times needed for the simulation of multiple codes using the common approach (green lines) or the simplified parametric one (red lines), is given as a function of the number of cylinder codes in Figure 3.5.

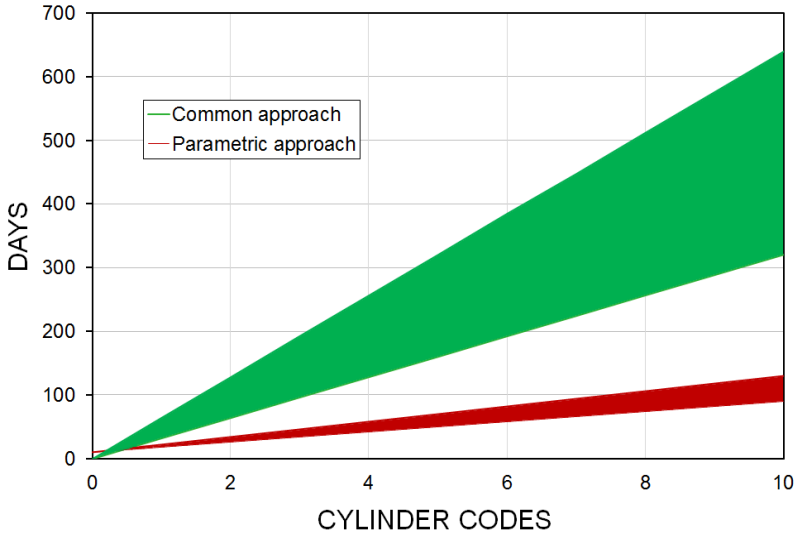

Figure 3.5 - Global times for the CFD steady state simulation of multiple codes

From Figure 3.5, it is possible to observe that the higher is the number of codes that could be simulated with the same *Master Model*, the higher is the reduction of the global simulation times.

Another important advantage connected with the use of a CFD parametric model is the possibility to run more simulations in parallel, with a further reduction of the global times. Nowadays, the possibility to use big clusters for the parallel running of more simulations allows the computational times to be reduced; however, in most cases, this opportunity is not adequately used, because the set-up effort required for the simulations settings is too high.

For this reason, it is clear that a parametric CFD routine could be an extremely useful solution, in order to obtain a reliable database for the global pressure losses estimation in an industrial application.

3.3.2 Reduction of the CFD simulations

Even in case of exploiting the use of a *Master Model*, the number of simulation cases that should be analyzed for each code is still too high. In fact, from each cylinder code it is possible to obtain different cylinders bore, changing the thickness of two components (liner and spacer) that are inserted in the compression chamber during the assembly of the reciprocating compressor.

The utilization of the same machine with different bore diameters, changing the thickness of liner and spacer, allows elaborating different mass flow rate using a single cylinder code.

In Figure 3.6 is shown an example of a double acting cylinder having three valves for every phase and for every effect. In particular, the dark grey component is the external case, while the other two components are the liner (yellow) and the spacer (clear grey). These last two components are inserted in the compression chamber during the compressor assembly. Usually, four different bore diameters are obtained for each code with the described procedure; the effect of the cylinder bore diameter on both the global pressure losses and the global flow coefficient evaluation will be shown in Paragraph 3.8.

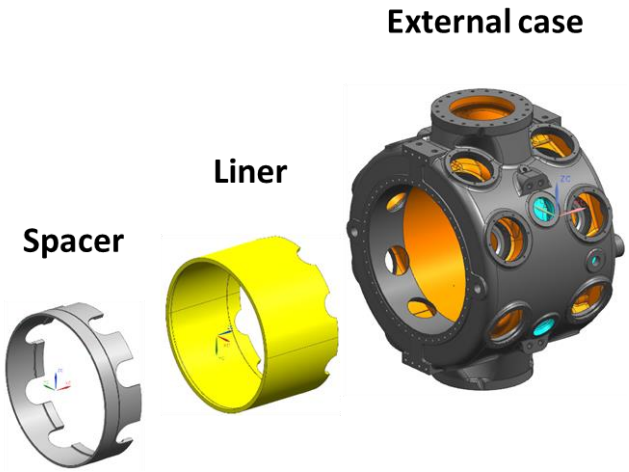

Figure 3.6 - Geometric CAD of external case, liner and spacer for a typical large bore reciprocating compressor

In addition, different valves can be used in a single cylinder. Two types of valves are commonly used; the ring type (D-valve) and the double ring type (M-valve) (Paragraph 1.7).

In the simplified CFD routine defined in this thesis, the actual valve is replaced with a cylindrical porous model according to the procedure proposed by Balduzzi [3], [34] (Paragraph 3.6.1). The valve pressure losses are obtained as a function of the valve flow coefficient and of the valve reference area (known from data sets provided by the valve manufacturers). The use of different valve typologies, involves the variation of both parameters and, consequently, the variation of the valve pressure loss.

Moreover, there is the possibility to use a single code with valves having different diameters. In fact, the number of valves and the valves diameter is strictly dependent by the cylinder bore diameter and, consequently, by the cylinder capacity. Usually the higher is the cylinder capacity, the higher is the number and the diameter of the valves. Nevertheless, the choice of the valve used is guided by two opposing aspects; the valve pressure losses and the cylinder dead volume. The greater is the valve diameter, the lower are the valve pressure losses. On the other hand, the greater is the valve diameter, the higher is the cylinder dead volume. For this reason, there is the possibility to choose different valve diameters with the same bore diameter, depending on the aspect that is chosen to privilege. Moreover, the possibility to use the same code with different bore diameters has an influence also on the choice of the valve diameter. For this reason, there are multiple combinations of bore diameters and valve diameters.

In this thesis, an analytic procedure is defined in order to reduce the number of simulations and, consequently, the calculation times (Paragraph 3.9). This procedure, is based on the "superposition principle", and allows obtaining the overall pressure losses in the suction and discharge gas path, knowing the flow coefficient and the reference area of the valve (given by the valve manufacturers) and the global pressure losses obtained by means of a single CFD simulation for a reference valve.

Another key aspect is the influence of the piston position on the global pressure losses and, consequently, on the flow coefficient evaluation. Using a steady state simulation, a fixed piston position is simulated without taking into account the piston motion. Considering the discharge phase, the pressure losses in the compression chamber are approximately constant during the first phase of the piston stroke. The losses increase when the piston moves close the cylinder head because of the phenomenon known as "piston masking effect". This phenomenon is due to the reduction of the passage area in the compression chamber for the masking of the passage window of the valve pocket, caused by the piston during his motion.

In Figure 3.7, an example of fluid domain for the compression chamber of a reciprocating compressor is shown. In Picture a, the piston is at bottom dead center and the passage window in the valve pocket is fully open. On the other hand, in Picture b, the piston is near to the head and the passage area is reduced for the "piston masking effect".

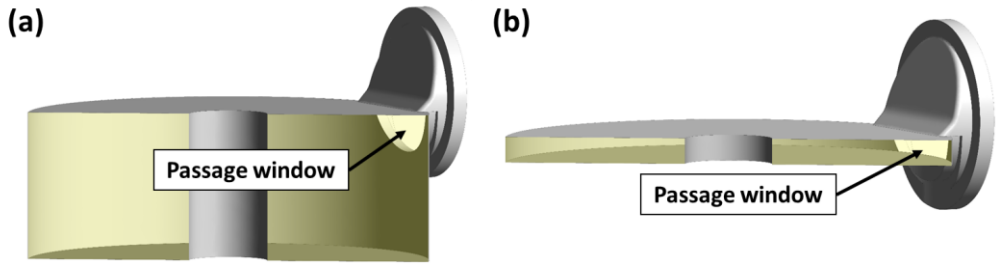

Figure 3.7 – Reduction of the passage window for the "piston masking effect"

Similar considerations can be done for the suction phase; in this case, the piston masking phenomenon happens in the initial part of this phase. Moreover, it is possible to observe that this phenomenon is less important for the suction phase because the suction valve is closed at the beginning of the piston masking.

Nevertheless, this phenomenon is not negligible both for suction and discharge phase, in view of a correct estimation of the global pressure losses in the machine. As it will be shown in Paragraph 5.4, the error in terms of *p-V* cycle estimation neglecting the piston masking effect and using a constant flow coefficient is not negligible during the first part of the suction phase and the last part of the discharge one.

For this reason, more simulations at different piston positions are needed in order to obtain an accurate evaluation of the pressure losses and a correct prediction of the *p-V* cycle by means of low orders models (Paragraph 3.10).

Finally, an accurate analysis is performed to understand the effect of the working fluid and of the operating conditions on the results. The Reynolds number for the large bore reciprocating compressors analyzed in this thesis can change of about three order of magnitude considering the working fluids that are commonly used and the typical operating conditions (two order of magnitude considering the same fluid at different operating conditions). For this reason, it is impossible to realize a reliable database without an accurate evaluation of the error committed when the machine works with different working fluids or in different operating conditions. The effect of the Reynolds number on the flow coefficient estimation is shown in Paragraph 3.11.

3.4 Case study

With reference to the cylinders of Baker Hughes, it is possible to find more than 100 cylinders codes. These cylinders could differ in terms of cylinder bore (the typical cylinder bore are variable between 100 mm and more than 1000 mm), number of valves (from 1 to 5) and cylinder materials (typically nodular cast iron (NCI) or cast steel (CS)). Moreover, it is possible to find codes having both symmetric and asymmetric domains.

The effect of these geometrical features on the global pressure losses evaluation is not negligible and 3D CFD steady state simulations for all these codes are necessary in order to obtain an accurate estimation of the overall pressure losses in the suction and discharge gas path.

In Figure 3.8 and Figure 3.9, an example of the typical fluid domains for a nodular cast iron cylinder (NCI) and for a cast steel (CS) is shown.

With reference to the compression chamber domain (yellow part), it is possible to notice the difference between the valve pocket of the nodular cast iron cylinder and the corresponding part of the cast steel one. Same considerations can be made for the suction and discharge plenum domains (orange part).

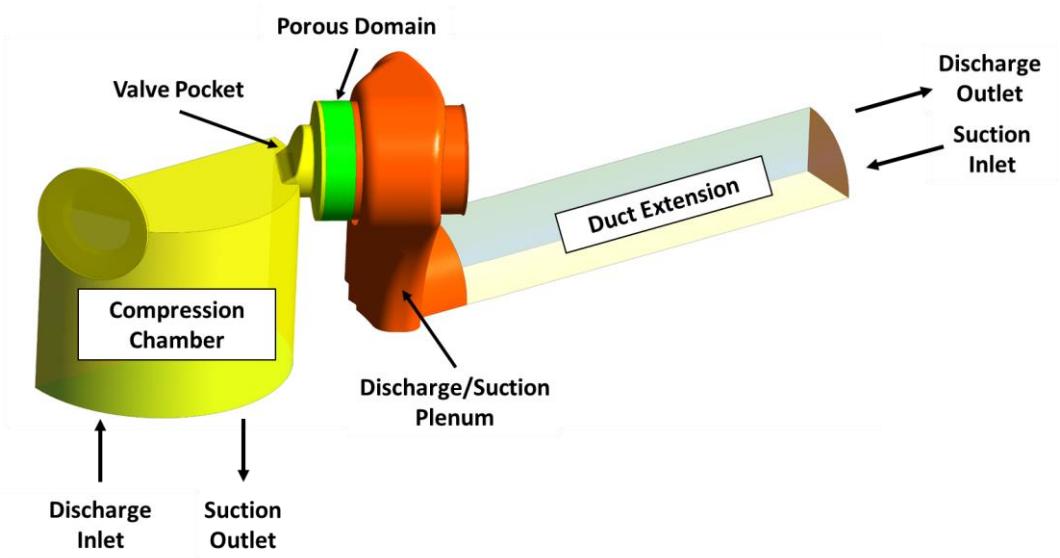

Figure 3.8 – Typical fluid domain for a Cast iron cylinder (NCI)

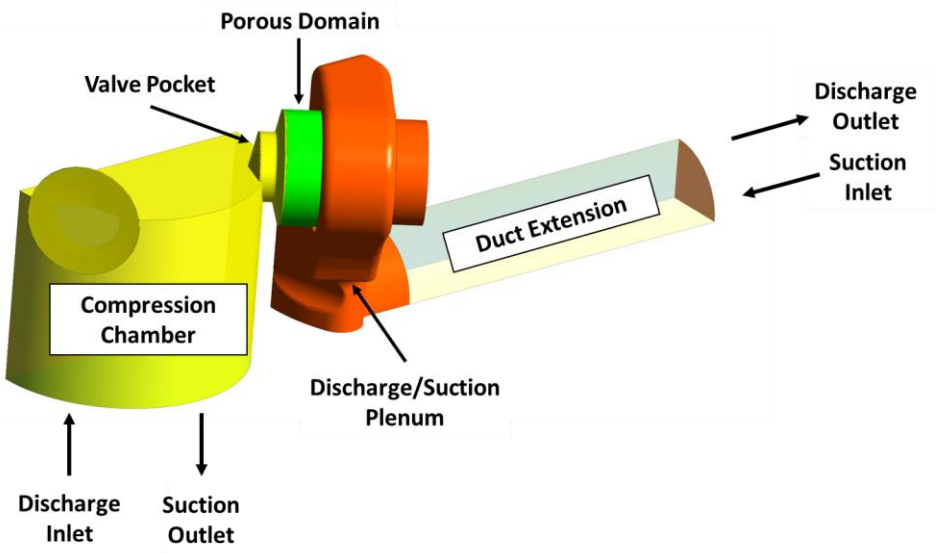

Figure 3.9 – Typical fluid domain for a Cast steel cylinder (CS)

As explained in Paragraph 3.3.1, the cylinder codes could be gathered in a smaller number of cylinder "families", having some common geometrical features (e.g. number of valves or cylinders materials). For each family a *Master model* can be created.

The classification of the overall cylinders codes of the Baker Hughes in cylinder "families" was made jointly with RAM Oil & Gas and was achieved by means of the following considerations;

- the deeper are the geometrical simplifications in the parametric CAD model, the greater is the number of codes that could be simulated with the same *Master model* (and consequently the lower are the set-up times for the realization of the global pressure losses database);
- it is impossible to simplify some geometrical feature, without an unreasonable increase of the error on the pressure losses evaluation.

Starting from these considerations and using the geometries shown in Figure 3.8 and Figure 3.9, in the first part of this work two simplified parametric CAD models were created by means of the software "Siemens NX" (Figure 3.3).

The results of the CFD simulations of these CAD were compared with the corresponding results obtained using detailed geometries. For the simulation of the detailed geometries, the common approach described in Paragraph 3.3.1 was used; the fluid domains of the compression chamber and of the suction and discharge ducts were extracted by solid CAD models given by Baker Hughes.

The objective of these comparisons was a first validation of the proposed routine and an indication of the error due to the simplifications of some geometrical features.

The first *Master model* was released for the NCI cylinder shown in Figure 3.8. This cylinder has two valves for every phase and for every effect (2+2) and a symmetric domain that allows reducing the computational times in a CFD simulation.

As it was revealed in Paragraph 3.3.2 and how it will be explained in Paragraph 3.6.1, the valves are not simulated in the defined routine, but their effect in terms of pressure losses is considered by means of a cylindrical porous model (green part).

The coupling between the valves domain and the compression chamber and ducts domain is obtained by means of interface conditions.

The suction and discharge ducts domain are extended using a duct extension with a length equal to five times the flange diameter. In a discharge duct simulation, this solution allows obtaining a fully developed flow, reducing possible problems in the solution convergence.

The simulated domain is characterized by a single inlet and by a single outlet; passing from a suction phase simulation to a discharge one, the inlet and the outlet are inverted. A no slip condition is imposed to the overall walls of the compression chamber and of the suction and discharge ducts that, at the same time, are considered like adiabatic walls.

Analogous considerations can be done also for the CS cylinder shown in Figure 3.9.

The errors on the evaluation of the overall pressure losses along the suction and discharge gas path and on the estimation of the corresponding global flow coefficients, using a simplified parametric CFD routine, are shown in Paragraph 3.7.

3.5 Definition of the calculation domains

The solution of the governing equations is sensitive to the cells size; however, this aspect has an important effect also on the calculation times. In fact, a fine mesh, characterized by the high elements' density, allows ensuring a good accuracy in the most critical zones for the evaluation of the global pressure drop. On the other hand, a similar mesh causes an increase of the computational times. For this reason, in the mesh definition, it is fundamental to choose the elements size that allows obtaining a compromise between the accuracy of the results and the simulations times. Therefore, a preliminary analysis on the fluid behavior in the machine is fundamental in order to understand the most critical zones (with the highest gradients) in the calculation domain. It is then possible to reduce the elements size (obtaining a finer mesh) in the zones where the higher gradients are expected maintaining a coarser mesh in the other zones. In this context, it is fundamental to avoid a sudden transition between zones having different densities of elements and at the same time to avoid too deformed or asymmetric elements that could cause problems for the solution convergence.

In this work, particular attention was paid to the mesh realization in order to obtain a mesh that allows respecting the aforementioned requirements and modelling the physical phenomena without an unacceptable increase of the calculation times.

The most important problem related to the mesh realization in a parametric CFD routine is due to the needed to model the physical phenomena for different geometries and for different operating conditions without to repeat a detailed mesh sensitivity analysis for each configuration.

For this reason, the mesh definition in the work described in this thesis was divided in two parts. At first, the elements size was chosen by means of the information obtained for different cylinders models in previous works of the REASE GROUP of the Industrial Department of the University of Florence (Paragraph 3.5.1). Then a parametric mesh was defined by expressing the mesh sizing a function of both the geometrical features and the operating conditions (Paragraph 3.5.2).

3.5.1 Mesh settings

For the mesh definition, the information obtained for different cylinders models in previous works of the REASE GROUP of the Industrial Department of the University of Florence were used. For this reason, a detailed mesh sensitivity analysis is not made in this work. Starting from the available information, the internal volume was filled with an unstructured mesh composed by tetrahedral elements. A finer mesh is used for the discretization of the valve pockets domain and of the suction and discharge ducts domain near to the valves. In particular, previous studies had highlighted that at least 100 elements along the bore circumference are needed for an accurate estimation of the fluid-dynamics phenomena in the compression chamber. The same studies allowed understanding that a finer mesh is needed for the valve pockets, for the valves itself (modeled as cylindrical porous domains) and for the ducts domain near to the valves. For a correct estimation of the global pressure losses in these parts of the domain, the circumference of the valves should be discretized with at least 150 elements.

Moreover, particular attention was paid to the definition of a mesh that allows modeling the boundary layer, for the influence of the fluid behavior near to the wall on the estimation of the overall pressure losses.

According with the arguments exposed in Paragraph 2.3 and Paragraph 2.4, in the CFD routine defined in this thesis, the turbulence was modeled by means of RANS approach, resolving the boundary layer using Low Reynolds modeling. This kind of model allows a more accurate estimation of the global pressure drop even if it causes an important increase of the computational times.

This approach requires a mesh near to the wall that allows resolving the laminar sublayer; for this goal, at least 5-6 elements are needed in this region of the boundary layer. The mesh near to the wall was then obtained by means of a certain number of prismatic layers. The height of the first layer was defined in order to obtain an y^+ approximately equal to one while the height of the others layers was increased with the increase of the wall distance.

Figure 3.10 shows an example of the mesh used for the discretization of the domain of the nodular cast iron cylinder described in Paragraph 3.4.

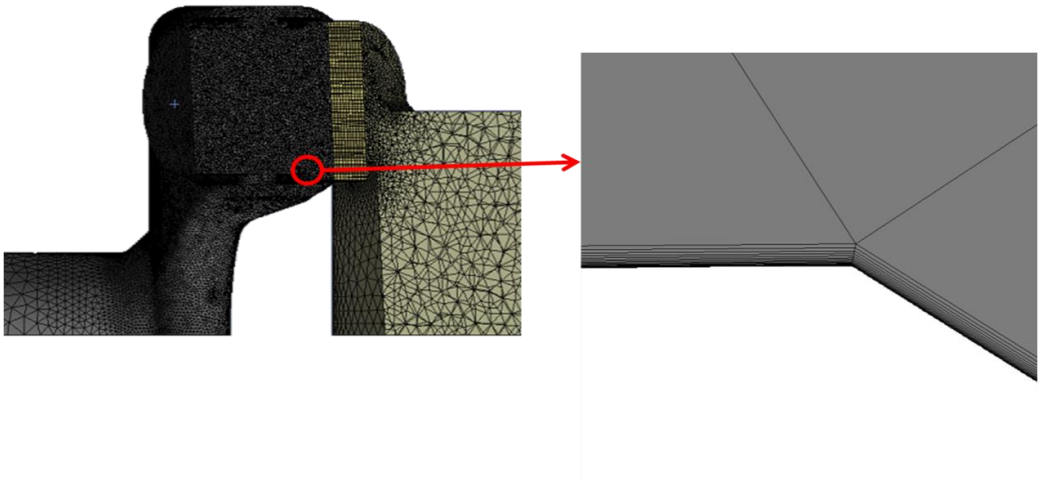

Figure 3.10 - Example of fluid domain discretization

From Figure 3.10, it's possible to observe that the size of the elements for the last prismatic layer is extremely lower than the size of the elements for the first tetrahedral layer.

As explained in Paragraph 3.5, sudden passages between zones having different densities of elements should be avoid because they could cause problems for the solution convergence. However, for the simulation of the overall suction and discharge gas path, it is impossible to respect these requirements. In fact, these kind of machines, usually work with very high velocities and pressures and for this reason it is needed a very low height of the first layer near to the wall in order to obtain an y^+ approximately equal to one.

The need to improve the stability of the simulations caused an increase of the number of layers used for the boundary layer resolution. In fact, for an accurate modelling of the boundary layer, 16-20 layers with a growth rate of 1.1-1.2 are sufficient, once that the first layer height is chosen in order to obtain an y^+ approximately equal to one.

Nevertheless, the analyses made for different cylinders codes with the goal to test the reliability of the mesh, showed possible problems on the stability of the simulation caused by the too high difference between the element sizes of the last prismatic layer and of the first tetrahedral layer (in particular for machines having the highest velocities).

For this reason, for the boundary layer resolution in the parametric CFD routine, 30 layers were used; this solution causes an increase of the number of elements of about 30%

(with a consequent increase of the calculation times). However, it represents the best compromise in order to guarantee the accuracy of the results (maintaining an y^+ approximately equal to one) and the stability of the simulations.

In Figure 3.11 and Figure 3.12 are shown the distributions of the velocity vectors in the regions near to the valves for the discharge domain and for the suction one.

These pictures confirm that the discretization of the fluid domain near to the wall by means of 30 layers of prismatic elements allows an accurate resolution of the boundary layer.

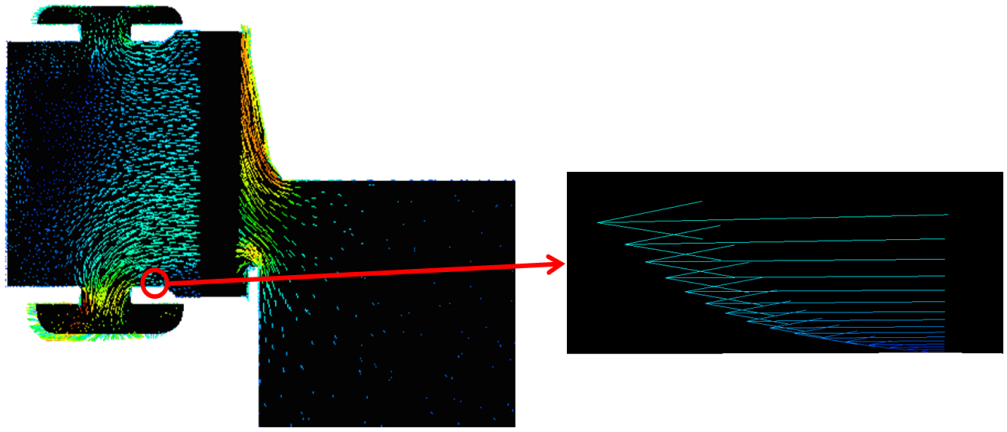

Figure 3.11 – Distribution of the velocity vectors in the discharge duct near to the valves

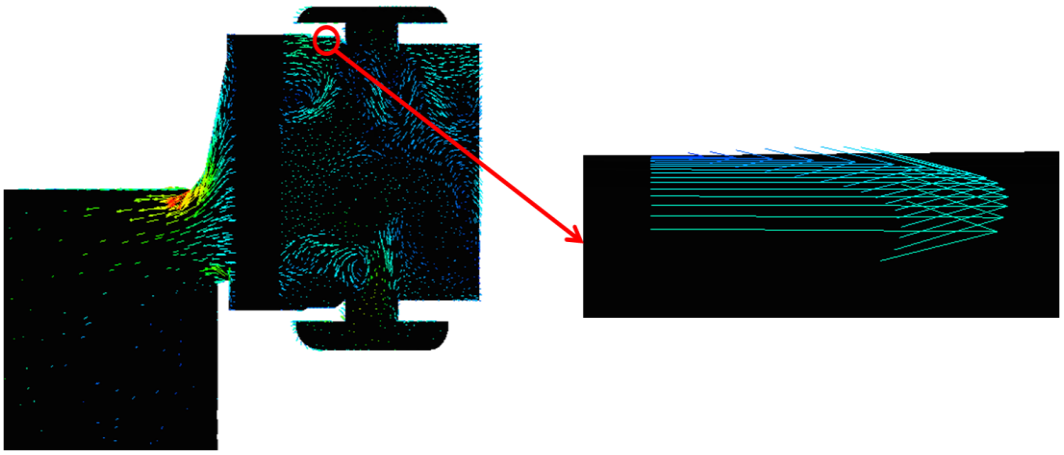

Figure 3.12 – Distribution of the velocity vectors in the suction duct near to the valves

3.5.2 Parametric sizing

Once that the mesh settings was defined, parametric relations have to be realized in order to obtain a mesh that allows maintaining the requirements described in Paragraph 3.5.1, when the geometries and the operating conditions change.

For the realization of fully automated mesh, the fluid domain was divided in named selections directly defined by means the software "Siemens NX".

The mesh was then realized using the software "Ansys meshing" obtaining a stable and fully automated mesh (Figure 3.13).

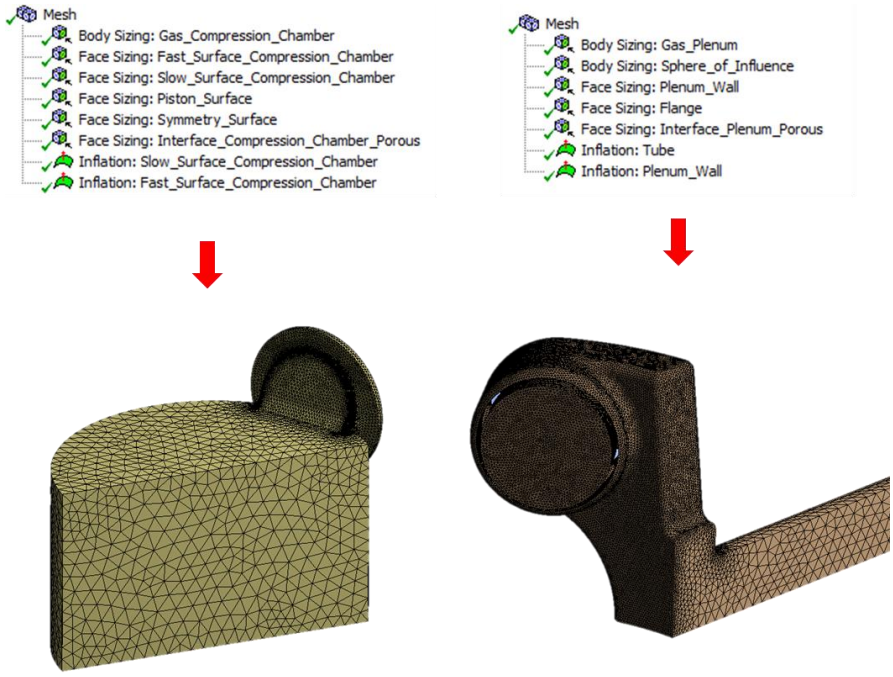

Figure 3.13 – Mesh structure in "Ansys Meshing"

The global body sizing used for the discretization of the compression chamber and of the suction and discharge ducts domains was obtained as a function of the cylinder bore. In fact, as exposed in Paragraph 3.5.1, at least 100 elements along the bore circumference are needed for an accurate estimation of the fluid-dynamics phenomena in the compression chamber. For this reason, the global body sizing was expressed as:

$$Global\ body\ sizing = \frac{\pi B}{100}$$

where B is the bore diameter.

At the same time, the finer mesh in the valve pockets, and in the ducts domain near to the valves, was obtained using a sphere of influence with a sphere diameter equal to the valve diameter and with elements sizing expressed as:

$$Sphere\ of\ influence\ element\ sizing = \frac{\pi D_v}{150}$$

where D_v is the valve diameter.

The porous domain used for the valve's modelling was discretized using the same element size of the sphere of influence (more details are given in Paragraph 3.6.1).

In this manner, the CFD parametric routine allows maintaining the mesh requirements showed in Paragraph 3.5.1, when the bore and the valve diameter change.

A schematic representation of the solution used for the parametric definition of the global body sizing and of the sphere of influence element sizing is shown in Figure 3.14

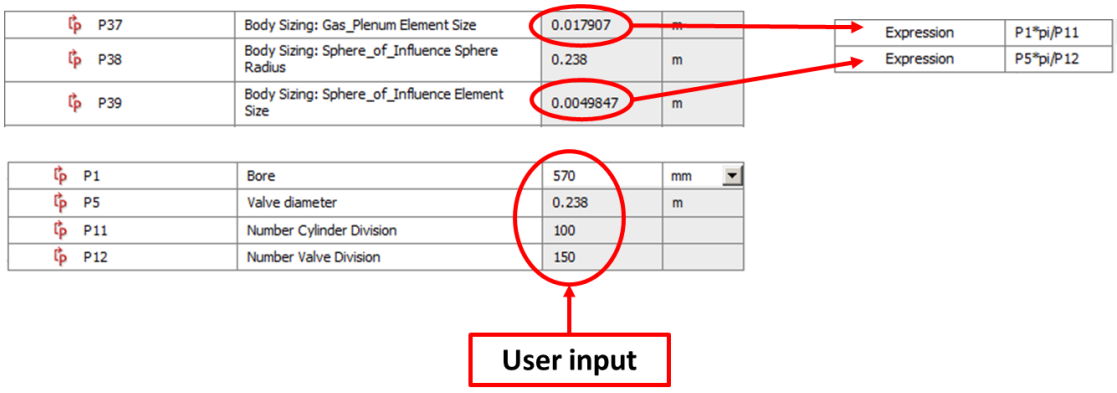

Figure 3.14 – Schematic representation of the parametric sizing

Another important aspect that occurs to take into account is the variation of the piston position in order to consider the phenomenon known as "piston masking effect". In fact, more simulations at different piston positions are needed in order to obtain an accurate evaluation of the global pressure losses and a consequently correct prediction of the *p-V* cycle by means of low orders models (Paragraph 3.3 and Paragraph 3.10).

Some difficulties could occur when the piston is positioned near to the head for the simulation of the small volume of the compression chamber between the piston and the compressor head. In fact, an accurate resolution of the fluid-dynamics phenomena in a so small volume is not guaranteed, without a significant increase of the density of the elements in this part of the domain.

On the other hand, a too small elements sizing could cause an unreasonable increase of the number of elements when the piston is positioned far from the head.

Starting from these considerations, the head and the lateral surface of the compression chamber were meshed using a parametric face sizing expressed as a function of the piston position, using the following relation:

$$Face\ sizing = \left((x - H_c) \frac{(SI_{ES} - B_s)}{-H_c} \right) + B_s$$

where:

- x is the simulated piston position, equal to the distance between the piston and the top dead center;
- H_c is the cylinder height, equal to the sum between the piston stroke and the clearance between the piston and the head at the top dead center (TDC);
- SI_{ES} is the sphere of influence element sizing;
- B_S is the body sizing.

Using this relation, the face elements sizing for these surfaces is equal to the global body sizing at the bottom dead center (BDC), to the valve pocket sizing at the top dead center (TDC) and reduces linearly when the piston moves from the BDC to the TDC.

This solution allows obtaining a finer mesh when the piston is near to the head of the compressor, with a more accurate evaluation of the physical phenomena in the reduced compression chamber domain. Moreover, the relation defined, allows maintaining the number of elements in the compression chamber domain almost constant with the piston position variation; in fact the smaller is the compression chamber domain, the higher is the density of elements used for the compression chamber discretization.

The choice to model the turbulence by means of RANS approach and resolving the boundary layer using Low Reynolds modeling, requires the use of parametric relation also for the definition of the first layer height in order to obtain an y^+ approximately equal to one when the operating conditions change.

In fact, as shown in Paragraph 2.4 the wall unit is defined as;

$$y^+ \equiv \frac{yu^*}{\nu}$$

and depends by the operating conditions of the machine.

For this reason, the first layer height (y) has to be expressed as a function of the operating conditions, once that the desired Wall Unit is chosen.

Starting from the y^+ definition, it is possible to obtain the first layer height (y) as:

$$y = \frac{y^+ \nu}{u^*}$$

where:

$$u^* \equiv \sqrt{\frac{\tau_w}{\rho}}$$

and:

$$\tau_w \equiv \mu \left.\frac{\partial u}{\partial y}\right|_{y=0}$$

However, it is possible to express the Wall shear stress τ_w also as [36]:

$$\tau_w = \frac{1}{2} C_f \rho U_{freestream}^2$$

where $U_{freestream}$ is the estimated velocity of the free-stream flow, while C_f is the Skin-friction that could be written as a function of the Reynolds number, using the following correlation [36]:

$$C_f = [2log_{10}(Re_x) - 0.65]^{-2.3}$$

valid for $Re_x < 10^9$. The Reynolds number could be expressed as:

$$Re_x = \frac{\rho U_{freestream} L_{boundary\ layer}}{\mu}$$

where $L_{boundary\ layer}$ is the characteristic length.

Using these correlations, it is possible to calculate the first layer height as a function of the geometrical features, of the working fluid and of the operating conditions.

In fact, chosen the working fluid and fixed the desired value of the Wall unit (usually 1), once that the $U_{freestream}$ and the $L_{boundary\ layer}$ are estimated, it is possible to calculate the Reynolds number and, consequently, the first layer height that allows the desired Wall unit to be obtained.

The only problem for a similar approach is due to estimation of the $U_{freestream}$ and of the $L_{boundary\ layer}$ in a machine like a reciprocating compressor, having extremely variable geometries and extremely different velocities. However, there is the possibility to use the indications obtained by the simulations of the cylinders shown in Paragraph 3.4, in order to have a quite good estimation of these variables for the others simulated machines.

Using this approach for the choice of the first layer height and modelling the boundary layer by means of 30 layers and of a growth rate of 1.2, it is possible to obtain an accurate discretization of the fluid domain near to the wall, also when the geometrical features and the operating conditions change.

The parametric relation defined in this paragraph are used for different codes with the goal to test the elements quality.

In particular, the *Skewness* was used as mesh quality indicator in the analyzed test cases. The *Aspect ratio* was not considered because all the prismatic elements for the boundary layer discretization have an extrusion height that is four orders of magnitude lower than the base size (i.e. *Aspect ratios* above 10^4), due to the necessity of guaranteeing y^+ approximately equal to one. For this test, it is important to remember that the desired *Skewness* should be lower than 0.5 and few elements having *Skewness* between 0.5 and 0.9 are tolerated. On the contrary, elements having a *Skewness* higher than 0.9 are unaccepted. Starting from these considerations, the element quality robustness is verified for some different cylinders of the NCI and CS "families" of Paragraph 3.4 with the objective to check the skewness variation, modifying the CAD dimensions.

The results confirm the robustness of the mesh obtained with the defined procedure. In fact, the average *Skewness* usually remains lower than 0.2 while roughly the 2-3% of elements have a *Skewness* between 0.5 and 0.9. The maximum value of the *Skewness* does not go above 0.9.

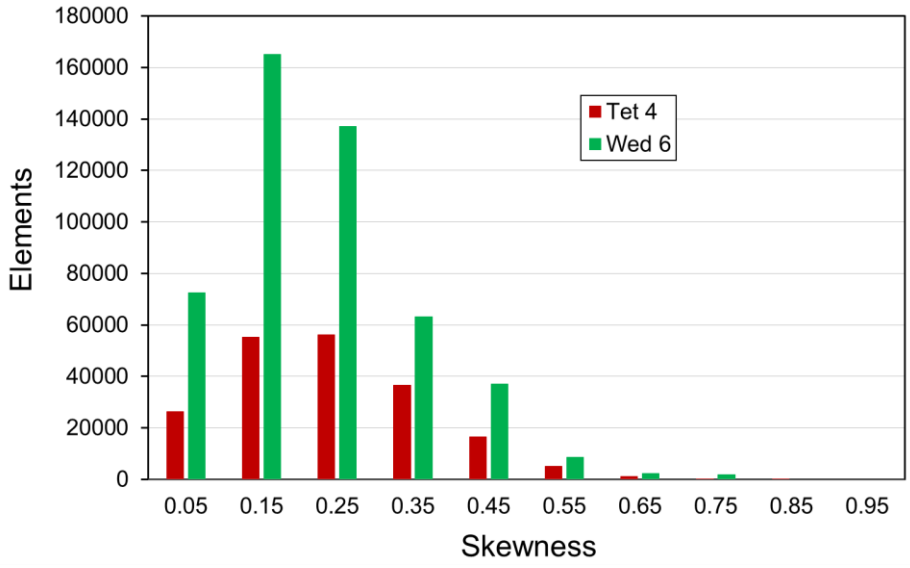

Figure 3.15 – Elements quality: Skewness for the mesh of the compression chamber of a NCI cylinder

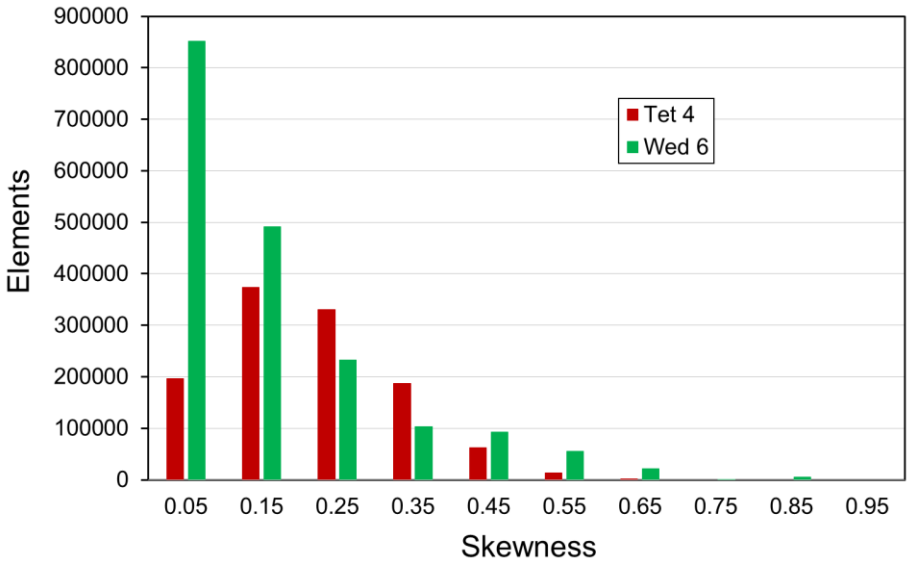

Figure 3.16 - Elements quality: Skewness for the mesh of the plenum of a NCI cylinder

An example of the *Skewness* obtained for the mesh of the compression chamber domain and of the plenum domain, for the NCI reciprocating compressor of Figure 3.8 is shown in Figure 3.15 and Figure 3.16.

3.6 Numerical settings

This section deals with the details of the simulation setup. The numerical approach employed a 3D steady state Reynolds Averaged Navier-Stokes (RANS), performed with the ANSYS CFX software package.

The *k-ω* model was adopted for modeling the turbulence while Low Reynolds modeling are used for the treatment of the boundary layer in the near-wall regions.

The choice to use the *k-ω* model is due to the indications obtained by previous works of the REASE GROUP of the Industrial Department of the University of Florence. In fact, this model showed better performance in terms of stability and reliability, quicker convergence to the final steady-state and the best agreement with experimental data. It was therefore chosen as the base scheme for the parametric CFD routine.

High resolution schemes were employed for both turbulence and convection schemes while the symmetry condition was used for all the simulated symmetric geometries in order to simplify the domain and to reduce the computational times.

The analysis of the evolution of residuals and of some variables (i.e. the total pressure losses and the mass flow rate) has shown that it is possible to obtain stable results after 1000 iterations; for this reason, a convergence control of maximum 1000 iterations was imposed.

The user inputs are the gas properties and the *RPM* while the boundary conditions are the static pressure at cylinder flange and the instantaneous velocity of the piston (calculated starting from the *RPM* and from the piston position) at the piston surface. Passing from a suction simulation to a discharge one the inlet and the outlet conditions are inverted: the static pressure at flange is then an inlet condition for a suction duct simulation and an outlet condition for a discharge duct one. At the same time, the piston velocity is an outlet condition for a suction duct simulation and an inlet condition for a discharge duct one.

The total temperature is always given as an inlet condition at the inlet surface (flange surface for a suction duct simulation and piston surface for a discharge duct simulation).

3.6.1 Valves modeling

As explained in Paragraph 3.3, in this work, the valves were modeled as cylindrical porous media. In fact, the simulation of an actual valve requires too high computational and set-up times; the modeling approach proposed by Balduzzi [3] and used in this thesis allows an important reduction of the global times considering the valves as localized pressure drops.

This very simple modeling can be implemented by using a cylindrical porous volume to replace the actual geometry of the valve. The CFD domain is therefore split into three different regions; the two zones, upstream and downstream the valve, were modeled as simple fluid regions (analogous to the simulation with the valve) and are in communication with a new central zone. The shape of this zone is a simple cylinder and the equations of the porous model are then applied only to this volume (Paragraph 2.5). The diameter of the cylinder is equal to the valve diameter while the length was imposed to be equal to the valve length.

Two interfaces were defined for the exchange of information with the inlet and outlet sections and the connection between the meshes was handled by adopting the General Grid Interface (GGI) method. In fact, the meshes of the two sides of the interfaces were not matching, since the grid generation was performed separately. The discretization of the fluid volume was obtained by means of tetrahedral elements (Figure 3.10), while the porous volume was discretized by means of an extrusion of triangular elements in the axial direction thus generating uniform layers of orthogonal prismatic cells.

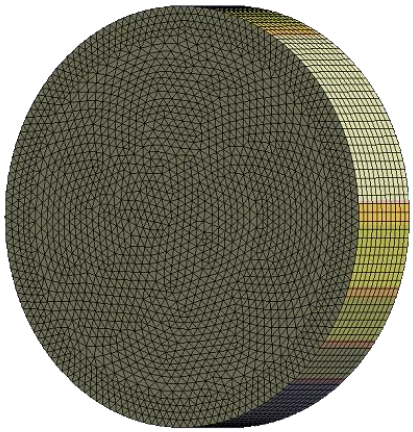

Figure 3.17 – Example of the mesh used for the discretization of a cylindrical porous medium

An example of the mesh used for the discretization of a cylindrical porous medium is shown in Figure 3.17.

The porous media element sizes was expressed as a function of the valves diameter, using the same relation defined for the sphere of influence elements size (Paragraph 3.5.2).

For the boundary layer treatment in the porous region, a free slip condition was imposed at the cylindrical wall, since all the fluid-dynamic losses are generated by the dissipation of the porous media.

As already explained in Paragraph 2.5, the porous model introduces a sink term in the Navier-Stokes equations for the momentum, representing a pressure drop per unit length. To adequately model a local pressure drop by means of a porous zone, calculated by means of the Darcy-Forchheimer (Paragraph 2.5), it is then sufficient to eliminate the permeability (Darcy) term and use the inertial loss term alone, which is proportional to the squared velocity, resulting in the following simplified form [3]:

$$\Delta p_i = \left(\frac{1}{2}\rho|v|F_{ij}v_i\right)\Delta x_i$$

Considering only the streamwise direction, along the valve axis (*x* axis), the pressure loss can be further simplified as:

$$\Delta p_i = \left(\frac{1}{2}\rho F v_x^2\right)L_v$$

where L_v is the valve length and v_x is the flow velocity inside the porous media, calculated by:

$$v_x = \frac{m}{\rho A_{por}}$$

where A_{por} is the transversal section of the porous cylinder

The resistance loss coefficient can be expressed as [3]:

$$F = \frac{1}{L_v {Ks_v}^2}\left(\frac{v_{lift}}{v_{por}}\right)^2 = \frac{1}{L_v {Ks_v}^2}\left(\frac{A_{por}}{A_{lift} * LIFT}\right)^2$$

where Ks_v is the valve flow coefficient, v_{por} is the fluid velocity in the porous medium (equal to v_x when only the velocity of the streamlines along the valve axis is considered) and $A_{lift}*LIFT$ is the passage area at the valve lift.

The definition of the resistance loss coefficient allows calculating the valve pressure losses as localized pressure drop.

The user input for the valve simulation are then the valve flow coefficient and the valve passage area at the valve lift. Knowing these parameters and the valve geometrical features (valve diameter and valve length), it is possible to calculate the resistance loss coefficient and consequently the valve pressure losses.

The loss in the transverse directions (radial and circumferential directions, in cylindrical coordinates) was simply specified by the introduction of a multiplier of the streamwise coefficient (C_{tr}). The assumption made was to force the flow to follow the axial direction without giving it any other degree of freedom, such as the possibility of turning inside the porous media; by doing so, the capabilities in controlling the losses are higher and there is no need to introduce any additional variable. Moreover, this condition is close to the real phenomenon since the valve channels act as a flow-straightening component, damping out, or even suppressing, all the vortex structures of the incoming flow. The purpose was then to obtain an anisotropic porous media with an "infinite" resistance in the transverse directions.

The value of C_{tr} is taken equal to 100, according with the results shown by Balduzzi [3]. In fact, this choice, allows obtaining a total pressure drop independent by C_{tr} itself (impossible to achieve using lower values of this parameter) with convergence times of residuals lower than the corresponding times for higher values of C_{tr}.

3.7 Validation of the parametric CFD routine

In order to validate the simplified procedure developed in this thesis, two *Master models* were created for the NCI and CS cylinders described in Paragraph 3.4.

At the same time, the fluid domains were extracted by the solid CAD models, meshed and simulated using the common strategy to realize a steady state CFD simulation (Paragraph 3.3.1).

The goal was the evaluation of the errors on the estimation of the overall pressure losses along the suction and discharge gas path and of the corresponding global flow coefficients, using parametric *Master models*. For this reason, the results obtained by means of the common approach and the parametric one were compared.

In order to understand the simplifications adopted in a typical *Master model*, an example of plenum domain of a NCI cylinder obtained by means of the fluid extraction approach (Picture a) or directly creating the parametric domain (Picture b) is shown in Figure 3.18.

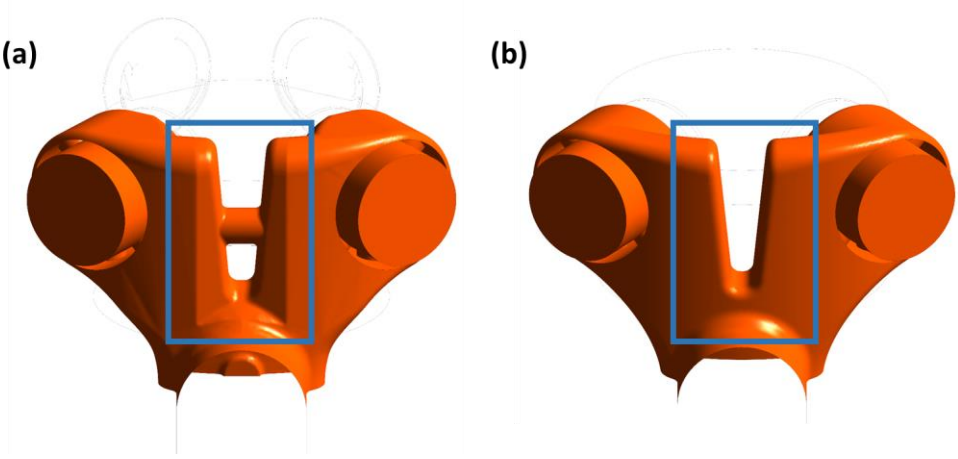

Figure 3.18 – Comparison between the plenum domain using the fluid extraction (Picture a) or the simplified parametric approach (Picture b)

The clearest difference in Figure 3.18 is the suppression of the duct between the two parts of the plenum domain in the parametric geometry. In fact, this kind of connection is used only for some codes and is not so influent on the reciprocating compressor performance because only a small percentage of fluid flows in this tube. Similarly, the cut visible in this zone in the detailed geometry was removed in order to simplify the *Master model*.

Particular attention was paid for the fillet radius creation; in fact, the fillet radius are often a critical part when the CAD parameters dimensions are changed and could cause a strong reduction on the stability of the *Master model*. On the other hand, some fillet radius could have a strong influence on the global pressure losses. For this reason, the choice of the fillet radius size is not a simple aspect; using the same size of the solid CAD model there is the possibility to obtain a not stable *Master model*. At the same time, too big change could cause a too high reduction of the accuracy of the results.

Starting from these considerations, the size of the biggest fillet radius were reduced while the fillet radius in not critical zones were eliminated.

The analogous comparison for the compression chamber domain is shown in Figure 3.19. In this case, it is chosen to avoid simplifications, for the strong influence of the valve pocket domain on the performance of the machine. In fact, small variations in the valve pocket geometrical features can have a strong influence on the global pressure losses evaluation.

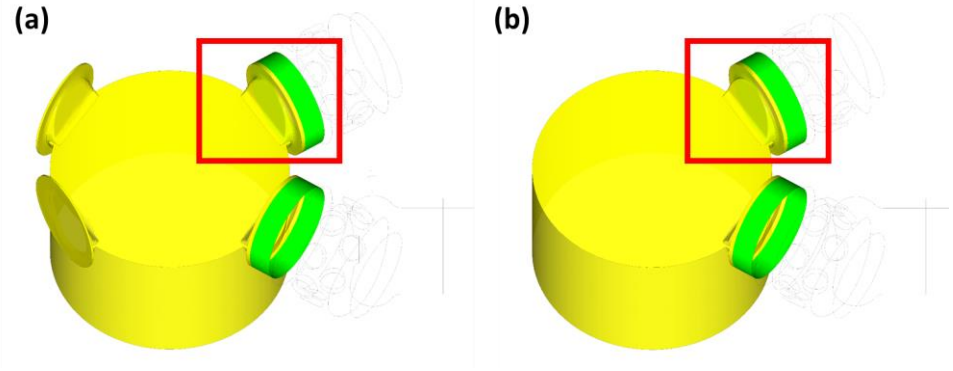

Figure 3.19 - Comparison between the compression chamber domain using the fluid extraction (Picture a) or the simplified parametric approach (Picture b)

The simplifications described allows reducing the computational times and increasing the stability of the *Master models*. Moreover, it is important to highlight that the biggest advantage of the defined parametric CFD routine is the set-up times reduction. As shown in Figure 3.5, this advantage is due to the possibility to simulate multiple cylinder codes using a single *Master model*. This is possible only simplifying the simulated cylinder domain and proving that the error committed is negligible; in fact, the lower are the simplifications of the geometrical features, the lower is the number of cylinder codes that could be simulated with the same parametric CAD model and, consequently, the lower is the set-up times reduction.

The comparison between the results obtained using the common approach and the simplified parametric one for the NCI cylinder of Figure 3.18 and Figure 3.19 are shown in Table 3.1, with reference to the crank end side and to the head end side effect of the suction and discharge phase.

	$\Delta p_{0,\,tot}$	$Ks_{,\,tot}$
SUCTION CRANK END	1.42%	-0.66%
SUCTION HEAD END	0.29%	-0.35%
DISCHARGE CRANK END	2.59%	-0.99%
DISCHARGE HEAD END	-3.87%	1.51%

Table 3.1 – Error in the global pressure losses and in the global flow coefficient evaluation using the simplified parametric approach instead of the common one for a NCI cylinder

From this table, it is possible to observe that the calculated error is negligible both for the overall pressure losses along the suction and discharge gas path and for the global flow coefficients. These errors confirm the potential of the proposed approach in order to obtain accurate results, reducing the global computational times. Moreover, it is important to remember the main objective of this parametric CFD routine; the estimation of the overall pressure losses and the calculation of the global flow coefficients to use in low order models in order to increase the performance predictability. Therefore, it is possible to highlight that an error of ± 2 % on the calculation of the global flow coefficients for both suction and discharge phase causes a maximum error of about ± 0.65 % on the estimation of the absorbed power by means of the 1D model described in Chapter 5.

Similar results were obtained for the cast steel cylinder showed in Figure 3.9. In this case, only the crank end side and the head end side effect of the suction phase were simulated (Table 3.2).

	$\Delta p_{0,\,tot}$	$Ks_{,\,tot}$
SUCTION CRANK END	1.58%	-1.88%
SUCTION HEAD END	-0.85%	1.08%

Table 3.2 - Error in the global pressure losses and in the global flow coefficient evaluation using the simplified parametric approach instead of the common one for a CS cylinder

In order to understand the effect of the simplifications of the geometrical features in the flow field, a surface of revolution was realized in the plenum domain for both NCI

and CS cylinders. The comparison between the velocity distribution in this surface for the suction phase of the NCI cylinder is shown in Figure 3.20.

In this this thesis, all velocity are reported in dimensionless form, normalized by the maximum in-cylinder value $\left(u^* = \frac{u}{u_{max}}\right)$.

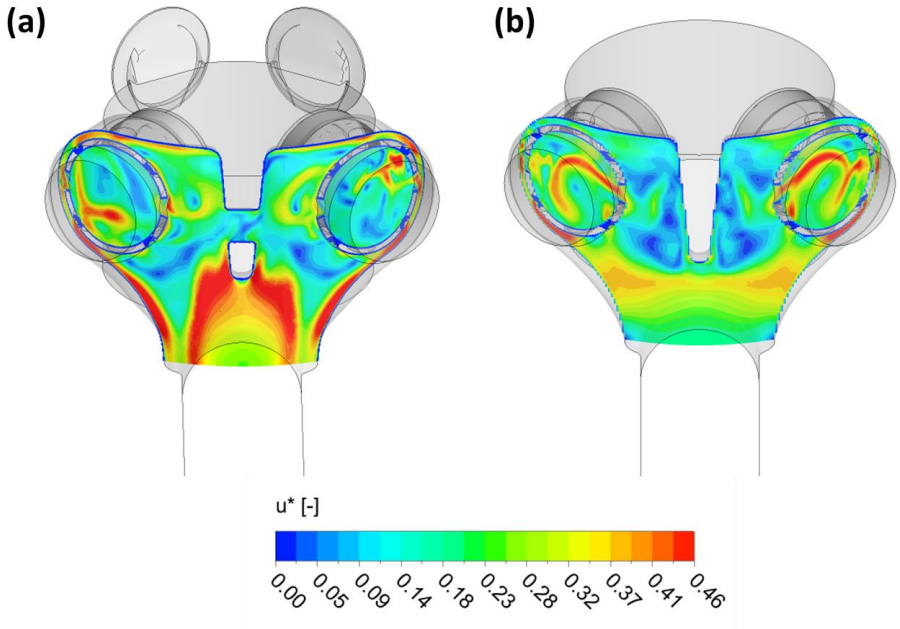

Figure 3.20 - Comparison between the velocity distribution in the plenum domain of a NCI cylinder using the common (Picture a) or the parametric approach (Picture b)

The results highlight the effect of the geometric simplifications of the plenum domain in the flow behavior. In particular, it is possible to observe how the simplifications realized for the parametric CAD model in the central part of the plenum have an effect on the flow field. The high accelerations shown in the central zone near to the flange in the extracted geometry are not visible in the parametric one. Moreover, also the lateral accelerations are avoided; in this case, the difference is probably due to the different fillet radius between the original and the parametric geometry. Globally, the flow in the parametric model seems to be more uniform. However, as highlighted by the results in Table 3.1, these differences have a reduced impact on the global performance evaluation.

Similarly, a cut plane was realized in the compression chamber domain; the comparison between the velocity distribution in this plane for the suction phase of the NCI cylinder is shown in Figure 3.21.

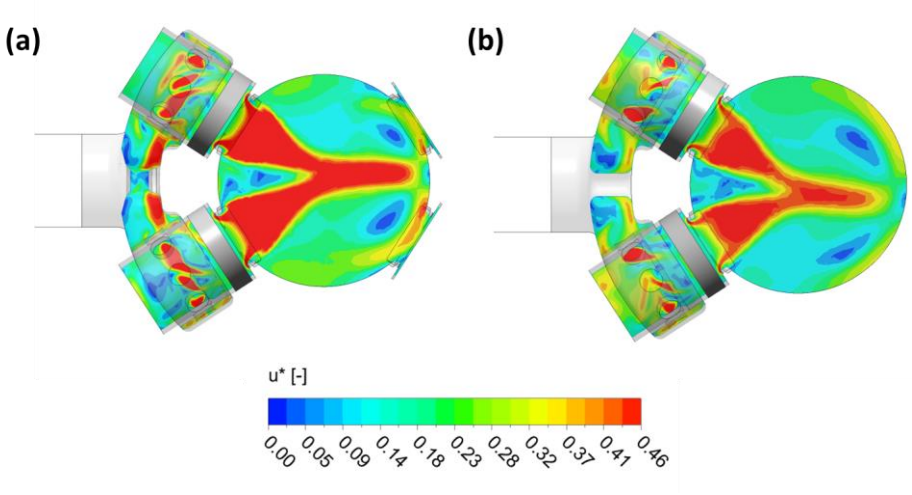

Figure 3.21 - Comparison between the velocity distribution in the compression chamber domain of a NCI cylinder using the common (Picture a) or the parametric approach (Picture b)

In this case, it is possible to notice that the flow behavior is similar between the parametric domain and the extracted one. In fact, as explained in the first part of this paragraph, it was chosen to avoid simplifications in the valve pocket domain for its strong influence on the performance of the machine.

The velocity distribution in the plenum domain and in the compression chamber one for the suction phase of the CS cylinder are shown in Figure 3.22 and Figure 3.23.

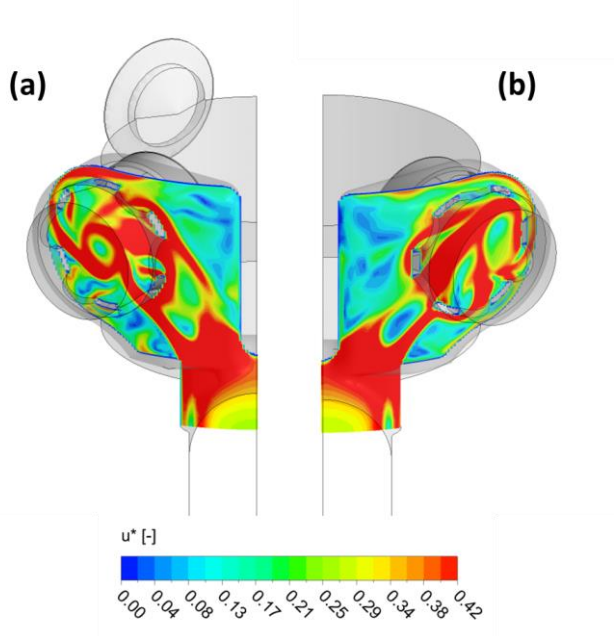

Figure 3.22 - Comparison between the velocity distribution in the plenum domain of a CS cylinder using the common (Picture a) or the parametric approach (Picture b)

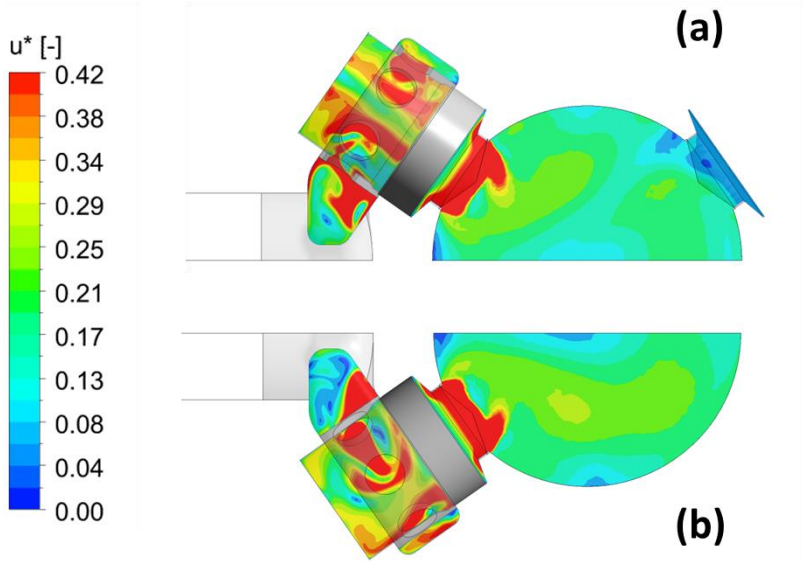

Figure 3.23 - Comparison between the velocity distribution in the compression chamber domain of a CS cylinder using the common (Picture a) or the parametric approach (Picture b)

For this cylinder, it is possible to notice the similarity between the flow field obtained in the plenum domain with the common approach (Picture a) and with the parametric one (Picture b). In fact, the differences between the two geometries are less important respect to the NCI cylinder; in particular, the original detailed geometry doesn't have both the connection duct between the two parts of the plenum and the cut plane in this zone of the domain. Without these important differences between the extracted geometry and the parametric one, the fluid behavior in the suction domain doesn't show the big differences highlight for the NCI cylinder.

With reference to the compression chamber domain, the considerations done for the NCI cylinder can be repeated.

The results achieved both for the NCI and CS cylinders, confirm the potential of the proposed approach showing that the errors introduced by the simplifications in the parametric *Master models* are compatible with the established target.

However, it is now important to highlight that these *Master models* have to be used for different cylinders codes, simply changing the dimensions of the parameters. In fact, a same *Master model* should be used for more cylinders codes of the same cylinder "family" (Paragraph 3.3.1).

These codes have typically similar geometries (e.g. the same number of valves) but can differ for some geometrical features that could have an influence on the global performance evaluation.

For this reason, the second step of the validation described in this paragraph was the comparison between the results obtained with the parametric approach (changing the parameter sizes) and the corresponding results achieved using the common approach.

In more detail, two others geometries were considered; one nodular cast iron cylinder having two valves for every phase and for every effect (belonging to the same "family" of cylinder of Figure 3.8) and one cast steel cylinder (belonging to the same "family" of cylinder of Figure 3.9). These cylinders were initially simulated changing the parameter in the corresponding *Master models*. At the same time, the fluid domains of these new codes were extracted by the solid CAD models and simulated using the common approach. The results obtained were compared: the errors are shown in Table 3.3, with reference to the simulations of the crank end side and of the head end side effect of the suction phase.

	$\Delta p_{0,\,tot}$	$Ks_{,\,tot}$
SUCTION CRANK END NCI	1.27%	-0.76%
SUCTION HEAD END NCI	2.13%	-1.24%
SUCTION CRANK END CS	3.47%	-1.90%
SUCTION HEAD END CS	2.88%	-1.30%

Table 3.3 - Error in the global pressure losses and in the global flow coefficient evaluation using the simplified parametric approach instead of the common one for cylinders belonging to the "families" 2+2 NCI and 2+2 CS

The errors are similar to the corresponding shown in Table 3.1 and Table 3.2, thus obtaining a further demonstration of the validity of the proposed approach. The considerations made for the velocity distributions in the suction plenum domain can be repeated also for these geometries. In fact, the differences between the fluid behaviors highlighted for the NCI cylinder are confirmed; at the same time, it is confirmed the reduced effect of these differences on the global performance evaluation. Analogously, the similar flow behavior between the parametric domain and the detailed one for the compression chamber domain is verified also for the new geometries simulated, confirming the accuracy achieved on the simulation of the valve pockets by means of the simplified parametric CAD models.

3.8 Effect of the bore diameter on the results

In the previous paragraphs, it was described and validated the procedure used for the realization of *Master models* that allows a substantial reduction of the global computational times for the global pressure losses evaluation, in particular for the reduction of the set-up effort required for the realization of these models.

However, the global times required for the creation of a reliable database in a common industrial application by means of CFD are still too high. In fact, there are a large number of variables that have an influence on the global pressure losses evaluation and, consequently, a large number of simulations that are needed for the realization of a reliable database.

For this reason, it is important to carry out an accurate study on the effects of these variables on the results in order to reduce the number of simulations that should be made for the realization of the database.

Starting from these considerations, the first aspect that occurs to consider is the dependence of the flow coefficient from the bore diameter. In fact, as explained in Paragraph 3.3, from each code, are usually extracted four different bore diameters, changing the thickness of liner and spacer (Figure 3.6).

The flow coefficient as a function of the bore diameter is shown in Figure 3.24 and Figure 3.25, respectively for the crank end side and for the head end side effect of the suction phase of the NCI cylinder of Figure 3.8.

In these figures, the flow coefficients and the bore diameters are normalized by means of the following relations;

$$Ks^* = \frac{Ks}{Ks_{max}}$$

$$Bore^* = \frac{Bore}{Bore_{max}}$$

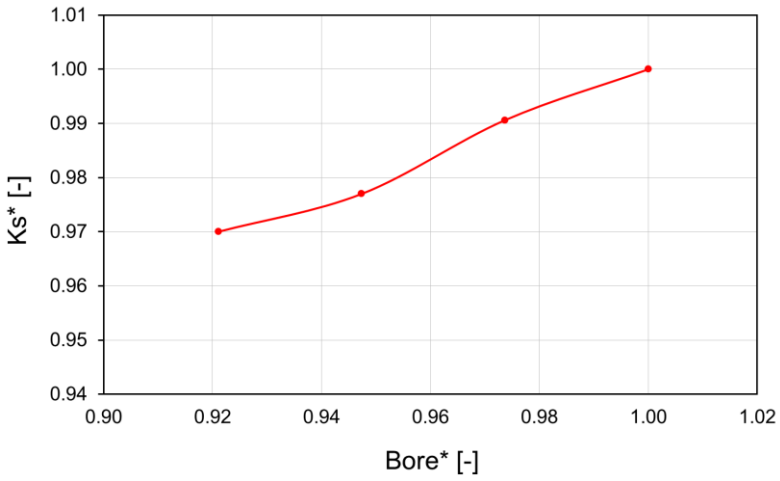

Figure 3.24 – *Ks as a function of *Bore**: suction crank end of a NCI cylinder**

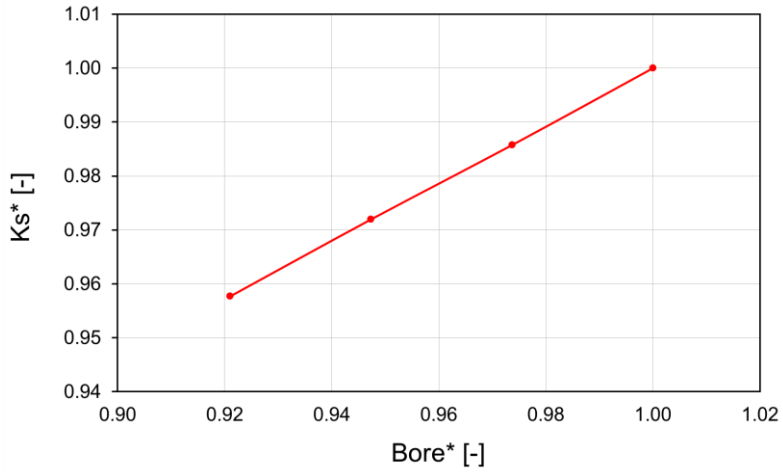

Figure 3.25 - *Ks as a function of *Bore**: suction head end of a NCI cylinder**

From these figures, it is possible to observe that the higher is the bore diameter of the machine, the higher is the calculated flow coefficient (and consequently the global fluid-dynamic efficiency). This is due to an increase of the pressure losses in the valve pocket when the bore diameter is reduced. In fact, the reduction of the bore diameter, is obtained by means of an increase of the thickness of the liner and spacer (Paragraph 3.3). This greater thickness causes an increase of the thickness of the valve pocket (Figure 3.26), and a less efficient behavior of the flow in this part of the machine. For this reason, the highest pressure losses (and lowest flow coefficients) are associated with the lowest bore diameters.

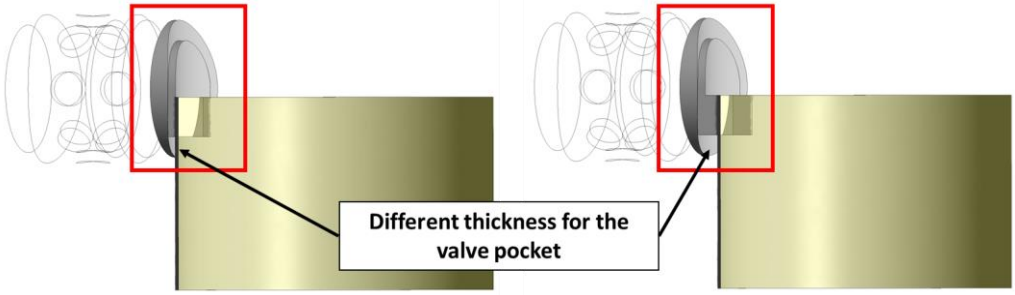

Figure 3.26 – Effect of the variation of the liner and spacer thickness in the valve pocket thickness

However, the most important aspect to highlight from Figure 3.24 and Figure 3.25 is the almost linear dependence of the calculated flow coefficient from the bore diameter. This relation allows reducing the number of configurations to simulate. In fact, it is possible to obtain the global flow coefficient at different bore diameters, knowing the flow coefficient at the highest diameter and at the lowest one by means of CFD simulations and obtaining the flow coefficients at the intermediate diameters by means of linear interpolations.

This solution requires only two simulations for every phase and for every effect (eight total simulations for each code), regardless of the number of diameters that are obtained of a single code.

The use of this solution in the parametric CFD routine defined in this thesis, allowed obtaining an important reduction of the global computational times.

3.9 Analytical procedure for the valve change

The second aspect that occurs to consider for the global times reduction in the realization of a reliable database by means of a parametric CFD routine, is the dependence of the global pressure losses and of the global flow coefficient by the valve used.

In the CFD routine developed in this thesis the actual valve is modeled by means of a cylindrical porous medium considering the valve as localized pressure drop. The user inputs for the valve simulation are then the valve flow coefficient and the valve passage area at the valve lift (Paragraph 3.6.1).

As explained in Paragraph 3.3.2, a same cylinder code could be used with different valve typologies (having different flow coefficients and different passage areas at the valve lift) and with different valve diameters.

The dependence of the global flow coefficient and of the global pressure losses by the valve used in the machine requires the definition of an analytic procedure in order to reduce the number of simulations and, consequently, the computational times. This procedure is based on the "superposition principle" and allows obtaining the overall pressure losses in the suction and discharge gas path changing the valve typology, once that the valve flow coefficient, the valve reference area and the global flow coefficient with a "reference" valve are known. In fact, the characteristics of the valve are given by the valve manufacturers while the global flow coefficient using a "reference" valve is calculated by means of a CFD simulation.

This methodology starts then by the flow coefficient definition (Paragraph 1.8);

$$Ks = \frac{m_{real}}{\frac{p_0 A_t}{\sqrt{\gamma R T_0}} \sqrt{\frac{2\gamma}{\gamma - 1}\left(\frac{p_t}{p_0}\right)^{\frac{2}{\gamma}}} \sqrt{1 - \left(\frac{p_t}{p_0}\right)^{\frac{\gamma-1}{\gamma}}}}$$

and by the calculation of the global flow coefficient for a cylinder code with a "reference" valve (called in example "*Valve A*") by means of a CFD simulation.

With reference to the simulations settings described in Paragraph 3.6 and considering a discharge phase simulation, it is possible to notice that the upstream total temperature T_0, the gas properties (R and γ) and the piston velocity are known, as user input of the CFD simulation. The other variable known is the static pressure at the flange surface; the upstream total pressure p_0, the corresponding density and consequently the

mass flow rate are then a function of the global pressure losses and have to be calculated by means of an iterative procedure.

The upstream total pressure for the first iteration of the iterative procedure is considered equal to the mean value between the flange static pressure and the critical pressure $p_{01,crit}$ defined as;

$$p_{01,crit} = p_2 \left(\frac{2}{\gamma + 1}\right)^{-\frac{\gamma}{\gamma-1}}$$

where p_2 is the flange static pressure.

Starting from this definition, the mass flow rate (m_{real}) and the overall pressure drop ($\Delta p_{TOT,A}$) with the "*Valve A*" can be achieved iteratively.

Similarly, the pressure drop of the "*Valve A*" ($\Delta p_{v,A}$) and the corresponding pressure drop ($\Delta p_{v,B}$) for another valve typology (called in example "*Valve B*") are calculated.

The overall pressure losses with the new "*Valve B*" ($\Delta p_{TOT,B}$) it is obtained using the "superposition principle" by means of the following relationship:

$$\Delta p_{TOT,B} = \Delta p_{TOT,A} - \Delta p_{v,A} + \Delta p_{v,B}$$

Known the overall pressure losses with the "*Valve B*", the global flow coefficient $Ks_{TOT,B}$ is computed.

The analytical procedure described in this paragraph is summarized in Figure 3.27.

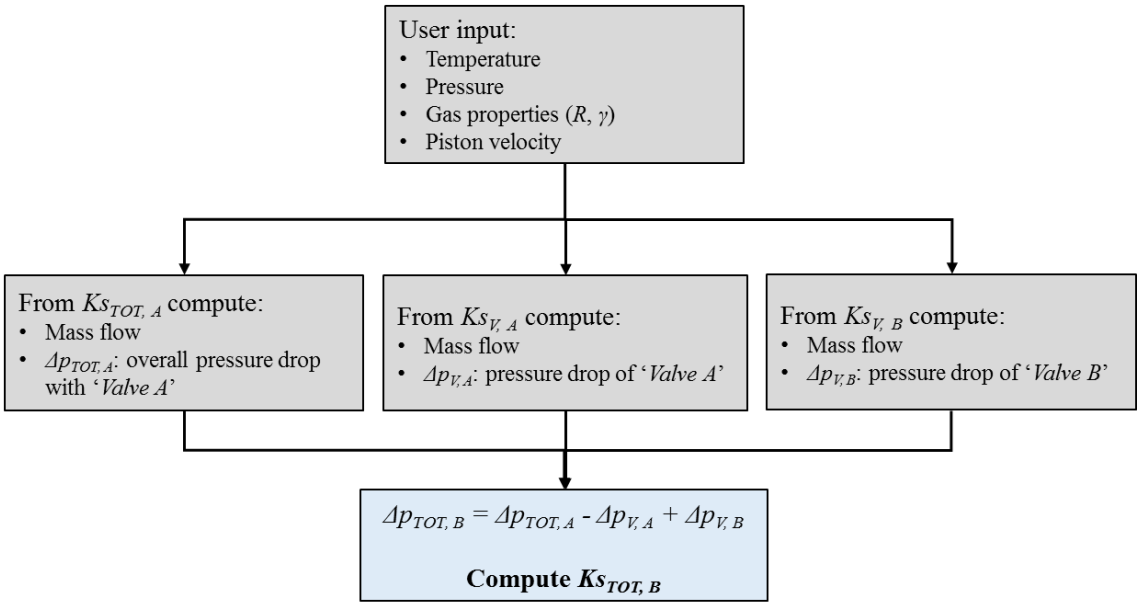

Figure 3.27 – Block scheme to summarize the analytical procedure for the valve change

This procedure could be used also for a suction phase simulations, remembering that in this case the inlet and outlet conditions are inverted (Paragraph 3.6).

The validation of the analytical procedure was obtained by means of CFD simulations, realized for the NCI and CS cylinders described in Paragraph 3.4.

At the beginning, the global flow coefficients ($Ks_{TOT,\,A}$) with a "reference" valve "*Valve A*") were calculated by the simulation of both codes considering different phases or effects and different piston positions. These global flow coefficients were used as input parameters in the analytic procedure in order to calculate the corresponding global flow coefficients ($Ks_{TOT,B}$) obtained with a different valve typology ("*Valve B*"). At the same time, the global flow coefficients with the "*Valve B*" were calculated by means of CFD simulations, changing the valve flow coefficient and the valve reference area at the valve lift and obtaining a new resistance loss coefficient (Paragraph 3.6.1) for the valve pressure losses evaluation.

The global flow coefficients obtained with the "*Valve B*" by means of the analytical procedure and of the CFD simulations were compared in order to quantify the error committed using the defined procedure instead of specific CFD simulations.

With reference the nodular cast iron cylinder, three simulations at different piston positions were realized for both suction and discharge phase and for both crank end side and head end side effect (12 total simulations for each valve).

Passing from "*Valve A*" to "*Valve B*", only the valve reference area was changed while the valve flow coefficient was maintained.

The global flow coefficients using the "*Valve A*" and the "*Valve B*" (both with CFD simulations and analytical procedure) and the error committed on the calculation of the $Ks_{TOT,\,B}$ by means of the analytical procedure instead of CFD simulations are shown for different piston positions in Figure 3.28 (suction phase) and Figure 3.29 (discharge phase). In these figures the piston position (x) is normalized with the piston stroke (S) while the global flow coefficients are scaled with the maximum in cylinder value obtained by means of the CFD simulations with the "*Valve B*" when the piston is far from the head (without "piston masking effect").

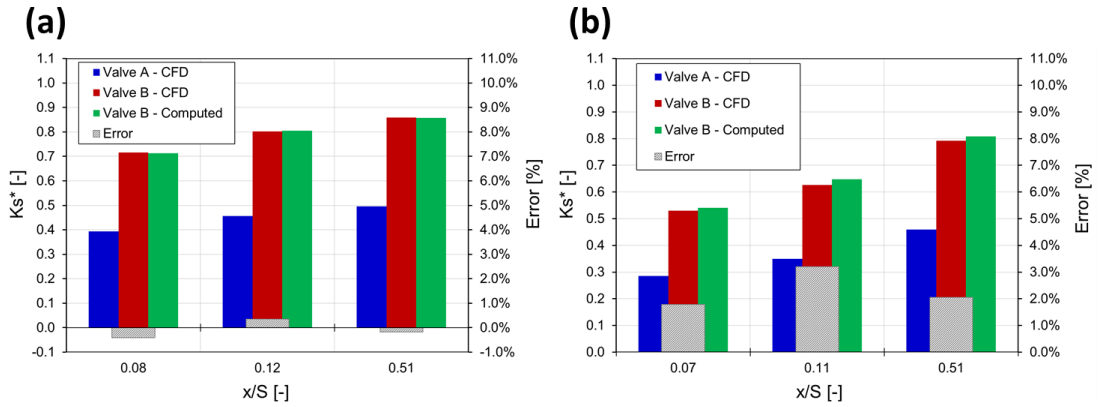

Figure 3.28 – Analytical procedure for the valve change: *Ks and error at different piston positions for the suction phase of a NCI cylinder. Crank end (Picture a) and head end effect (Picture b).**

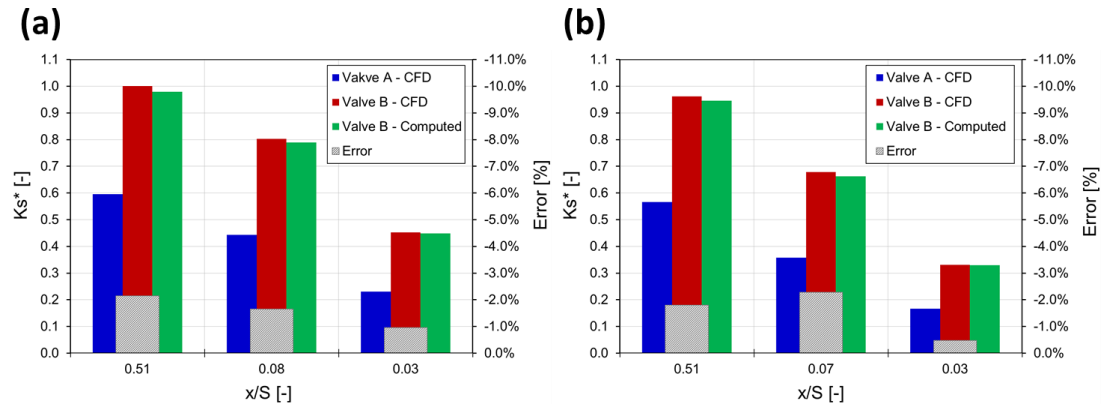

Figure 3.29 - Analytical procedure for the valve change: *Ks and error at different piston positions for the discharge phase of a NCI cylinder. Crank end (Picture a) and head end effect (Picture b).**

The results shown in Figure 3.28 and Figure 3.29 confirm the potential of the proposed approach with a maximum error on the global flow coefficient evaluation equal to 3.2% (obtained for the head end side effect of the suction phase).

The same validation approach was used for the CS cylinder. In this case, only the crank end side effect of the discharge phase was simulated for three different piston positions. Passing from "*Valve A*" to "*Valve B*", both the valve reference area and the valve flow coefficient were changed.

The results obtained are shown in Figure 3.30.

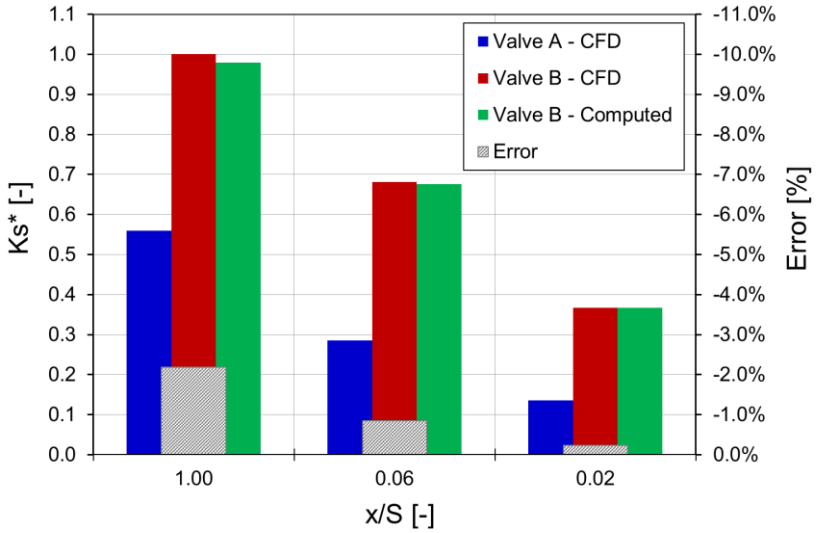

Figure 3.30 - Analytical procedure for the valve change: *Ks and error at different piston positions for the crank end effect of the suction phase of a CS cylinder**

A further validation of the analytical procedure was achieved; in fact, the maximum error is lower than 2%.

The procedure developed and validated in this paragraph, allows calculating the overall suction and discharge pressure losses by means of a single CFD simulation for every phase and for every effect, regardless of the number of valves typologies that are used for a single code.

However, it is important to highlight that this procedure doesn't allow obtaining an accurate flow coefficient evaluation when the valve diameter change. In fact, as explained in Paragraph 3.3, a single cylinder code could also be used with different valve diameters. The variation of this parameter has a not negligible effect on the fluid dynamics interactions between the valve itself and the plenum and compression chamber domains. The defined analytical procedure doesn't allow taking this interaction into account; for this reason, specific CFD simulations are needed each times that the valve diameter changes.

In conclusion, the analytical procedure described in this paragraph requires specific CFD simulations for each valve diameter used but allows a substantial reduction of the simulations number because allows avoiding to repeat the CFD simulations when the valve type (and consequently the valve flow coefficient and the reference area) change.

3.10 Piston masking effect

In Paragraph 3.3.2 the phenomenon known as "piston masking effect" and its importance for an accurate prediction of the *p*-*V* cycle was explained.

This phenomenon is due to the reduction of the passage area in the compression chamber domain for the masking of the passage window in the valve pocket, caused by the piston during his motion (Figure 3.7). Working with steady state simulations it is impossible to take the effect of the piston movement into account; for this reason, more simulations are needed in order to evaluate the influence of the piston masking phenomenon on the global pressure losses estimation.

It is then extremely important to choose a number of simulations that allow obtaining a compromise between the simulations times and the results accuracy. Obviously, the higher is the number of simulations, in particular in the masking zone, the higher is the results accuracy. On the other hand, the increase of the simulations number causes an unreasonable increase of the simulations times.

The flow coefficient (scaled by means of the maximum in-cylinder value) as a function of the ratio between the piston position (x) and the piston stroke (S) is shown in Figure 3.31 and Figure 3.32 for the NCI and CS cylinders of Paragraph 3.4 (the dashed lines in both figures shows the piston masking starting). Both figures are referred to the head end side effect of the discharge phase.

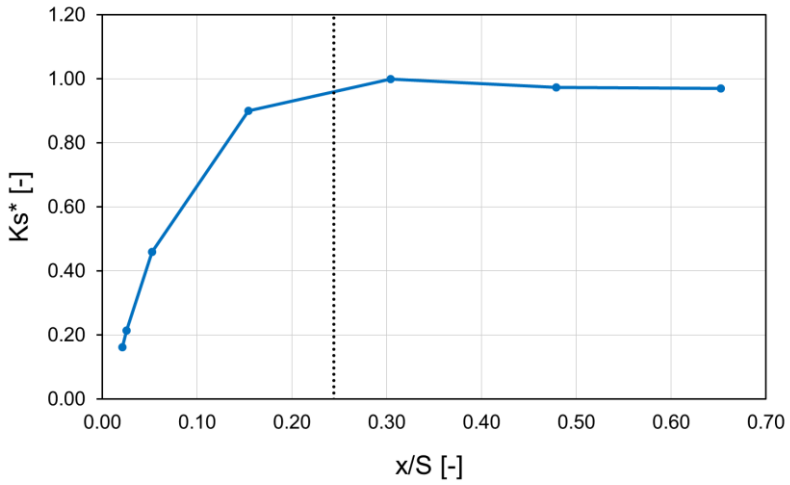

Figure 3.31 - *Ks as a function of the piston position: discharge head end of a NCI cylinder**

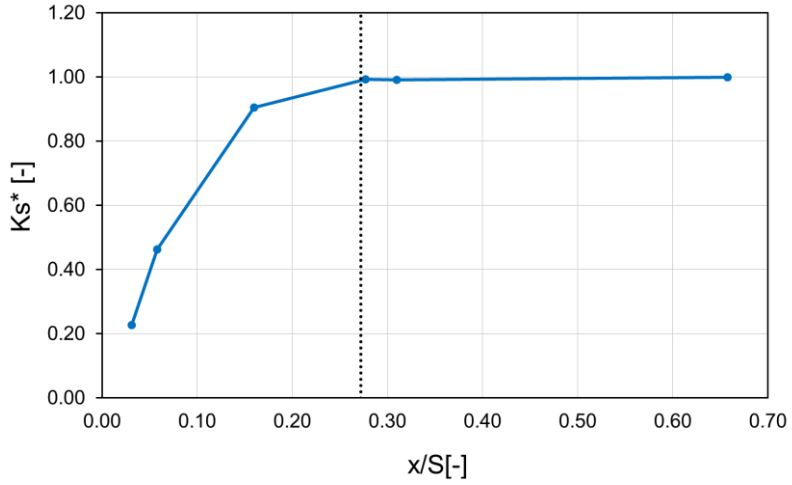

Figure 3.32 - *Ks as a function of the piston position: discharge head end of a CS cylinder**

The first aspect that occurs to highlight is the quite constant flow coefficient before the piston masking starting; in the first part of the piston stroke is then useless to simulate more than one piston position. The flow coefficient achieved when the piston is in the middle of its stroke is then supposed to be constant during the piston stroke without piston masking effect.

On the other hand, more attention has to be paid on the definition of the number of simulations in the masking zone. If no simulation are made in this zone and the flow coefficient obtained without piston masking is used for all the discharge phase in low orders models, the error introduced in the *p-V* cycle prediction is not negligible (Paragraph 5.4). From both Figure 3.31 and Figure 3.32, it is possible to notice that the flow coefficient reduction during the piston masking phenomenon follows a quite linear line during the first part of the masking, increasing its pendency in the last part. For this reason, it is possible to obtain an accurate prediction of the global pressure losses in the machine during the piston masking effect, using two simulations; one with the piston located approximately at the midpoint of the masking height and one with the piston near to the compression chamber head.

Starting from these considerations, in the simplified CFD routine it was chosen to consider the effect of the piston position on the flow coefficient by means of three simulations. The first one was realized with the piston located at the mid stroke position (point 1 in Figure 3.33 and Figure 3.34), the second at the midpoint between the point 3

and 4 in the following figures and the third one with the piston located at 10 mm from the compression chamber head (point 3).

In Figure 3.33 and Figure 3.34 an estimation of the results achieved using only three CFD simulations is shown (red lines); the overlapping between this estimation and the results obtained in Figure 3.31 and Figure 3.32 allows understanding the error introduced in the defined CFD routine. Points 1, 2 and 3 in both figures are referred to the three CFD simulations at the defined piston positions. On the other hand, point 4 was not calculated by means of a CFD simulation but was obtained as a construction point, knowing the piston masking starting and supposing a constant flow coefficient for all the discharge phase without piston masking effect.

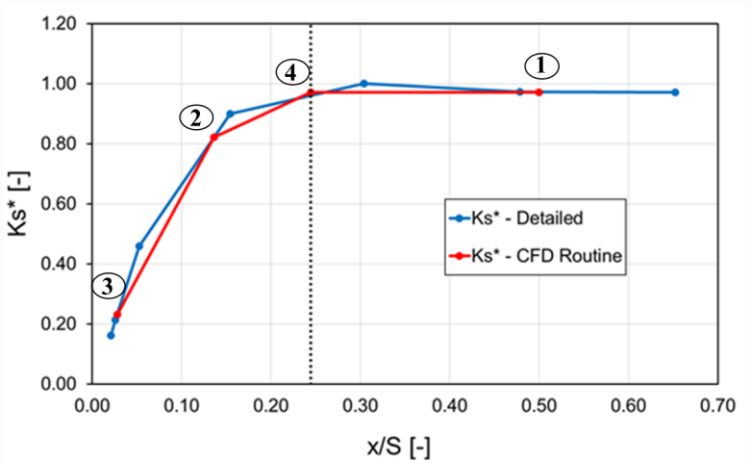

Figure 3.33 - *Ks as a function of the piston position for a NCI cylinder: overlapping between the detailed curve (blue curve) and the curve obtained with three CFD simulations (red curve)**

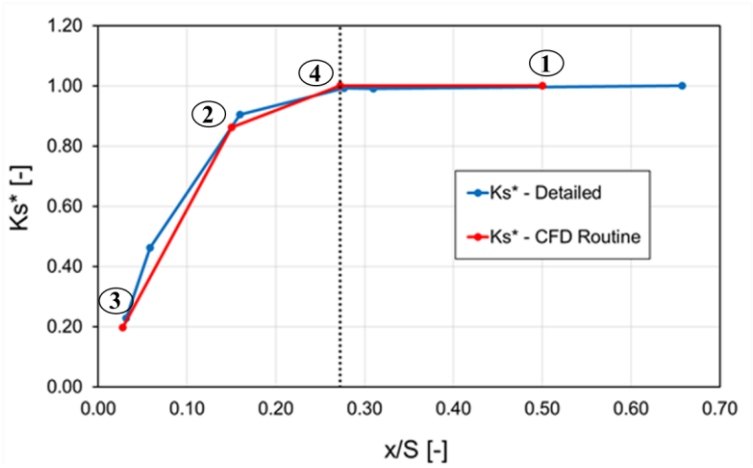

Figure 3.34 - *Ks as a function of the piston position for a CS cylinder: overlapping between the detailed curve (blue curve) and the curve obtained with three CFD simulations (red curve)**

Both figures show an almost perfect overlapping between the red curve and the blue one in the zone of the piston stroke without piston masking. On the other hand, a small underestimation of the global flow coefficient during the piston masking is achieved using the simplified CFD routine instead of a biggest number of CFD simulations.

However, the error introduced in the *p-V* cycle estimation by means the 1D model described in Chapter 5 is not so high; the difference on the absorbed power using the red flow coefficient curve instead of the blue one is lower than 0.3% for both cylinders.

More details on the effect of the number of simulations in the *p-V* cycle prediction will be given in Paragraph 5.4.

Moreover, it is possible to observe that the use of the number of simulations defined in the CFD routine causes always an underestimation of the global flow coefficient and a consequent overestimation of the absorbed power; this solution gives then a precautionary estimation on the performance predictability of the machine.

Similar considerations can be made also for the suction phase even if the piston masking happens during the first part of this phase and not at the end like in the discharge phase. Moreover, the piston masking phenomenon is less important because the suction valve is closed during the first part of masking. However, it was chosen to use three simulations also for the suction phase in order to avoid a further increase of the error on the performance evaluation.

In conclusion, the approach proposed in this paragraph allows obtaining a compromise between the results accuracy and the computational times with small and precautionary errors on the estimation of the *p-V* cycle both for suction and discharge phase.

3.11 Effect of the operating conditions on the results

A typical reciprocating compressor can work with different working fluids and in different operating conditions (Paragraph 3.3.2). In fact, dealing with large bore machines, a wide range of Reynolds numbers can be experienced during the operation, which can differ of about three orders of magnitude, depending on the working fluid and the operating conditions (two order of magnitude considering the same fluid at different operating conditions). For this reason, an analysis on the flow coefficient variation with the Reynolds number is fundamental in order to quantify the error introduced when the working condition of the machine differs from the simulated one.

Therefore, eight simulations were carried out for the NCI cylinder of Paragraph 3.4; the most common working fluids used by Baker Hughes were tested at different operating conditions (pressure, temperature and mean piston speed). These operating conditions were chosen in order to obtain the maximum and minimum Reynolds number achievable for each fluid in the simulated reciprocating compressors.

In Table 3.4 the tested working fluids and the maximum and minimum Reynolds numbers (evaluated at the flange section) are summarized. It can be noticed that the lowest Re value is obtained for the H2 at the minimum mean piston speed, due to the smallest molecular weight. Conversely, the highest Re value is obtained for the N2 at the maximum mean piston speed. The crank end side effect of the suction phase was simulated, with a piston position chosen in order to consider the piston masking phenomenon. In fact, it was noticed that the highest Reynolds numbers are usually obtained in the valve pocket when the piston is near to the head for the reduction of the passage area due to the piston masking effect.

	$Re_{min.}$	$Re_{max.}$
HYDROGEN (H_2)	3.83E+03	5.08E+05
METHANE (CH_4)	2.42E+04	6.99E+05
NITROGEN (N_2)	2.65E+04	5.30E+05
CARBON DIOXIDE (CO_2)	4.94E+04	1.04E+06

Table 3.4 - Tested working fluids and Reynolds numbers at the flange section for a NCI cylinder with piston masking effect

The obtained flow coefficients (scaled by means of the maximum in-cylinder value at the simulated position) as a function of the Reynolds number are shown in Figure 3.35.

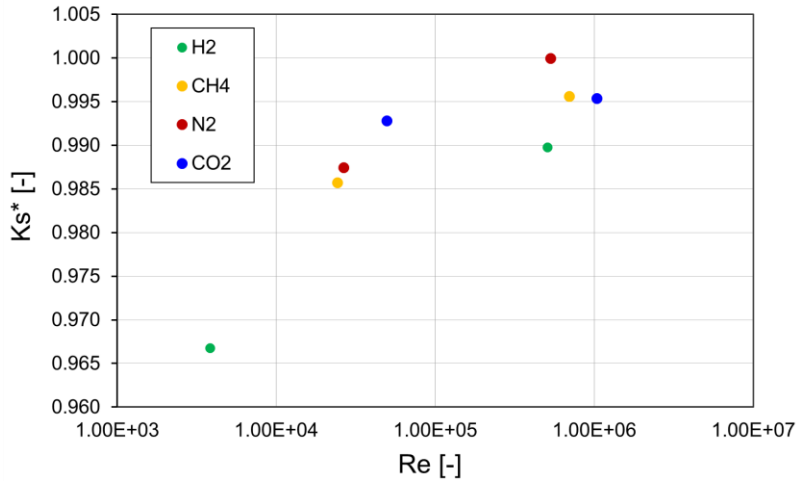

Figure 3.35 - *Ks as a function of the Reynolds number for a NCI cylinder during the piston masking phenomenon**

From this figure, it is possible to observe that the variation of the working conditions in the machine can introduce an error on the evaluation of the flow coefficient. In fact, fixed the working fluid, the global flow coefficient increase with the Reynolds number. However, the error introduced neglecting the flow coefficient variation with the Reynolds number is not so high; in fact, passing from the maximum to the minimum Reynolds number (that differ of about three order of magnitude) it is obtained a maximum difference on the flow coefficient evaluation lower than 3.5%. Moreover, the maximum difference with a same fluid in different operating conditions is equal to 2.38%.

These results allow understanding the influence of the working fluids and of the operating conditions on the flow coefficient evaluation. Nevertheless, the error related to the choice of a "reference" condition for a CFD simulation instead of the actual condition is not so high and allows respecting the established target.

Moreover, it is important to highlight that the error in the absorbed power prediction by means of low order models due to a non-correct flow coefficient evaluation depends by the working fluid. In fact, the lower is the molecular weight of the fluid, the lower is the influence of the flow coefficient on the estimation of the *p-V* cycle.

More detail regarding this aspect are given in Paragraph 5.4; however, it is possible to explain that the error on the absorbed power estimation neglecting the variation of the operating conditions is usually lower than 1% regardless of the fluid used.

Starting from these considerations, it is possible to conclude that the flow coefficients calculated by means of a CFD simulation using established "reference" working fluid in "reference" operating conditions are useful to obtain a quite accurate estimation of the overall pressure losses in the machine also when the operating conditions change.

Therefore, in the parametric CFD routine defined in this thesis it is possible to simulate only one working condition; the calculated flow coefficients can be used in low orders models also for different working conditions without the introduction of unacceptable errors in the *p-V* cycle prediction.

4 Application of the parametric approach to an industrial case

4.1 Introduction

Chapter 3 was focused on the description of the steps that have been followed for the realization of a new simplified parametric CFD routine.

The starting point was the definition and the validation of CFD *Master models*; in more detail, mesh and numerical settings were defined in order to obtain accurate results with stable models. Moreover, the effect of the simplification of some geometrical features were evaluated and described. The second step was the analysis of the effect of the variation of some variables (i.e. bore diameter, valve, piston position and operating conditions) on the global pressure losses. In particular, different solutions were proposed in order to reduce the number of simulations that needed for the realization of a reliable database in a common industrial application.

The possibility to have an accurate estimation of the global pressure losses for different machines, which are characterized by different geometrical features and which work with different operating conditions, is extremely important in order to increase the performance predictability. In fact, the prediction of the *p-V* cycle it is nowadays possible in a few seconds by means of low order models (0D-1D). However the accuracy of the results achieved is strictly dependent by the evaluation of the flow coefficient (*Ks*) commonly used in these models to take the global pressure losses into account.

A non-accurate estimation of the global flow coefficient causes high error in the predictability of the *p-V* cycle and of the absorbed power. On the other hand, the

evaluation of the global pressure losses by means of solutions that require too high computational and set-up times is unacceptable because doesn't allow taking advantage of the reduced computational times of low order models.

The possibility to simulate a large number of codes by means of the CFD routine developed in this work is then extremely interesting in order to use the results obtained in low order models.

In this scenario, the described procedure was used in an industrial application; in fact, the whole fleet of cylinders of Baker Hughes was simulated making use of simplified CFD parametric models together with the solutions proposed in Chapter 3 for the reduction of the simulations number.

In this chapter, a brief summary of the simulations made is given (Paragraph 4.2) as well as a detailed analysis of the achieved results (Paragraph 4.3).

4.2 Description of the simulations campaign

The CFD routine described in Chapter 3 was used for the simulation of 123 double acting cylinder codes of Baker Hughes.

All codes are gathered in multiple "families" defined as a function of:

- cylinder casing (HA, HB, HD, HE, HG, HM, HF);
- number of valves (1+1, 2+2, 3+3, 4+4, 5+5);
- cylinder material (cast steel (CS)), nodular cast iron (NCI));
- cylinder manufacturing (forged, melt);
- cylinder application (high pressure, low pressure).

For each cylinder code, two different bore diameters were simulated; in fact, as explained in Paragraph 3.8, four different bore diameters are usually extracted by a single cylinder code changing the thickness of liner and spacer. The almost linear relationship between the bore diameter and the global flow coefficient shown in Figure 3.24 and Figure 3.25 allowed simulating only the maximum and minimum diameter obtaining the global flow coefficient at the intermediate diameters by means of linear interpolations.

Moreover, each code is usually used with two valves diameters; therefore, two different simulations were made using a small and a big valve. The only exception is due to the cylinders with a single valve (1+1); in fact, these cylinders are usually used with a single valve diameter.

All the simulations were made using a single "reference" valve, whose pressure losses are evaluated at the maximum valve lift. For this reason, a single valve flow coefficient was used for all the simulated cylinders.

If the same code is used with different valve types (having different flow coefficients or different valve areas at the valve lift) the new global flow coefficients will be calculated by means of the analytic procedure described in Paragraph 3.9.

Three different piston positions were simulated to take the piston masking phenomenon into account (Paragraph 3.10).

It was chosen to simulate all codes using N_2 as working fluid and considering a single operating condition. In fact, pure nitrogen is the most common fluid used in these machines; moreover, the maximum error introduced when the working fluid or the operating conditions change was considered admissible (Paragraph 3.11).

Starting from these considerations, 48 simulations were made for each cylinder code (24 for the cylinders having a single valve);

- two different bore diameters and valve diameters (4 configurations for each code);
- one simulation for every phase and for every effect (4 simulations for each configuration);
- three different piston positions (3 simulations for each phase and effect).

For the realization of the whole database, more than 4000 simulations were realized by means of 21 *Master models*. The classification of the overall cylinders codes in cylinder families and the realization of the CAD models was done jointly with RAM Oil & Gas.

The simulations campaign was divided in two phases; in the first one all the cylinders of the families HG and HF (33 cylinder codes) were simulated, in the second one the database was completed with the simulation of all the others cylinder "families".

A cluster having 1280 CPU was used; each simulation was realized adopting a parallelization strategy on 80 CPU. Four hours were necessary for the simulation of the biggest domains while the smallest machines were simulated in less than 2 hours.

The first phase of the campaign was completed in 4 months while other 6 months were needed to complete also the second phase.

In Paragraph 5.4, it will be shown how the results obtained from this simulations campaign can be used in an in-house one dimensional model, allowing a strong increase of the performance predictability.

Moreover, some fluid dynamic considerations obtained from the results of the first phase of the simulations campaign are shown in Paragraph 4.3.

4.3 Results

In this paragraph, the results of the first phase of the simulations campaign are analyzed and discussed. The typologies and the number of cylinders simulated, as well the maximum and minimum bore and valve diameter (in dimensionless form by means of their maximum values) are summarized in Table 4.1.

Cylinder type	N° of codes	Min. Bore*	Max. Bore*	Min. Valve Diam.*	Max. Valve Diam.*
1+1 NCI	14	0.108	0.248	0.322	0.661
2+2 CS	9	0.220	0.552	0.492	1.000
2+2 NCI	4	0.296	0.456	0.525	0.831
3+3 NCI	2	0.468	0.552	0.661	0.831
4+4 NCI	3	0.632	0.840	0.729	1.000
5+5 NCI	1	0.936	1.000	0.898	1.000

Table 4.1 – Summary of the most important characteristics of the cylinders codes simulated during the first phase of the simulations campaign

The calculated flow coefficients as a function of the bore diameters are plotted in Figure 4.1 and Figure 4.2. Both figures are referred to the head end side effect of suction (Picture a) and discharge phase (Picture b). In more detail, Figure 4.1 shows the results of the simulations without piston masking effect ("*Piston position 1*") while Figure 4.2 shows the results of the simulations with the piston located at 10 mm from the compression chamber head ("*Piston position 3"*).

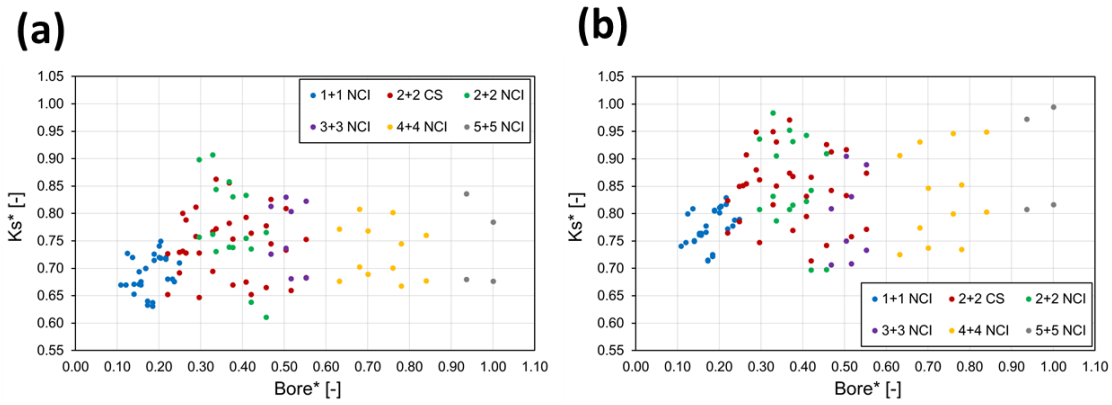

Figure 4.1 - *Ks as a function of *Bore** for different cylinders codes at "*Piston position 1"*: suction head end (Picture a) and discharge head end (Picture b)**

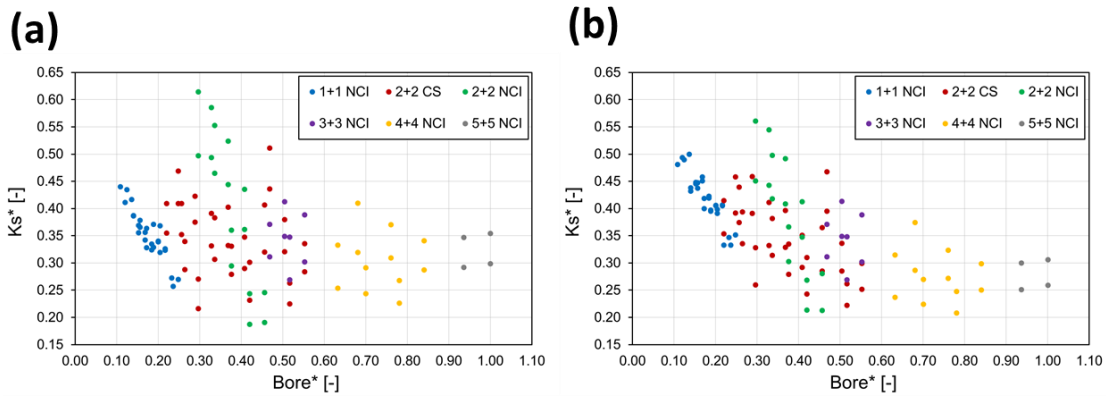

Figure 4.2 - *Ks as a function of *Bore** for different cylinders codes at "*Piston position 3*": suction head end (Picture a) and discharge head end (Picture b)**

These results confirm the influence of the geometrical features on the global pressure losses estimation and, consequently, on the global flow coefficient evaluation. In fact, the *Ks** calculated for different codes by means of CFD simulations is extremely variable: the maximum difference is around 30% for both suction and discharge gas domain at "*Piston position 1*". This difference, allows understanding the difficulty on the evaluation of the global flow coefficient by means of a Pocket Factor (*PF*) for the valve flow coefficient correction. In fact, the large variability on the geometrical shape of each code and the influence of this variability on the results requires this parameter to be tuned for the specific case, with the possibility to achieve an incorrect estimation of the losses or incorrect results. On the other hand, the use of CFD simulations, allows overcoming this problem taking the geometrical features into account for the global pressure losses estimation.

Similar considerations can be made also for the results obtained at "*Piston position 3*" (Figure 4.2); in this case, the maximum difference is around 60%-70%.

An interesting aspect that could be highlighted by a comparative analysis of the results shown in Figure 4.1 and Figure 4.2 is the different behavior of 2+2 nodular cast iron and 2+2 cast steel cylinders during the piston masking phenomenon.

As shown in Figure 3.8 and Figure 3.9 the fluid domains of these two cylinders "families" are extremely different for both the compression chamber and plenum domain. For this reason, it is not simple to understand the effect of a single geometrical feature on the results; in fact, there are too many different geometrical variables between the simulations of these two cylinders "families".

However, from Figure 4.1 and Figure 4.2 it is possible to observe the similar flow coefficients between the cast steel cylinders and the nodular cast iron at "*Piston position 1*". On the other hand, NCI cylinders show a clear better behavior at "*Piston position 3*"; the efficiency reduction during the piston masking phenomenon for the NCI cylinders is then lower than the cast steel one.

In order to understand this different behavior it is possible to refer to Figure 4.3 where the valve pockets of the head end side effect are shown for CS (Picture a) and NCI cylinders (Picture b). From this figure, it is possible to observe that CS cylinders have usually a higher passage window than the NCI (Figure 4.3) at "*Piston position 1*"; this is due to a different alignment between the valve axis and the compression chamber head for these two cylinders "families". In fact, the valve axis of CS cylinder is usually aligned with the compression chamber head. On the other hand, the valve axis of a NCI cylinder is usually in a highest position with respect to the compression chamber head. This different constructive solution causes a highest passage window reduction during the piston masking phenomenon for the CS cylinders and consequently a highest efficiency reduction.

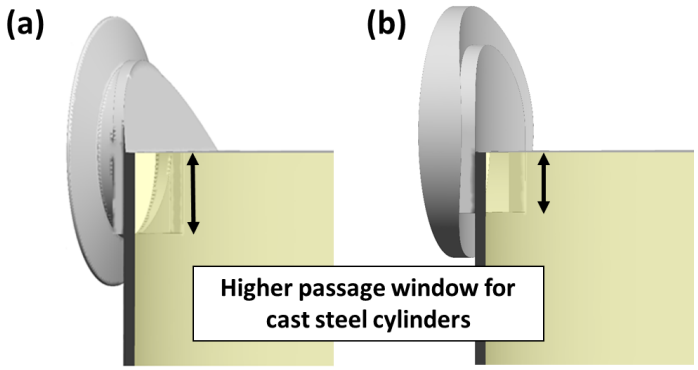

Figure 4.3 – Different height for the passage window of cylinders 2+2 CS (Picture a) and 2+2 NCI (Picture b)

To better understand the effect of the piston masking phenomenon on the global flow coefficient, in Figure 4.4 the *Ks** obtained for the head end side effect of suction (Picture a) and discharge phase (Picture b) are plotted as a function of the bore diameter for the 2+2 CS cylinders. All the piston positions simulated are illustrated; the flow coefficient reduction due to the piston masking phenomenon is extremely variable.

However, by means of the comparison between the "*Piston position 1*" and the "*Piston position 3*" it is possible to say that the efficiency reduction is usually highest for the cylinders having the biggest bore diameters. This relationship is once again due to the passage window height: in fact, usually, the higher is the bore diameter, the higher is the passage window height and consequently the higher is the flow coefficient reduction during the piston masking phenomenon for the reduction of the passage window area in the valve pocket.

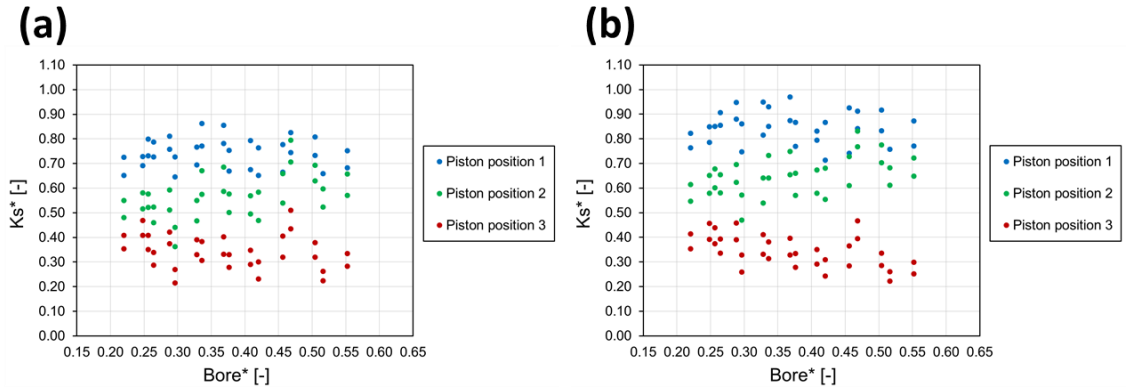

Figure 4.4 – Piston masking effect of cylinders 2+2 CS: *Ks as a function of *Bore** for suction head end (Picture a) and discharge head end (Picture b)**

Another interesting aspect to highlight is the effect of the valve diameter on the flow coefficient evaluation. In Paragraph 4.2, it was explained that two different valve diameters were simulated for each cylinder code (with the only exception of cylinders having a single valve). In Figure 4.5 a comparison between the flow coefficients obtained for a same code using different valve diameters is shown with reference to the head end side effect of cylinders 2+2 CS at "*Piston position 1*". The flow coefficients calculated for a same code using a smallest valve are always higher than the corresponding calculated with a valve having a biggest diameter. However, this effect is not necessarily due to a highest fluid dynamic efficiency with a smallest valve diameter; in fact, it is useful to remember that the reference area at the valve lift used for the flow coefficient definition (Paragraph 1.8) is a function of the valve diameter. To correct understand the results of Figure 4.5 it is then important to take into account that the flow coefficient calculated for the simulations with the smallest valve is referred to a smaller reference area than the flow coefficient achieved for the simulation of the same code with the biggest valve.

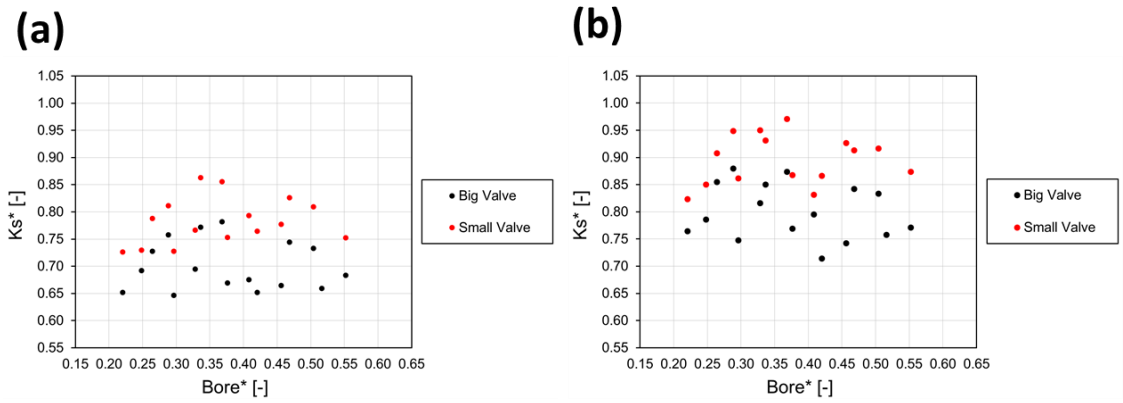

Figure 4.5 – Valve diameter effect for cylinders 2+2 CS at "*Piston position 1*": *Ks as a function of *Bore** for suction head end (Picture a) and discharge head end (Picture b)**

On the other hand, the results obtained by the simulations of a same code changing the bore diameter by means of the variation of the thickness of liner and spacer confirm the considerations made in Paragraph 3.8. In fact, the higher is the bore diameter of the machine, the higher is the calculated flow coefficient and the global fluid-dynamic efficiency. This is due to a worst fluid dynamic behavior in the valve pocket for the cylinders having the smallest bore diameter (Figure 3.26).

Figure 4.6 shows a comparison between suction and discharge phase of cylinders 2+2 CS with reference to "*Piston position 1*" and "*Piston position 3*" for both head end (Picture a) and crank end effect (Picture b).

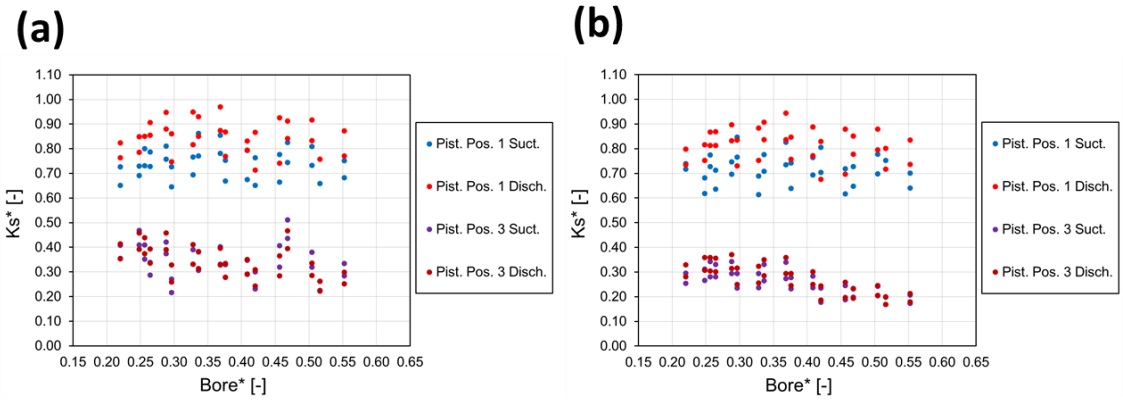

Figure 4.6 – Comparison between suction and discharge phase of cylinders 2+2 CS: *Ks as a function of *Bore** for head end (Picture a) and crank end effect (Picture b)**

Regarding the results at "*Piston position 1*", it is possible to observe that the *Ks** of the discharge phase is always higher than the *Ks** of the suction phase for both head end and crank end effect. To understand this difference, Figure 4.7 shows the velocity streamlines in both the compression chamber and plenum domain for suction (Picture a) and discharge phase simulation (Picture b).

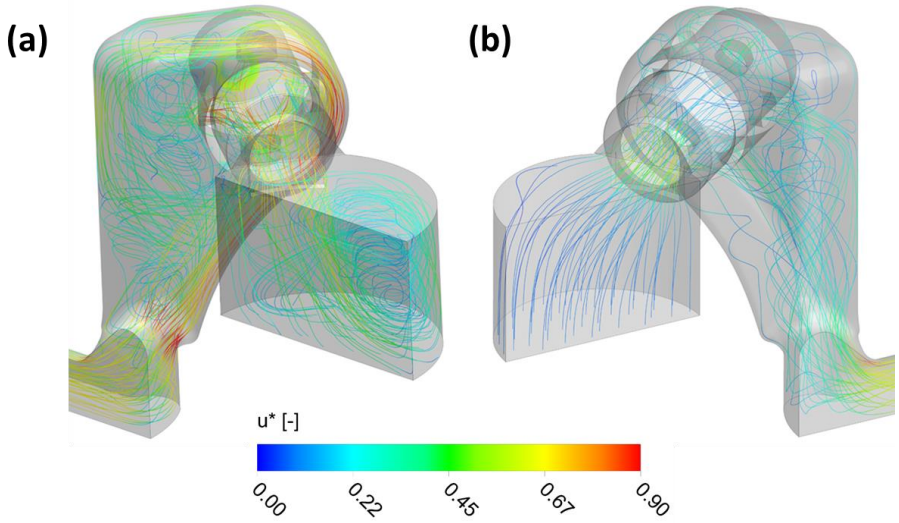

Figure 4.7 – Cylinders 2+2 CS at "*Piston position 1*": velocity streamlines during suction (Picture a) and discharge phase (Picture b)

The fluid dynamics structures are extremely different between the two phases; in particular, the suction phase shows a chaotic fluid in the compression chamber domain with the creation of strong recirculation. On the other hand, the fluid behavior in this part of the domain is more uniform during the discharge phase.

This different behavior allows understanding the higher flow coefficient calculated for the discharge phase simulations; in fact, it is clear that the strong recirculation in the compression chamber domain during the suction phase simulations causes an increase of the global pressure losses with a reduction of the global flow coefficient with respect to the discharge phase simulations.

Different considerations can be made for the results at "*Piston position 3*"; in this case, the recirculation in the compression chamber domain during the suction phase persists but is lower than the corresponding recirculation at "*Piston position 1*" (Figure 4.8).

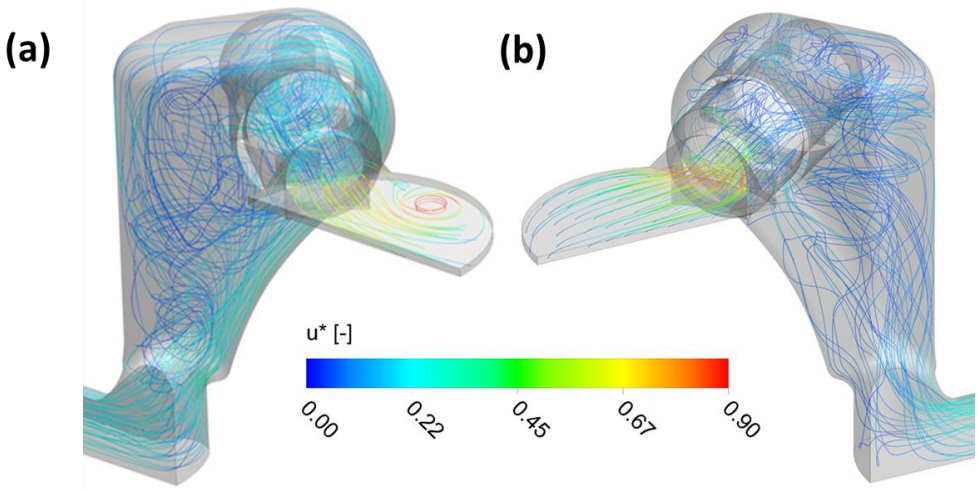

Figure 4.8 - Cylinders 2+2 CS at "*Piston position 3*": velocity streamlines during suction (Picture a) and discharge phase (Picture b)

Moreover, the fluid streamlines in the compression chamber domain for the discharge phase show a preferential direction to the flange side when the piston is located near to the compression chamber head; for this reason, the fluid velocity at the valve inlet is strongly non uniform (Figure 4.9). This effect is visible also for the suction phase; however, the velocity variations for this phase are less important and the fluid in the porous volume shows a more uniform behavior.

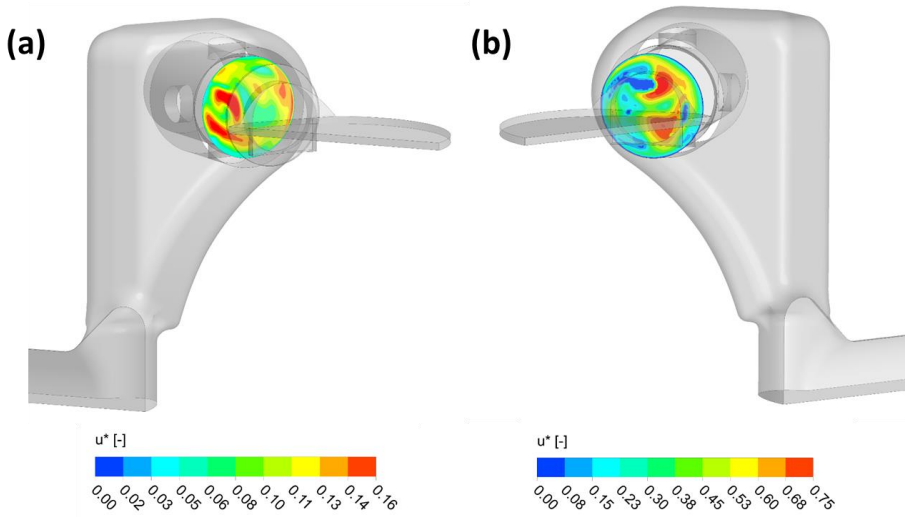

Figure 4.9 – Cylinders 2+2 CS at "*Piston position 3*": velocity contours at the valve inlet interface during suction (Picture a) and discharge phase (Picture b)

For this reason, the suction and discharge global flow coefficients at "*Piston position 3*" (Figure 4.6) are affected by these two phenomena. The suction *Ks** should be lower than the discharge one for the recirculation in the compression chamber domain. On the other hand, the non-uniformity at the valve inlet causes an increase of the global pressure losses in the valve domain during the discharge phase. These considerations allows understanding the results of Figure 4.6. In fact, the highest discharge *Ks** at "*Piston position 1"* are not repeated also for "*Piston position 3*" both for the lowest recirculation in the compression chamber domain during the suction phase and for the non-uniform fluid distribution at the valve inlet during the discharge one.

The last interesting aspect highlighted in this paragraph is the different fluid dynamic efficiency between head end and crank end effect.

Figure 4.10 shows the comparison between the two effects for both suction (Picture a) and discharge phase (Picture b).

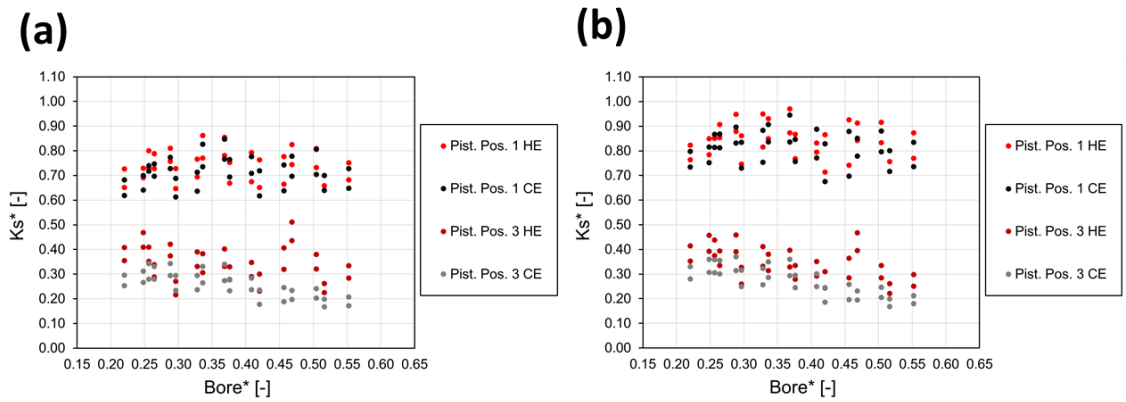

Figure 4.10 - Comparison between head end and crank end effect for cylinders 2+2 CS: *Ks as a function of *Bore** for suction (Picture a) and discharge phase (Picture b)**

From these results, it is possible to observe that the head end *Ks** for cylinders 2+2 CS is always higher than the crank end *Ks**, regardless by the phase or by the piston position. The velocity streamlines in the compression chamber and plenum domain are shown in Figure 4.11 (suction phase) and Figure 4.12 (discharge phase) for both head end (Picture a) and crank end effect (Picture b).

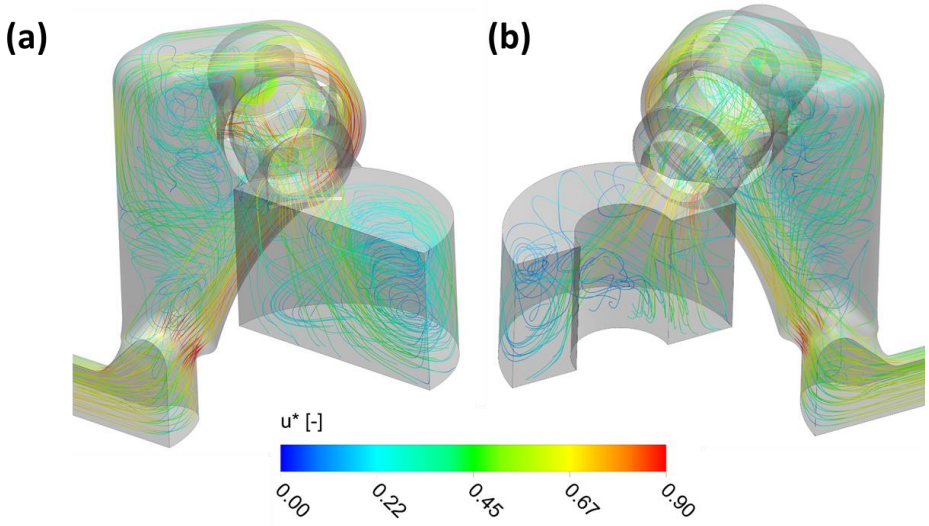

Figure 4.11 - Suction phase of cylinders 2+2 CS at "*Piston position 1*": velocity streamlines for head end (Picture a) and crank end effect (Picture b)

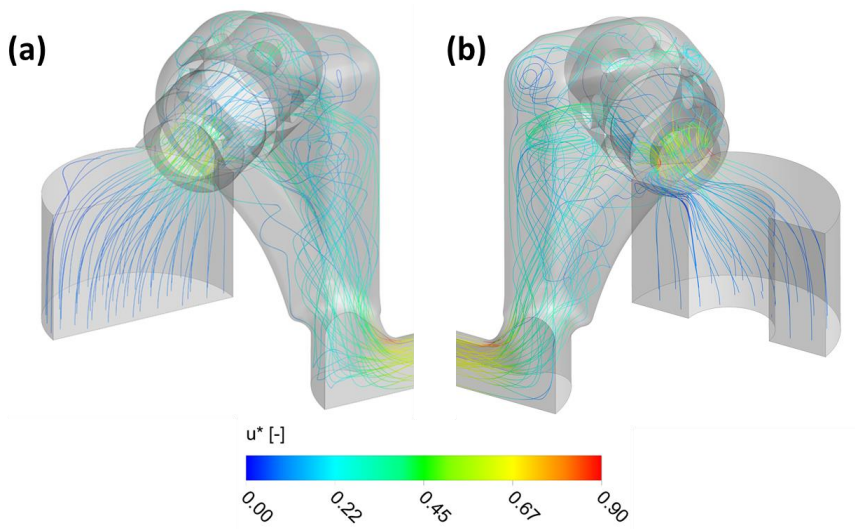

Figure 4.12 - Discharge phase of cylinders 2+2 CS at "*Piston position 1*": velocity streamlines for head end (Picture a) and crank end effect (Picture b)

The most important differences between the two effects are due to the valve pocket domain and to the existence of the piston rod in the crank end effect. Both differences are displayed in Figure 4.13 where the compression chamber domain of a cylinder 2+2 CS is shown for the head end (Picture a) and crank end effect (Picture b).

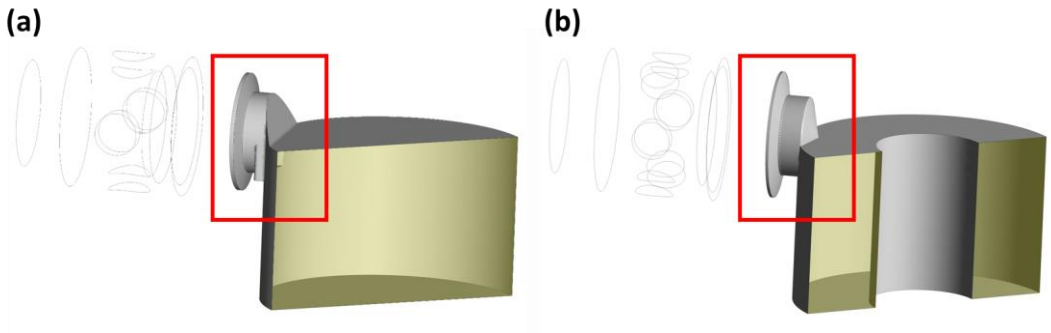

Figure 4.13 – Compression chamber domain of cylinders 2+2 CS: comparison between head end (Picture a) and crank end effect (Picture b)

The effect of these differences on the global flow coefficient depends by the valve pocket geometry and by the piston rod diameter.

In more detail, the higher is the piston rod diameter the higher is the efficiency reduction in the crank end domain caused by the disturbance of the piston rod on the fluid dynamic behavior in the compression chamber domain.

On the other hand, it is not simple to correct understand the effect of the valve pocket geometry on the global flow coefficient evaluation. In fact, different important geometrical features characterize the valve pocket geometries of different cylinders "families". Moreover, as explained by Balduzzi [15], small differences in the valve pocket geometry have a strong influence on the fluid dynamic efficiency in the compression chamber domain.

For this reason, the comparison between the head end and crank end effect is extremely case dependent. In other words, the highest efficiency shown in Figure 4.10 for the head end effect is not always repeated for all the simulated cylinders "families".

Starting from these considerations, it is possible to conclude that the highest *Ks** shown by all the 2+2 CS cylinders at the head end side, regardless by the phase and by the piston position is an intrinsic characteristic of this cylinders "family". It is due to the lowest fluid dynamic efficiency of the valve pocket at the crank end side and to the quite big rod diameters used for these cylinders. However, these results can be different for others cylinders "families" having most efficient valve pockets at the crank end side and lowest piston rod diameters

5 Finite volume one dimensional model

5.1 Introduction

In the reciprocating compressor design process, the performance predictability plays a key role since the early stages.

For an accurate prediction of the global performance, three-dimensional CFD transient simulations should be used: however, the computational costs of these simulations are too high and not compatible with any industrial process. For this reason the thermodynamic cycle of a reciprocating compressor is often calculate by means of lumped parameter numerical models, with a substantial reduction of the calculation times. These models allow a good prediction of the compressor performance but neglect the presence of unsteady phenomena such as pressure waves travelling inside cylinder bore and suction/discharge gas chambers. Dealing with a large size compressor, it can be observed that the time needed for the pressure waves to travel the whole cylinder bore is comparable with the duration of the physical phenomena of the thermodynamic cycle. This affects the gas transfer process inside the cylinder chamber, mostly during the suction and discharge phases, and thus the compressor performance [2].

A more realistic way to simulate the mass flow inside the compression chamber is to increase the spatial dimension of the fluid domain representation. This leads to a numerical model that includes a spatial definition of the cylinder chamber, in order to account for the fluid inertial effects. In order to meet this need and to increase the accuracy of the thermodynamic cycle simulation, a one-dimensional compressor model that solves

the fluid dynamic equations by applying the finite volume method (FVM) was developed by the REASE GROUP of the Industrial Department of the University of Florence jointly with Baker Hughes, a GE company.

This model requires the knowledge of the flow coefficient (*Ks*) to account of the global pressure losses along the suction and discharge flow path; for this reason, the results of the simulations campaign described in Chapter 4 were used.

The implementation of the 1D model was not the main objective of this work; therefore, the details of this model are not shown in this thesis. However, a brief description of the model and a comparison between the numerical results and the measurements collected on a dedicated test bench are given.

In particular, the aim of this chapter is to investigate the effect of the approximations introduced in the flow coefficient evaluation on the performance prediction of a large size reciprocating compressor. For this reason, different approaches in the definition of the global flow coefficient were used; the results showed the influence of such approaches on the working cycle prediction.

The study described in this chapter is carried out for three different compressor sizes and three different working gases, showing that the requirements in terms of flow coefficient accuracy depend on the specific case.

5.2 State of the art

Numerical models that simulate the thermodynamic cycle of the compressor are widely used with the aim of analyzing the phenomena involved in the thermodynamic cycle and predicting the compressor performance.

In the first phases of the design, lumped parameter models are widely used for preliminary analysis because of the low computational cost. These models simulate the cylinder chamber as a lumped element, whose volume varies with time. The thermodynamic properties (e.g. pressure, temperature and density) are uniform in the whole fluid domain that the volume represents and the change of state in the cylinder chamber follows quasi-static transformations [2].

Dealing with large size reciprocating compressors, the performance predictability of the lumped parameter models has limits that cannot be neglected. This was addressed

to the inability of such models in simulating the pressure waves propagation phenomena that affects the thermodynamic cycle. For this reason, an upgrade of the fluid domain discretization is needed.

A first study of the effect of waves and unsteady flow inside the cylinder was realized by E. Machu [37]. In his work, he calculated simple waves by using the method of characteristics.

Later G. Machu [38] described a numerical model based on the one dimensional Euler equations: the model was able to describe also laterally running waves moving inside the compressor chamber.

Aigner [39] and Steinrück [40] presented a compressor model focusing on the evaluation of a compressor performance with improved description of the physical phenomena involved in the compressor thermodynamic cycle. A spatial discretization was considered inside both the cylinder chamber and the compressor plena.

Starting from these works, the REASE GROUP of the Industrial Department of the University of Florence jointly with Baker Hughes, a GE company, developed a FVM numerical model based on the F-wave solution method of the Euler equation in the fluid domain of the compressor chamber. The model has a 1D spatial distribution: the cylinder chamber is discretized in a finite number of volumes that change size during the simulation because of the piston movement during the compressor operation.

In case of multi-valve configurations, in the FVM model a single valve with an equivalent section is used in order to represent the total valves.

The flow coefficients obtained by means of the parametric routine described in Chapter 3 for the global pressure losses evaluation allows increasing the numerical accuracy of the model.

5.3 Mathematical model

The FVM one-dimensional model starts by the conservation laws of the three basic physic properties (mass, linear momentum and energy) described in Paragraph 2.1.

Assuming isentropic conditions (*s=const.*), pressure can be expressed in terms of density and entropy:

$$p = p(\rho, s)$$

In order to solve conservation laws that describe the fluid motion, the system of hyperbolic equations can be written in conservative form as [2]:

$$\frac{\partial \vec{q}}{\partial t} + \frac{\partial \vec{f}(q,x)}{\partial x} = 0$$

where the state vector $\vec{q}$ and the flux function $\vec{f}(q,x)$ are defined as follows:

$$\vec{q} = \begin{Bmatrix} R \\ u \end{Bmatrix}$$

$$\vec{f}(q,x) = \begin{Bmatrix} Ru \\ \frac{u^2}{2}\frac{p_0}{\rho_0^{\gamma}}\left(\frac{R}{A}\right)^{\gamma-1} \end{Bmatrix}$$

with $R=\rho A$.

In the Finite Volume Method, the computational domain is divided into cells and the unknown quantity that is numerically computed is the cell average of q on each cell (Q). Following the F-Wave approach, this system was reduced to the form [39]:

$$\vec{Q}_i^{n+1} = \vec{Q}_i^{n} - \frac{\Delta t}{\Delta x}\left(\vec{Z}^1_{i+\frac{1}{2}} + \vec{Z}^2_{i-\frac{1}{2}}\right)$$

where Z is the F-Wave numerical flux increments.

The interaction between two cells is done through the cell interface, which separates the two different states at the left and at the right side.

In the 1D model, the diameter that links the suction and discharge central valves has been chosen as the main direction of mass flow rate inside the cylinder (x axis). The equations of motion (Euler equations) are integrated over a cross section *A(x,t)* perpendicular to the x axis. The cross section areas vary with time due to the piston motion. The computational domain consists of the interior of the compressor, including the cylinder, the valve pockets and the pressure chambers. Cylinder, suction and discharge pressure chambers are considered as three different domain linked at the same compressor

boundary through which the communication is done with the mass flow rate.

Figure 5.1 and Figure 5.2 show respectively an example of compression chamber domain for multi-valve cylinder (3+3 NCI) and its schematic representation of the fluid volume discretization.

The pocket volumes are split into two volumes: one that is located in the cylinder head (Cylinder pocket) and the other is facing the valve (Pocket valve). This configuration allows taking into account the whole length of propagation of the pressure waves (valve to valve) inside the cylinder.

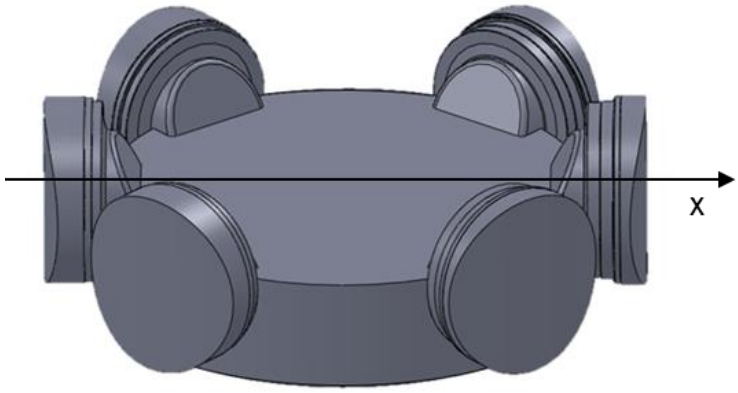

Figure 5.1 – Fluid domain of the compression chamber of a nodular cast iron cylinder (NCI)

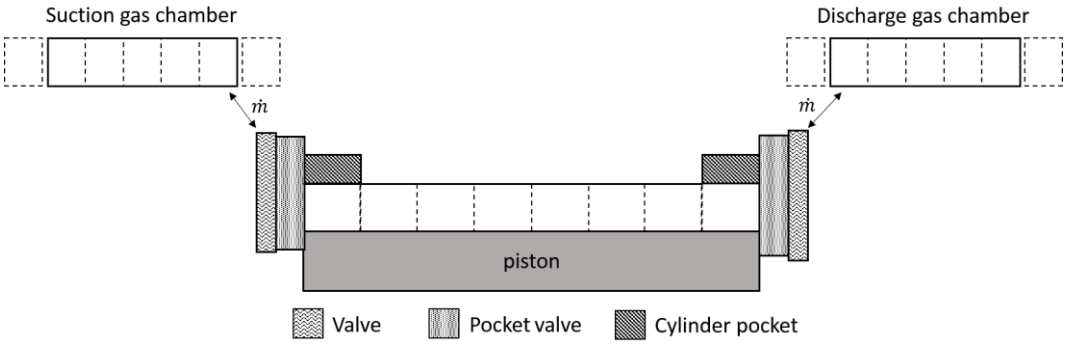

Figure 5.2 - Discretization scheme of the fluid domain

In order to obtain a good predictability of the FVM model, the choice of boundary conditions is of primary relevance [2].

The state variables values at the boundary of the fluid domain are set by imposing the proper $\vec{Q}$ value in the ghost cells. In other words, the values of $\vec{Q}$ in the ghost cells are set in order to obtain specific state variable values at the boundaries.

During compression and expansion phases, a rigid wall boundary condition is imposed in the cylinder domain. In this case, the values of variables of the ghost cell are set to ensure a zero speed at the wall (Figure 5.3):

$$\vec{Q}_{k+1} = \begin{Bmatrix} R_k \\ -u_k \end{Bmatrix}.$$

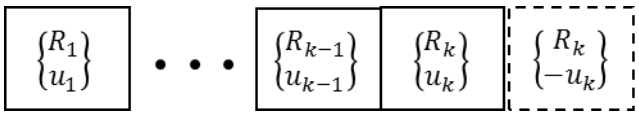

Figure 5.3 - Subdivision of the computational domain into grid cells; dashed line represents the ghost cell at the right boundary.

When the valves open, mass flow rate is computed at the interface between the compression chamber and the suction and discharge gas chamber (Figure 5.2).

It is done by considering the flow through the valve as the (stationary) outflow of a gas from a pressurized container through a convergent nozzle (Paragraph 1.8);

$$m_{id} = \frac{p_0 A_t}{\sqrt{\gamma R T_0}} \sqrt{\frac{2\gamma}{\gamma - 1}} \left(\frac{p_t}{p_0}\right)^{\frac{2}{\gamma}} \sqrt{1 - \left(\frac{p_t}{p_0}\right)^{\frac{\gamma-1}{\gamma}}}$$

The real mass flow rate can be calculated by means of the flow coefficients obtained from CFD simulations (Chapter 4).

By taking advantage of the flow coefficient *Ks*, it is possible to compute the mass flow rate in the FVM model and the boundary values are so set [2]:

$$\vec{Q}_k = \begin{Bmatrix} R_k \\ \frac{m_{out}}{R_k} \end{Bmatrix}$$

Non-reflecting condition has been used at the external boundaries of gas chambers;

$$\vec{Q}_{k+1} = \vec{Q}_k$$

$$\vec{Q}_0 = \vec{Q}_1$$

5.4 Experimental test case

The FVM numerical model was used to simulate the working cycle of three different cylinders codes, whose data are summarized in Table 5.1 (bore and valve diameter are expressed in dimensionless form with the same maximum values of Table 4.1).

	Material	**N° of valves**	**Working fluid**	**Bore***	**Valve Diam.***
Cylinder 1	NCI	3+3	N_2	0.616	1.000
Cylinder 2	NCI	2+2	CH_4	0.368	0.661
Cylinder 3	CS	2+2	H_2	0.504	0.898

Table 5.1 – Summary of the most important characteristics of the cylinders codes simulated by means of the FVM 1D model

The *p-V* cycle of the cylinders shown in Table 5.1 were evaluated using the FVM model described in Paragraph 5.3 with flow coefficients calculated by means of the following approaches;

- *Detailed*: the global flow coefficients for both suction and discharge phase were obtained using a high number of steady state CFD simulations at different piston positions. The CFD simulations were realized using the common strategy described in Paragraph 3.3; in fact, the fluid domains of the compression chamber and of the suction and discharge ducts were extracted by solid CAD model given by Baker Hughes.
- *CFD Routine*: the suction and discharge flow coefficients were calculated by means of the parametric CFD routine described in Chapter 3. Three simulations were realized for both suction and discharge phase (Paragraph 3.10).
- *Constant*: the effect of the piston masking phenomenon was neglected. Therefore, only the global flow coefficients calculated at piston position 1 by means of the parametric CFD routine (Paragraph 3.10) were used for both suction and discharge phase.
- *Valve*: the valve flow coefficient was used as a global flow coefficient for both suction and discharge phase.

The numerical results achieved using these different approaches were compared with measurements collected at the test bench during experimental campaigns on the compressors. The objective of these comparisons was to understand the influence of the accuracy in the flow coefficient evaluation on the working cycle prediction.

As shown in Table 5.1, the cylinders simulated have extremely different characteristics for both geometrical features (i.e. number of valves, cylinder material, bore and valve diameters) and working fluids in order to understand how the requirements in terms of flow coefficient accuracy depend by the specific case.

Figure 5.4 shows the suction and discharge flow coefficients (scaled by means of the maximum in-cylinder value) as a function of the ratio between the piston position (x) and the piston stroke (S) of the 3+3 nodular cast iron cylinder of Table 5.1 ("*Cylinder 1*") calculated by means of the CFD parametric routine described in Chapter 3.

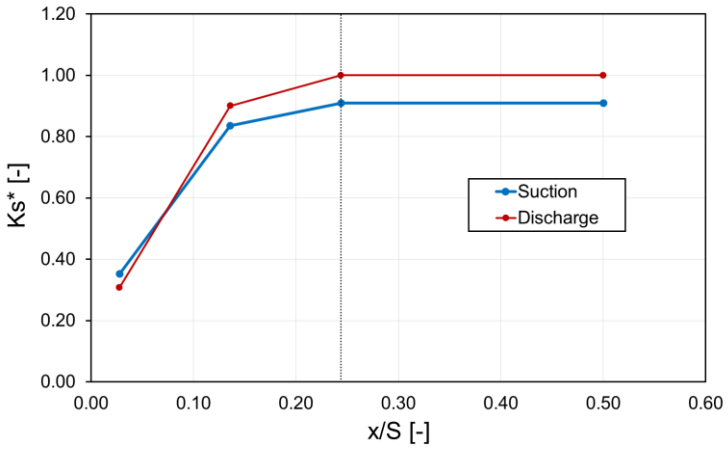

Figure 5.4 – 3+3 NCI cylinder: suction and discharge global flow coefficients at different piston positions

The comparison of the experimental p-V cycle with the results of the 1D model are shown in Figure 5.5, using the global flow coefficients obtained with all the approaches described.

In all the next figures, the values of pressure are reported in a dimensionless form (p^*), normalized by the suction pressure (p_s) and the discharge pressure (p_d) as follows:

$$p^* = \frac{(p - p_s)}{(p_d - p_s)}$$

Therefore, $p^*=0$ corresponds to the suction pressure and $p^*=1$ corresponds to the discharge pressure.

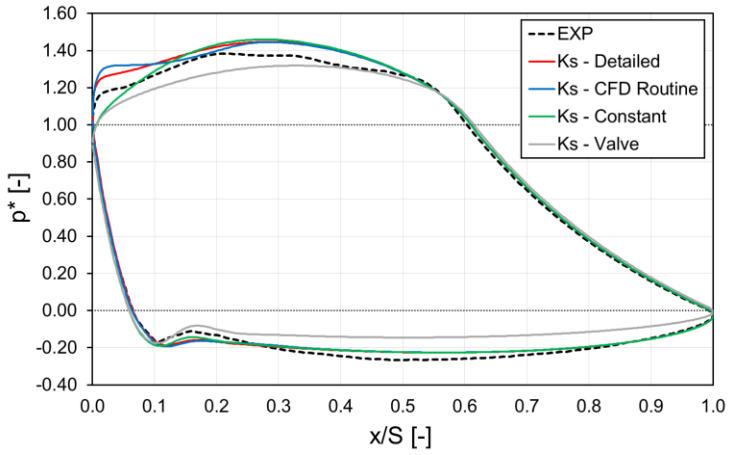

Figure 5.5 – 3+3 NCI cylinder: comparison between measured and numerical *p-V* cycle using the FVM numerical model with different *Ks*

The results confirm the importance that a correct estimation of the global flow coefficients for both suction and discharge phase has for the prediction of the *p-V* cycle by means of low order models. In fact, the error introduced when the valve flow coefficient is used as global flow coefficient is extremely high with an underestimation of the global pressure losses in both suction and discharge phase. This underestimation allows understanding the effect of the valve pocket and plenum losses on the performance of the machine. In fact, the valve flow coefficient doesn't allow considering the overall pressure losses in the compression chamber and plenum domain and results in an overestimation of the efficiency of the reciprocating compressor.

On the contrary, the results of the simulation with constant flow coefficients reveal a better agreement with the experimental measurements for both suction and discharge phase. In this case, also the valve pocket and the plenum losses are taken into account, thus obtaining a more accurate estimation of the overall pressure losses in the machine. However, the use of a constant flow coefficient neglects the piston masking effect and the increase of the pressure losses when the piston is located near to the compression chamber head. This effect is extremely evident in the last part of the discharge phase when the numerical results using the constant *Ks* (green line) highlight an underestimation of the pressure losses with respect to the experimental results. On the other hand, this underestimation is less evident during the suction phase; in fact, the suction valve is closed at the beginning of the piston masking phenomenon that, for this reason, affects a smaller part of the piston stroke than the discharge phase.

A further increase of the numerical *p-V* cycle agreement with the experimental results is then achieved considering the piston masking effect by means of multiple CFD simulations realized with the piston located near to the compression chamber head. The numerical results obtained using the flow coefficients calculated by means of steady state CFD simulations showed an overestimation of the global pressure losses at the end of the discharge phase for both detailed approach and simplified parametric one. However, the trend of the experimental curve is correctly reproduced by the results of the FVM model with both flow coefficients.

Moreover, it is possible to observe that the results of the 1D model are similar when the detailed approach or the parametric one are used, thus confirming the validity of the parametric approach on the enhancement of the performance predictability of a reciprocating compressor with a strong reduction of the computational and set-up times.

To quantify the accuracy and reliability of the FVM model using different *K*s for the global pressure losses evaluation, the prediction capability of the compressor performance was assessed in terms of both the indicated absorbed power and on an evaluation of the matching of *p-V* cycle.

The first was evaluated by calculating the absolute error in the predicted power between the numerical results and the experimental measurements.

The latter was addressed making use of the coefficient of determination R^2 [41], defined as:

$$R^2 = 1 - \frac{\sum_{\vartheta=0^\circ}^{360^\circ}\left(p_{EXP}(\vartheta) - p_{NUM}(\vartheta)\right)^2}{\sum_{\vartheta=0^\circ}^{360^\circ}\left(p_{EXP}(\vartheta) - p_{EXP,AVE}\right)^2}$$

The experimental pressure was selected as the reference data to which the pressure variations of numerical models can be compared and $p_{EXP,AVE}$ represents the average pressure over a revolution of the crank-shaft.

Figure 5.6 and Figure 5.7 shows the values of the two parameters obtained for the 3+3 nodular cast iron cylinder, using the four different approaches described for the flow coefficient evaluation.

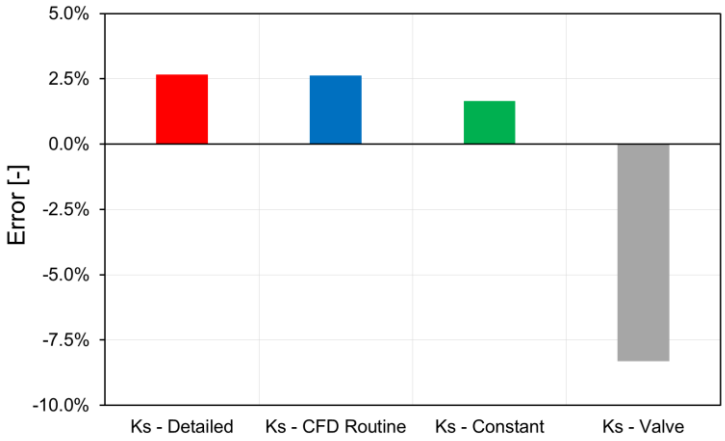

Figure 5.6 – 3+3 NCI cylinder: error in the prediction of the absorbed power using the FVM numerical model with different *Ks*

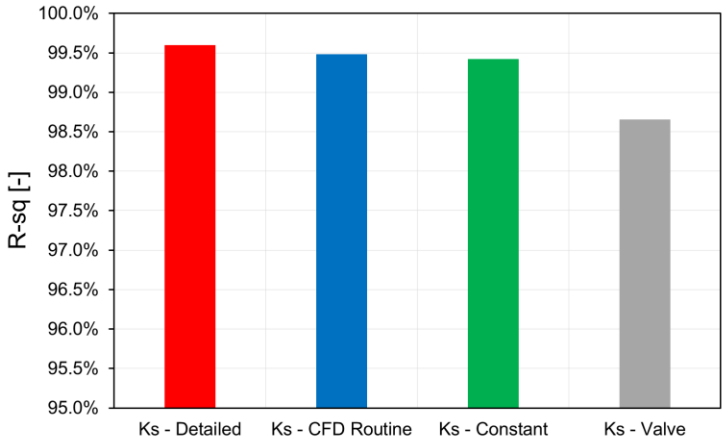

Figure 5.7 – 3+3 NCI cylinder: coefficient of determination using the FVM numerical model with different *Ks*

As expected, the error introduced using the valve flow coefficient is considerably higher than the corresponding achieved with the other approaches since it does not allow computing the compressor performance with an adequate accuracy. A power underestimation of about 8.5% was shown and the matching between the in-cylinder pressure cycles is the poorest since the R^2 is equal to 98.6%.

The detailed approach provides the best estimate of the trend of the pressure profile (R^2=99.6%) although in terms of absorbed power is slightly worse than the constant approach, with an error of 2.66%.

The CFD parametric approach gives similar results for both the absorbed power and the coefficient of determination (R^2=99.5%).

On the contrary, the numerical results obtained with a constant flow coefficient give the smallest error in the absorbed power estimation. However, this is not due to a better prediction of the *p-V* cycle (R^2=99.4%) but to an underestimation of the pressure losses at the end of the discharge phase (Figure 5.7) that allows balancing the overestimation in the first part of this phase. In other words, the global error in the absorbed power is lower than the other approaches only for the combination of two opposite errors during the discharge phase simulation.

In order to understand if the considerations made for the cylinder 3+3 NCI are confirmed also for cylinders having different geometrical features and working with different operating fluids, the *p-V* cycles of "*Cylinder 2*" and "*Cylinder 3*" in Table 5.1 were evaluated by means of the 1D model.

The suction and discharge global flow coefficients calculated by means of the CFD parametric routine for the 2+2 NCI cylinder are plotted in Figure 5.8.

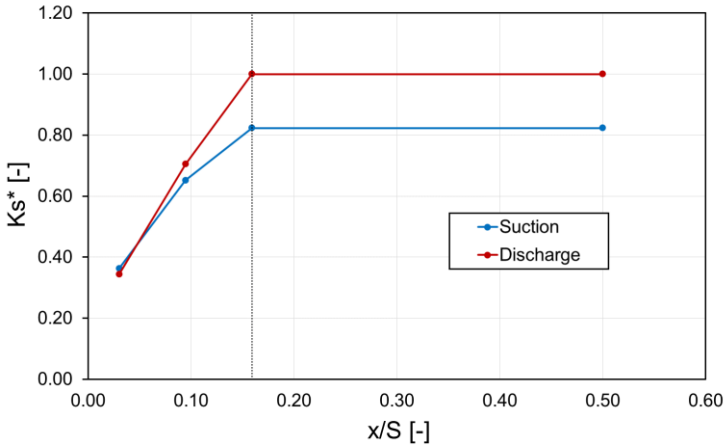

Figure 5.8 – 2+2 NCI cylinder: suction and discharge global flow coefficients at different piston positions

The *p-V* cycle was achieved using the flow coefficients of the parametric approach and the results were compared with the experimental measurements.

Moreover, the working cycle was calculated also using the constant and the valve flow coefficient (Figure 5.9).

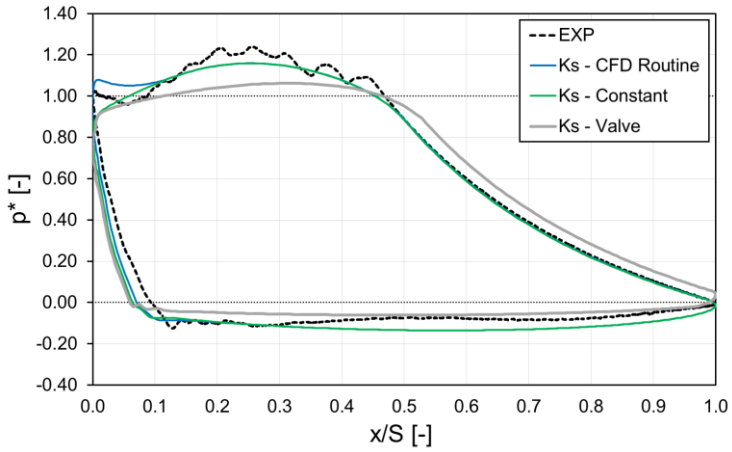

Figure 5.9 – 2+2 NCI cylinder: comparison between measured and numerical *p-V* cycle using the FVM numerical model with different *Ks*

The global agreement between the numerical results and the experimental measurements is worse than the corresponding obtained for the "*Cylinder 1*".

The comparison between the numerical and the experimental *p-V* cycles confirms that the error introduced using the valve flow coefficient is again the highest. In particular, for this cylinder, also the compression and the expansion phases are not correctly reproduced. Moreover, the underestimation of the discharge pressure losses shown by the "*Cylinder 1*" is repeated, thus confirming the importance to take the compression chamber and the plenum pressure losses into account for an accurate prediction of the *p-V* cycle.

A better agreement is achieved when CFD simulations are used for the flow coefficients evaluation (green and blue lines in Figure 5.9). In fact, a perfect overlapping of the compression curve between the numerical and experimental results is obtained; however, the error in the expansion curve persists also for these approaches.

The global errors in the absorbed power (Figure 5.10) are higher than the "*Cylinder 1*" with the only exception of the valve flow coefficient approach that nevertheless shows the lowest coefficient of determination (R^2=96.2% in Figure 5.11) due to the low matching between the numerical and the experimental in-cylinder pressure cycles.

On the other hand, the best agreement with the experimental measurements revealed by the *p-V* cycle is confirmed when the *Ks* of the CFD parametric routine is used (R^2=98.9%). Moreover, the experimental trend at the end of the compression phase is once again correctly reproduced only when the flow coefficient evaluation is made by means of multiple CFD simulations (blue line in Figure 5.9).

Figure 5.10 – 2+2 NCI cylinder: error in the prediction of the absorbed power using the FVM numerical model with different *Ks*

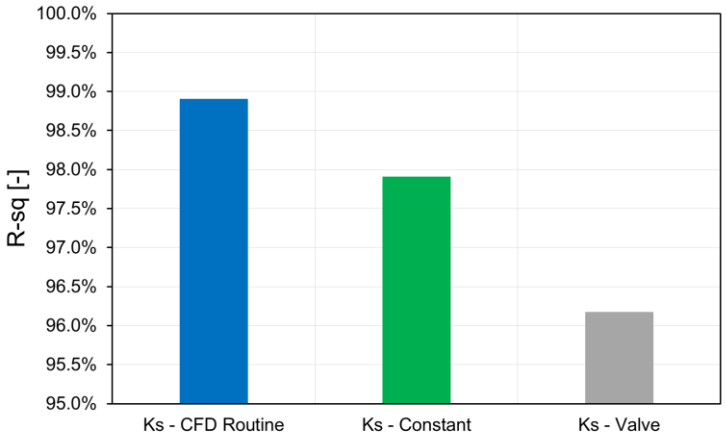

Figure 5.11 – 2+2 NCI cylinder: coefficient of determination using the FVM numerical model with different *Ks*

Finally, a third cylinder ("*Cylinder 3*" in Table 5.1) was simulated and the numerical results were compared with the experimental measurements. The most important objective of this final comparison was to understand the effect of the working fluid on the requirements in terms of flow coefficient accuracy.

For this reason, a cylinder that works with H_2 as working fluid was chosen; in fact, the hydrogen has the lowest molecular weight with respect to the typical operating fluids used in the large bore reciprocating compressors analyzed in this work.

The suction and discharge global flow coefficients of this last cylinder (2+2 CS cylinder) calculated by means of the CFD parametric routine are shown in Figure 5.12.

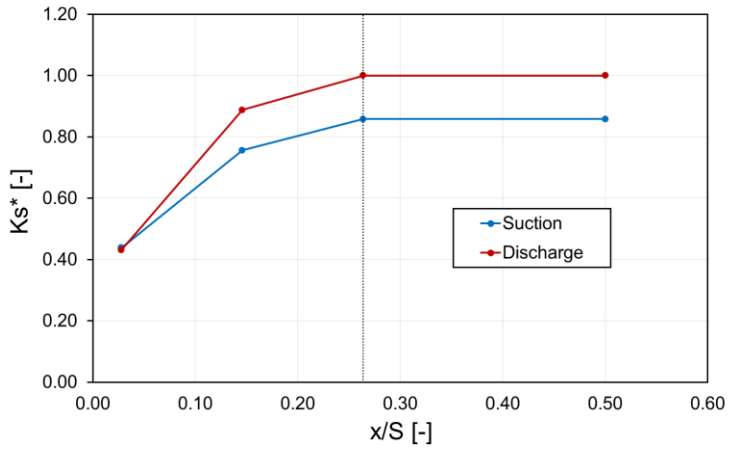

Figure 5.12 – 2+2 CS cylinder: suction and discharge global flow coefficients at different piston positions

With reference to Figure 5.12, it is important to remember that all the results of the CFD parametric routine were obtained using pure nitrogen as working fluid (Paragraph 4.2). For this reason, they include the error due to the variation of the operating fluid with respect to the "reference" one used for the CFD simulations (Paragraph 3.9). On the other hand, the fluid used in the 1D model is the actual one.

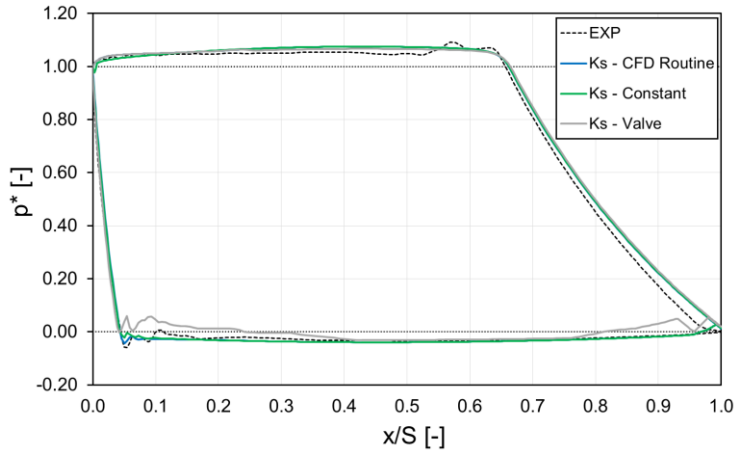

Figure 5.13 – 2+2 CS cylinder: comparison between measured and numerical *p-V* cycle using the FVM numerical model with different *Ks*

The comparison between the numerical results achieved with different approaches for the flow coefficient evaluation and the experimental measurements is shown in Figure 5.13. The clearest difference with the *p-V* cycles of the "*Cylinder 1*" and "*Cylinder 2*" shown in Figure 5.5 and Figure 5.9 is the lowest global pressure losses during the suction and discharge phases.

In fact, both phases have quite constant curves; moreover, the pressure difference during the discharge phase with respect to the value in the discharge ambient is extremely lower than the corresponding exhibited by the others cylinders.

This pressure increase after the valve opening is due to the inertia of the outflowing gas caused by the large extension of the compression chamber. The lowest inertia of the hydrogen with respect to the others working fluids allows explaining the lowest pressure difference between the actual discharge pressure and the theoretical one. Similar considerations can be made also for the suction phase.

Another important aspect to highlight from Figure 5.13 is the similarity between the numerical curves obtained using different flow coefficients. This aspect allows understanding that the *Ks* accuracy has a less important effect on the *p-V* cycle prediction when the working fluid has a low molecular weight.

Nevertheless, also for this cylinder the numerical curve obtained with the valve flow coefficient shows the worst agreement with respect to the experimental measurements, in particular for the suction phase prediction. On the other hand, the other curves highlight a best agreement with the experimental results and an almost perfect overlapping with one another thus explaining that the piston masking effect is negligible in this case.

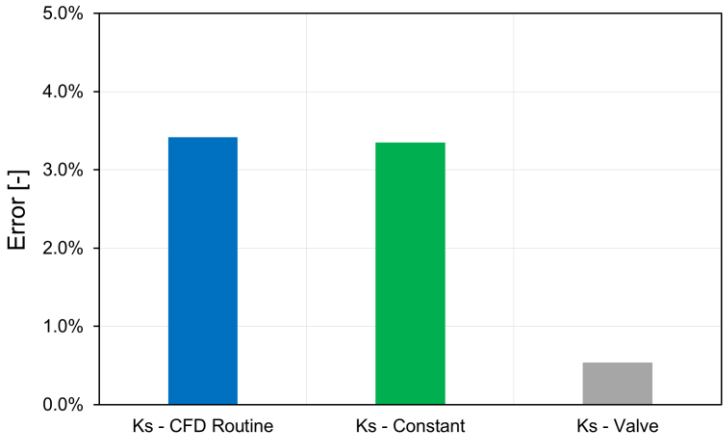

Figure 5.14 – 2+2 CS cylinder: error in the prediction of the absorbed power using the FVM numerical model with different *Ks*

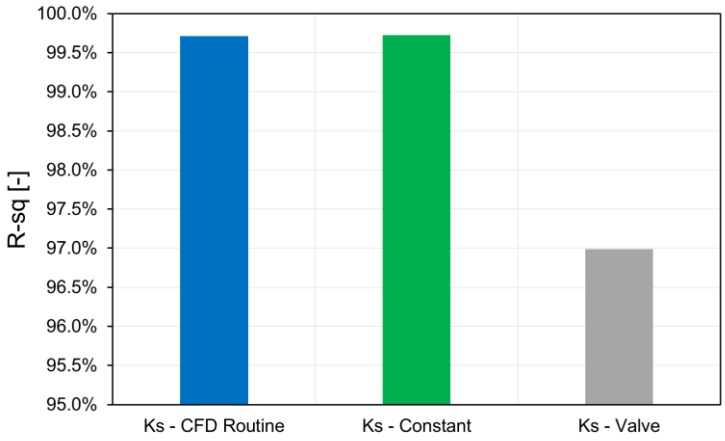

Figure 5.15 – 2+2 CS cylinder: coefficient of determination using the FVM numerical model with different *Ks*

Good results are achieved for both the error in the absorbed power (Figure 5.14) and in the coefficient of determination (Figure 5.15).

The error in the absorbed power evaluation using the CFD global flow coefficients is due to a not perfect overlapping in the compression curve. However the good agreement with the *p-V* cycle is confirmed by the high coefficient of determination (R^2=99.7% for both the CFD Routine and the Constant flow coefficient approaches).

A lower error in the absorbed power is obtained with the valve flow coefficient; however, the lower coefficient of determination (R^2=97.0%) confirms the worst agreement between these results and the experimental one. The lower difference shown in Figure 5.14 is once again due to the combination of two opposite errors; in fact, the underestimation of the working cycle area during the suction phase allows balancing the corresponding overestimation during the compression one.

These considerations allows concluding that the lower is the inertia of the working fluid, the lower is the influence of the flow coefficient in the *p-V* cycle prediction; nevertheless, the importance to use CFD simulations for the performance predictability enhancement is confirmed also for a working fluid having a low molecular weight.

6 CFD two-dimensional approach

6.1 Introduction

In Chapter 5 the *p-V* cycles obtained with a finite volume 1D model for different cylinders were shown; the accuracy of the results were highlighted by means of the comparisons of the numerical results with the experimental data collected on dedicated tests bench.

As explained in Paragraph 5.2, 0D-1D models represent the most common approach for predicting the compressor performance because of the low computational cost.

However, CFD simulations can represent a viable tool for the analysis of the working cycle. Due to the complexity of the geometry and the large extent of the fluid domain, unsteady three-dimensional CFD simulations are very demanding in terms of computational resources, resulting in unreasonably lengthy simulations and specialized hardware requirements.

The use of a two-dimensional CFD modeling strategy could be a solution aimed at reducing the computational effort by ensuring a compromise between the accuracy of the results and the simulation costs.

In this chapter, a methodology to perform a 2D CFD simulation of the working cycle of a reciprocating compressor is defined in order to provide more accurate results than low-order models and, at the same time, to guarantee the reduction of the computational effort with respect to unsteady 3D CFD simulations.

In more detail, the analysis presented in this chapter were carried out for the double-acting large bore cast iron cylinder, whose compression chamber was shown in Figure 5.1. The simplifications required to allow the reduction of the three-dimensional fluid domain to an equivalent two-dimensional configuration are shown. In particular, the suction and discharge duct pressure losses are modeled making use of the flow coefficients calculated with the parametric CFD routine described in Chapter 3.

The obtained results are compared to experimental measurements; a satisfactory agreement was achieved when comparing the numerical data to the measurements of dynamic pressure sensors placed in the cylinder head, clearance volume adjustment plugs and suction and discharge nozzles.

A comparison with the simulation results of low-order numerical models is also shown to highlight the enhancement in the performance predictability.

The matching between experimental and simulated results, together with the short calculation time, confirms the high potential of the proposed solution in predicting the expected performance of the machine, in terms of indicated power and specific work. Moreover, additional benefits are related to the possibility of investigating the pressure oscillations and distributions in the cylinder chambers, and the mass flow rates for the analysis of the suction and discharge pipelines.

6.2 Case study

As explained in Paragraph 6.1, the 2D CFD numerical model was used to simulate the working cycle of the compressor of Figure 5.1, using pure nitrogen (N_2) as working fluid.

Numerical results were compared with measurements collected at the test bench during an experimental campaign on the compressor. Experiments have been conducted on the compressor at full load conditions at a rotating speed of 375 rev/min. The head end side of the cylinder was equipped with multiple dynamic pressure sensors for monitoring the compressor operation.

The pressure in the compression chamber was monitored using a pressure sensor located in the center of the head (P_H). Three sensors are used to monitor the suction valves head pressure (P_{S1}, P_{S2}, P_{S3}), three for the discharge valves head pressure (P_{D1}, P_{D2}, P_{D3}) and two sensors for the suction and discharge nozzles (P_{N1}, P_{N2}).

In Figure 6.1 and Figure 6.2 are shown respectively the global domain of the head end side effect of the simulated cylinder and the location of the pressure sensors.

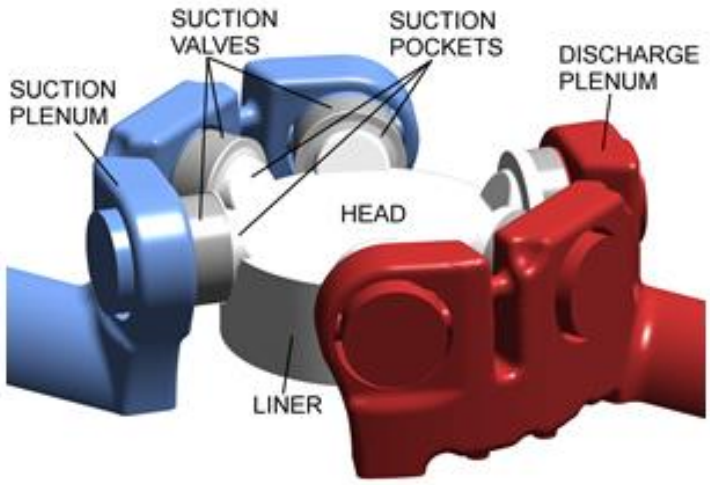

Figure 6.1 – Global fluid dynamic domain for head end side effect of the cylinder

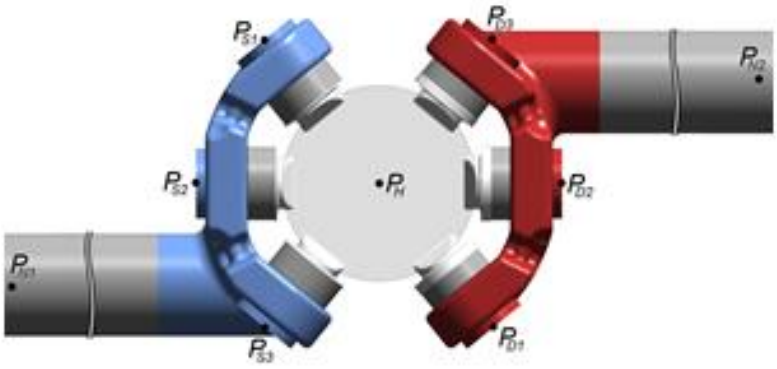

Figure 6.2 - Locations of the pressure sensors

Figure 6.3 shows the experimental data collected as a function of the ratio between the piston position (x) and the piston stroke (S), where the values of pressure are reported in a dimensionless form (p^*), normalized by the suction pressure (p_s) and the discharge pressure (p_d) (Paragraph 5.4):

$$p^* = \frac{(p - p_s)}{(p_d - p_s)}$$

The pressure trend in both suction and discharge valves is referred to the central valve.

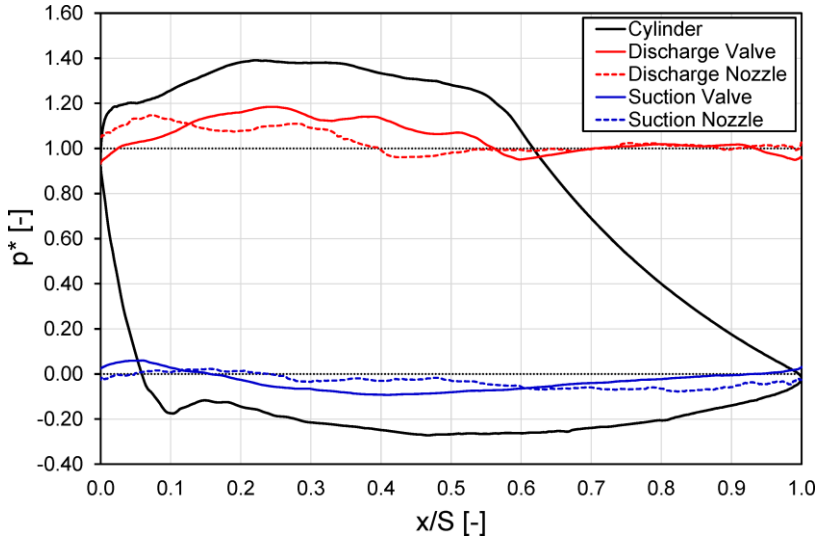

Figure 6.3 - Experimental diagram of the working cycle

6.3 Two-dimensional strategy

The three-dimensional approach is the only able to really describe the actual functioning of the machine. The valves orientation, the valve-retainer geometry and the complexity of the plenum shape impose the fluid flow to follow a strongly three-dimensional path. Notwithstanding this, the development of a robust transient 3D CFD approach requires unreasonably lengthy simulations and large computational resources, due to the huge extension of the overall fluid domain.

On the other hand, lumped parameter models, which are the easiest models to implement, fail to correctly predict the working cycle.

One-dimensional models (Chapter 5) are thought to be the best compromise in terms of accuracy of the prediction and computational costs and complexity, but they require a much greater effort from the point of view of the numerical implementation since no dedicated software is available. However, both lumped parameter and 1D models require the knowledge of the global flow coefficient to correct predict the performance of the machine.

Therefore, the goal of the model described in this chapter was to define an approach ensuring the best compromise between performance predictability, computing effort and programming of numerical code.

The computational resources required for a 2D simulation are compatible with the requirements in the design phase, although much higher in comparison to low-order models. Notwithstanding this, the main advantage is the possibility of using general purpose commercial or open-source CFD codes, thus avoiding the need of writing and implementing an in-house FVM software.

Within these preconditions, in this work it was investigated the potential of a 2D simulation strategy in enhancing the predictability of the thermodynamic cycle of reciprocating compressors.

The first step for the definition of the 2D model is the transformation from the original 3D geometry into an equivalent 2D representation [42].

For this purpose, the idea is to extend the methodology proposed by Balduzzi [3] and [15] to transient simulations for the working cycle prediction. As shown in Paragraph 3.6.1 this methodology is based on a simplified CFD approach in which the valve geometry is replaced with an equivalent porous medium that generates a localized pressure drop equivalent to the actual valve. Starting from this idea and considering the complex geometry of both valves and plenums, their fluid volumes was treated as porous mediums, without the need of a geometrical characterization. In this way, the fluid-dynamic parameters (Ks_v and Ks_p) can be calculated by means of the simplified CFD parametric routine described in Chapter 3, with the benefit of a reduction both in the runtime and in the time required for setting up the model.

Therefore, the plenums and valves regions were simply modeled as rectangular equivalent porous regions with the purpose of replicating the main effect of the actual geometry on the flow (i.e. the same pressure drop).

The length of each porous region, which acts as an equivalent distributed source of pressure loss, is analogous to the actual length of each correspondent component. Each porous coefficient is computed by means of its correspondent flow coefficient.

As a result, the fluid domain is decomposed in seven separate regions, as shown in Figure 6.4.

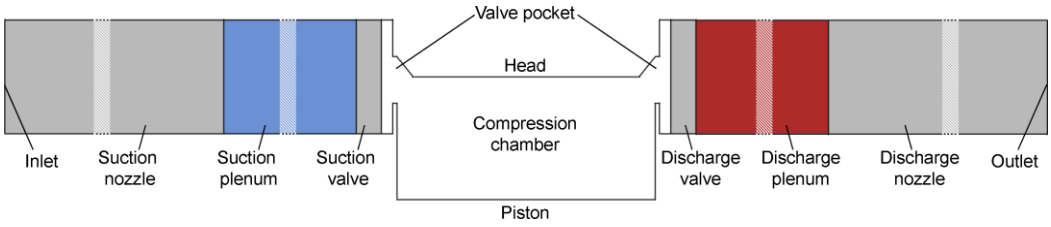

Figure 6.4 - 2D computational domain

In addition, also the reduction of the compression chamber volume required a special treatment [42]. When dealing with large size reciprocating compressors, the flow inside the cylinder has a preferential direction (i.e. the flange-to-flange direction). The results of the 1D FVM model shown in Paragraph 5.4 revealed that a discretization of the compression chamber volume along the diametrical axis connecting suction and discharge central valves is suitable to catch the main phenomena of pressure wave propagation and mass flow of gas inside the cylinder.

For the 2D representation, the second dimension was added in the direction of the cylinder axis, since the flow is strongly guided by the valve pocket shape and by the interaction with the moving piston. The transversal direction is therefore neglected, suppressing directional effects caused by lateral valves, which anyhow are deemed to be of secondary relevance.

As a result, the geometry of the cylinder and the valve pockets was modeled through a simplified 2D representation (Figure 6.5) in the plane containing the cylinder axis and parallel to the flanges axes, by means of the following features [42]:

- The cylinder is reduced to a rectangular area, defined by the cylinder bore (B) and the cylinder height (H_c), expressed as the sum of the piston stroke (S) and the clearance (c) between the piston and the head at the Top Dead Center (TDC);
- For both suction and discharge geometries, the three valve pockets are reduced to a single equivalent pocket defined by two critical cross-section: the pocket throat (t) and the pocket height (H_P). Both cross sections are computed by

imposing the same ratio of the actual flow sections, by means of the following relations:

$$\frac{H_P}{B} = \frac{3\frac{\pi {D_v}^2}{4}}{\frac{\pi B^2}{4}}$$

$$\frac{t}{B} = \frac{3A_t}{\frac{\pi B^2}{4}}$$

where A_t is the throat area of the three-dimensional pocket.

Moreover, the angle (β_s) and the length (L_s) of the slide due to the machining on the cylinder head are analogous to the actual ones. Due to the 2D approximation, the constraint on the pocket throat does not allow preserving the angle when the piston starts the masking of the window of the valve pocket, since the masking height is not preserved.

- The pocket length (L_P) was computed in order to guarantee the same volumetric compression ratio; the area at TDC is equal to 12% of the displacement ($B \times S$ in the 2D case).

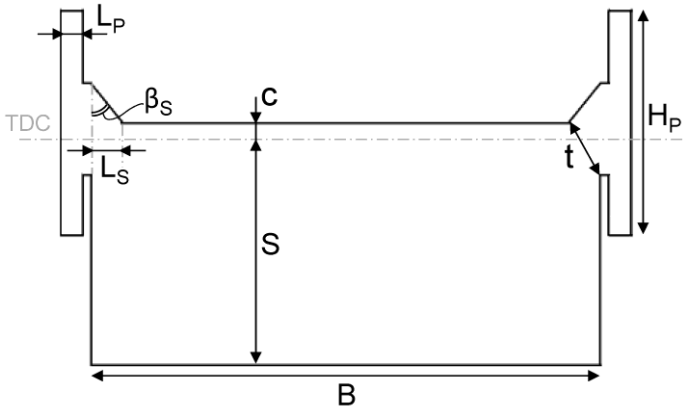

Figure 6.5 - Relevant dimensions for the 2D representation of the compression chamber

Finally, the inlet and outlet ducts shown in Figure 6.4 have the same length of suction and discharge nozzles.

6.4 Numerical setup

The time-dependent unsteady Reynolds-averaged Navier-Stokes equations were solved with the commercial code ANSYS FLUENT in a two-dimensional form by employing a finite-volume method.

As discussed in Paragraph 6.2 the working fluid was pure nitrogen (N2), modeled as an ideal compressible gas. The PISO scheme was selected for the treatment of the pressure–velocity coupling. The governing equations were discretized by a second-order upwind scheme for spatial discretization while the turbulence model adopted was the Standard k-ε in combination with the enhanced wall treatment for the computation of the boundary layer in the near-wall region. The temporal discretization was obtained using an angular time step of 0.1°.

The compression chamber was discretized by means of a Cartesian grid, featuring 60659 rectangular elements at the Bottom Dead Center (BDC), in order to allow the simulation of the piston motion during the working cycle. The mesh motion was performed by adopting a dynamic layering on the piston (i.e. by adding or removing layers of cells adjacent to the boundary).

The suction and discharge porous mediums used for the modelling of the valves and plenum were meshed using a Cartesian grid of 2825 and 23391 rectangular elements, respectively, while an unstructured grid of 36428 triangular elements was used for the inlet and outlet ducts in order to allow a faster coarsening of the grid. As a result, the total number of elements at BDC is 185947. Due to the piston layering, the number of elements at TDC decreases down to 133262.

A pressure-inlet boundary condition is imposed at the inlet of the suction nozzle domain. The values of pressure and temperature measured inside the suction vessels were defined in the model. A pressure-outlet boundary condition is imposed at the outlet of the discharge nozzle domain, where only the value of experimental pressure is provided.

Wall boundaries are considered adiabatic; in fact, the studied cylinder is water-cooled thus avoiding the heat conduction from the hot discharge zone to the suction and compression chambers. More details on the thermal state of the compressor cylinder are

given in Chapter 7 where the results of a conjugate heat transfer (CHT) simulation, validated against experimental measurements, will be shown.

The opening and closing of the suction and discharge valves is automatic and it is regulated by the pressure differences between the compression chamber and the suction and discharge ducts. When a valve is closed, a wall is placed between the pocket and the adjacent porous medium. During the valve opening, the wall condition is substituted with an interface that allows the communication between the porous medium and the fluid region of the pocket. The valve dynamics can be neglected, since the duration of opening and closing phases is in the order of 1÷2°, due to the low revolution speed.

6.5 Results

Based on the methodology described in Paragraph 6.3, the working cycle of the head-end of the double-acting cast iron cylinder was simulated and compared to both measured data and numerical predictions of low-order models (both the 1D model described in Chapter 5 and lumped parameter numerical model).

Figure 6.6 shows the comparison of the experimental in-cylinder pressure with the results of the 2D CFD simplified model. The computed suction and discharge mass flow rates are also reported.

The instantaneous values of mass flow rate are in a dimensionless form (m^*), normalized by average mass flow rate for cycle:

$$m^* = \frac{m}{\frac{1}{T}\int_0^T m(t)dt}$$

where T is the global time for cycle.

Both the mass flow rate and the in-cylinder pressure are shown as a function of the ratio between the TDC distance (x) and the piston stroke (S).

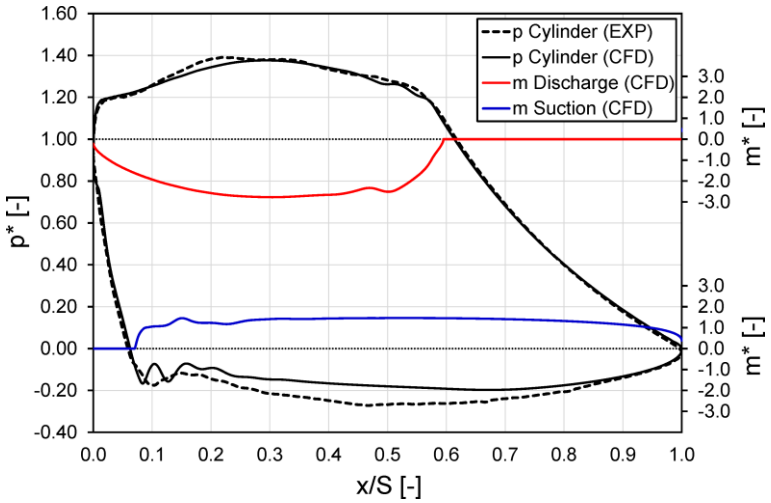

Figure 6.6 - Comparison between computed and measured in-cylinder pressure; computed suction and discharge mass flow rate profiles

From the results in Figure 6.6, some first outcomes become apparent:

- Compression and expansion phases are matching perfectly. This is indeed an important outcome as it testifies the consistency of the modeling approach in evaluating the correct elaborated mass of gas per cycle;
- The pressure trends during the discharge phase are almost superimposed. It is apparent that both the distribution of pressure losses and the gas inertial and dynamic effects are correctly reproduced. In particular, after the valve opening, the inertia of the outflowing gas can be seen from the gradual increase of the discharge mass flow rate, due to the large extent of the compression chamber. As a result, the piston keeps compressing the gas up to 20% above the value in the discharge ambient even if the discharge valve is already open.
- The computed pressure during the suction phase is higher than the measured values. This behavior is probably due to an underestimation of the pressure losses. Notwithstanding this, the pressure values at the BDC are matching, denoting an analogous volume filling.

Focusing the attention on the matching between pressure trends during the suction and discharge phases, Figure 6.7 and Figure 6.8 show the instantaneous pressure as a function of the piston position considering the discharge and suction sensors, respectively. The comparison between measured and computed values is carried out for the cylinder head, the valves and the nozzles sensors.

From a perusal of both figures, it is possible to note that the global amplitude and the phasing of pressure oscillations are comparable. In particular, the discharge wave reaches the valve and nozzle sensors at the correct time, then the trends of increasing pressure have analogous slopes and the maximum overpressure is correctly predicted in terms of both position and magnitude.

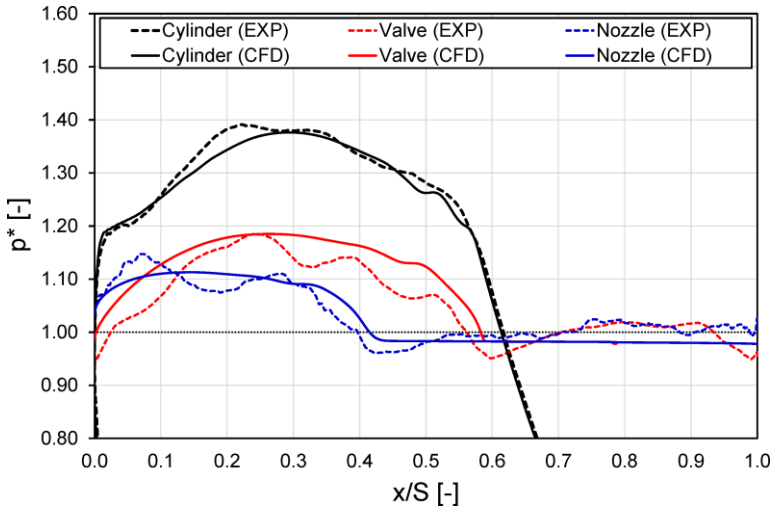

Figure 6.7 - Comparison between computed and measured pressure during the discharge phase at three locations: cylinder head, discharge valve head and discharge nozzle

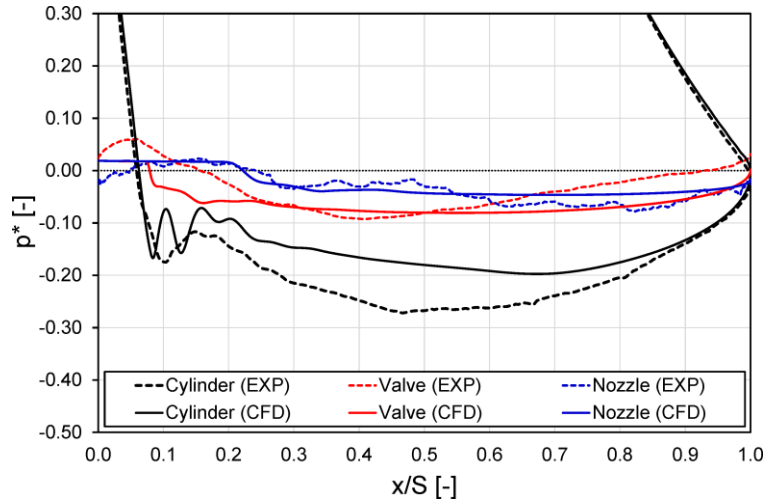

Figure 6.8 - Comparison between computed and measured pressure during the suction phase at three locations: cylinder head, suction valve head and suction nozzle

The only difference lies in the presence of high-frequency fluctuations in the experimental data due to reflections of the pressure waves along the components of the gas chamber. The presence of valve cages, bend ducts and T-junctions is indeed ignored in the simplified 2D geometry and only their primary effect is introduced through a distribute source of pressure loss. However, wave reflections inside these components represent a secondary effect that is less significant for the *p-V* cycle prediction.

To better clarify some of the phenomena described in the analysis of the compression cycle, Figure 6.9 and Figure 6.10 show the contours of pressure (expressed in a dimensionless form by means of the discharge pressure) and the flow streamlines in the cylinder and in the discharge line at two different crank-angle (ϑ) positions.

In particular, Figure 6.9 refers to ϑ=266°CA, corresponding to few degrees after the discharge valve opening (x/S≈0.6). The pressure wave traveling along the plenum volume is clearly visible, as well as the "advancing front" of discharge gases. Focusing on the cylinder volume, a non-uniformity on the pressure distribution is apparent. This latter phenomenon is related to the inertia of the outflowing gas, as illustrated by the streamlines: only the portion of gas close in proximity of the discharge pocket is starting the discharge process, while the largest amount of volume is "undisturbed", therefore is still experiencing the compression.

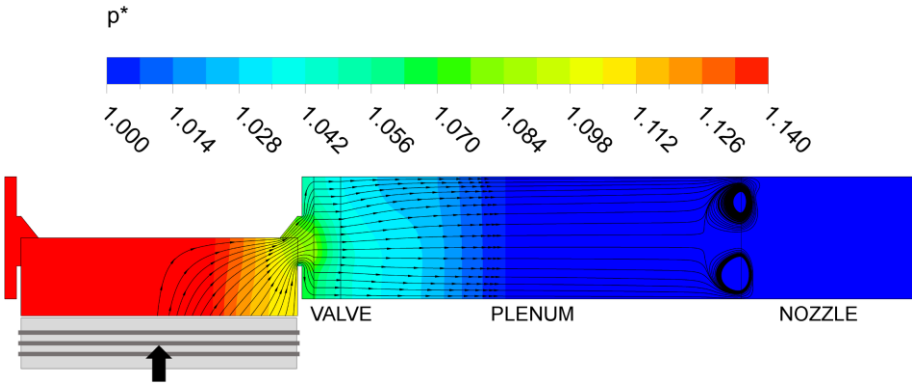

Figure 6.9 - Discharge phase @266°CA: pressure contours and flow streamlines

Figure 6.10 refers to ϑ=300°CA, corresponding to the position where the cycle reaches the maximum pressure (x/S≈0.3). In this condition, the discharge flow is experiencing the maximum pressure drop and the distribution of the losses can be easily observed.

As expected, the largest drop is localized inside the porous medium of the valve, representing roughly half of the global loss (~48%). However, also the valve pocket and the gas plenum have a strong impact on the irreversibility associated with viscous friction, since they contribute to ~23% and ~29% of the global loss, respectively. Therefore, an accurate prediction of their losses and a suitable representation of their fluid-dynamic response are pivotal to correctly account for all of the effect that contribute to the gas exchange process of the machine.

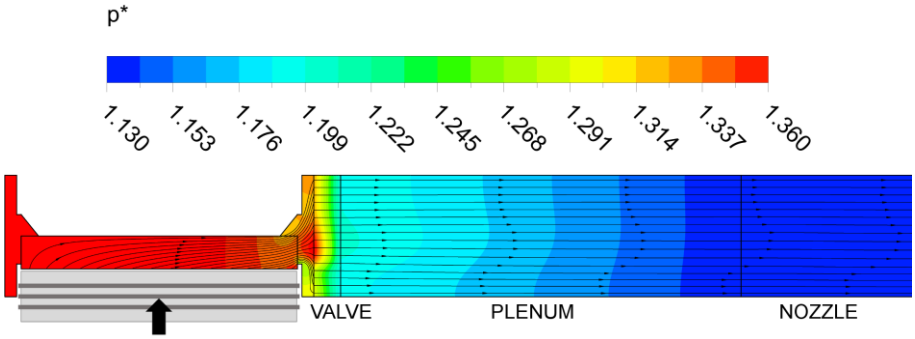

Figure 6.10 - Discharge phase @300°CA: pressure contours and flow streamlines

The results of the 2D CFD simulations were finally compared with the results obtained on the same test case with low-order numerical models (Figure 6.11).

In more detail, the comparison were made with the results of the 1D model described in Chapter 5 and with the corresponding results achieved with a lumped parameter numerical model (0D) developed by the REASE GROUP of the Industrial Department of the University of Florence [2].

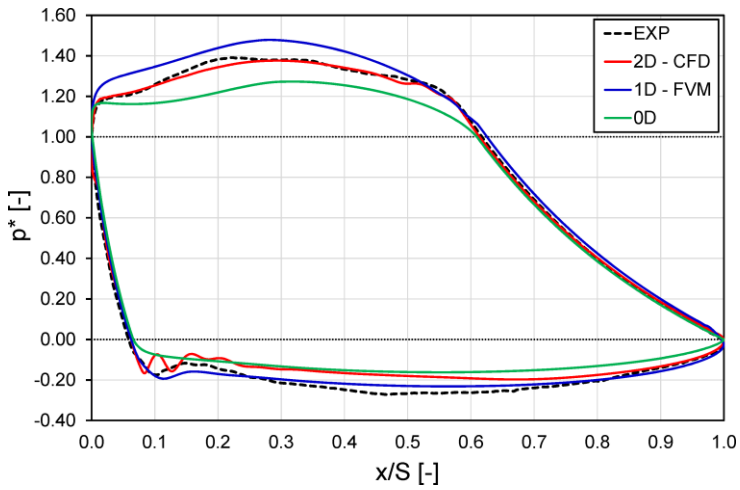

Figure 6.11 - In-cylinder pressure: comparison between measured values and results of different numerical approaches

The lumped parameter model underestimates the absorbed work, since the predicted pressure is higher than the measured pressure during the suction phase and lower during the discharge phase. In particular, the deviation from the experimental curve occurs at the angular positions of valves opening: the 0D approach does not allow accounting for the inertial effect of the mass flowing in and out the compression chamber. It is possible to clarify this behavior focusing on the discharge phase: the pressure variation inside the cylinder at each step depends on both the amount of mass flowing out from the cylinder and the volume reduction. Since the volume reduction is the same for all of the models, the lower in-cylinder pressure predicted by the 0D model is due to a higher mass flow rate after the valve's opening. The mass flow rate depends on the flow coefficients, which are the same for all of the models, and on the pressure difference between cylinder and discharge plenum. Thanks to the volume discretization, the 1D and 2D models evaluate the local pressure difference across the throat section, while the 0D model performs the calculation with averaged values. The local reduction of pressure shown in Figure 6.9, which delays the discharge of gas, is not accounted for in the 0D model, thus leading to a faster discharge process.

On the contrary, both the FVM and the 2D model are able to correctly reproduce the pressure increase after the discharge valve opening and the pressure reduction after the suction valve opening.

Finally, the absolute error in the predicted power between the numerical models and the experimental measurements and the coefficient of determination R^2 (Paragraph 5.4) were evaluated in order to quantify the accuracy and reliability of the numerical models.

Figure 6.12 shows the values of the two parameters for all of the three analyzed numerical models.

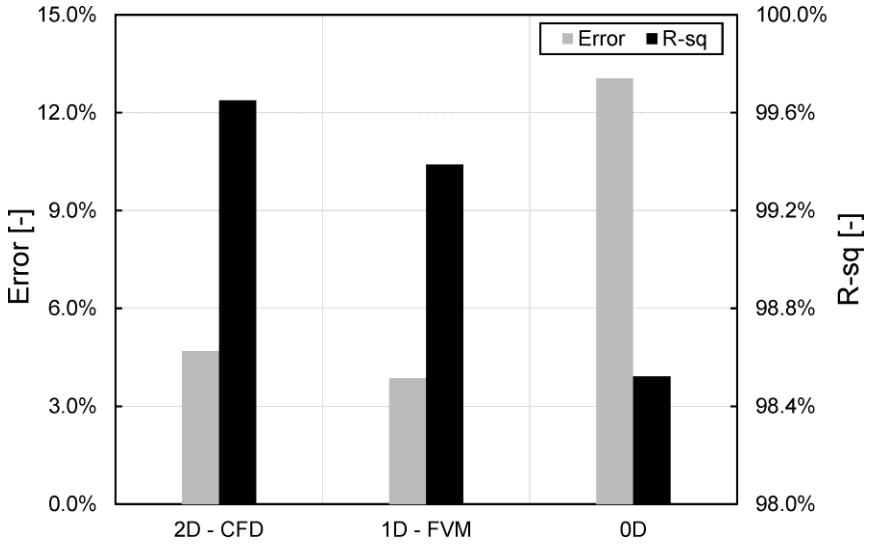

Figure 6.12 – Error in the prediction of the absorbed power and coefficient of determination: comparison between different numerical approaches

As expected, the lumped parameter model is considerably worse than the other approaches since it does not allow computing the compressor performance with an adequate accuracy. A power difference of about 13% was estimated and the matching between the in-cylinder pressure cycles is the poorest since the R^2 is lower than 98.5%. The 2D CFD model provides the best estimate of the trend of the pressure profile (R^2=99.6%) although in terms of aggregate parameter is slightly worse than the FVM model, with an error in the absorbed power of 4.7%.

Concerning the calculation time, low order models are very fast if compared to CFD models. Indeed, 0D and 1D models have a time scale of few seconds to achieve convergence. Conversely, a 2D simulation has a time scale of few hours for a single run, while the simulation time for a full 3D run is estimated in 4÷6 days.

6.6 Modeling strategies

An extended sensitivity analysis for the assessment of the proper simplifications required to allow the reduction of the three-dimensional fluid domain to an equivalent two-dimensional representation was carried out in a preliminary stage [42].

Different configurations were tested by varying the pockets simplification, the porous mediums definition and extension and the compression chamber geometry.

In the present paragraph, the results of some preliminary choices are shown, aimed at highlighting the effect of some critical features for an accurate two-dimensional simulation of a reciprocating compressor. In more detail, three particular geometrical configurations were selected; these configurations serve as a representative sample and cover the most important aspects in order to differentiate between influential or non-influential characteristics, with respect to the results described in the previous paragraph for the "*Baseline*" configuration.

It is worth pointing out that all of the investigated features not only directly affect the accuracy of the final result but also have a mutual influence between themselves; the analysis tried to decouple the effects of each choice and to highlight their impact on the simulation outcomes.

Concerning the modeling of the valve pockets, the results of a more simplified geometry are reported to assess the required detail level of the pocket shape to adequately predict the pocket losses.

Figure 6.13 shows the computational domain of the analyzed configuration (indicated in this work as "*Configuration 1*") where a basic rectangular shape was used, therefore neglecting the shape of the pocket window and the machining on the head.

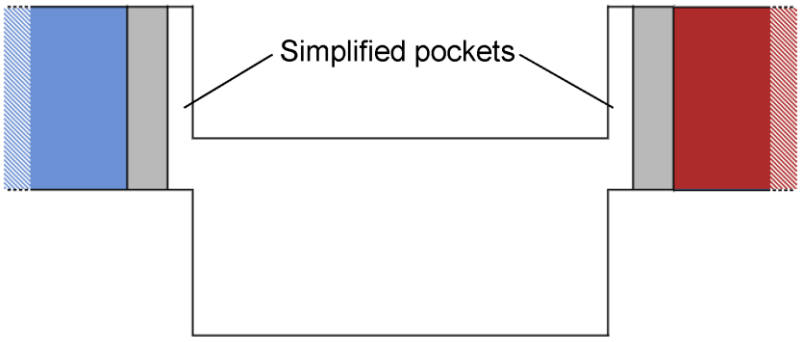

Figure 6.13 - Computational domain of the "*Configuration 1*" with simplified pocket shape

With respect to the "*Baseline"* geometry, the pocket length (L_P) is increased in order to guarantee the same dead volume while the masking height is not modified.

In order to evaluate the influence of the modeling of porous mediums, a simplified configuration that uses a single porous medium for modeling the pressure losses of valve and plenum is analyzed. This configuration is indicated in this work as "*Configuration 2*" and is shown in Figure 6.14.

In the "*Baseline"* configuration, the valve loss and the plenum loss were modeled separately using two different flow coefficients for each phase, acting as two equivalent distributed sources of pressure loss. The new combined porous medium length is calculated considering the sum of the valve and plenum length while the global resistance coefficient *F* is computed in order to obtain the analogous global pressure drop of valve and plenum, as reported in the following equation:

$$F = \frac{1}{(L_v + L_p)Ks^2_{(v+p)}}\left(\frac{A_{por}}{A_{ref}}\right)^2$$

The cylinder geometry is not modified with respect to the "*Baseline"* configuration.

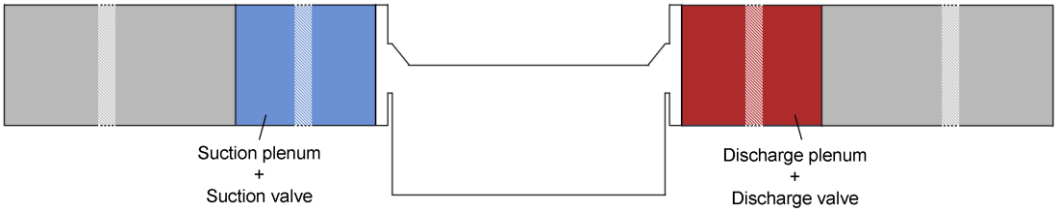

Figure 6.14 - Computational domain of the "*Configuration 2"* with combined porous mediums

Finally, to examine the effect of fine details of the compression chamber geometry on the response of the model, a different strategy for the definition of the two critical cross-section of the pockets is analyzed ("*Configuration 3*").

In place of the imposition of the equivalence of the pocket throat *t*, as for the "*Baseline*" configuration, the pocket shape is defined by maintaining the same masking height H_m of the 3D geometry (Figure 6.15). This implies that, conversely to the "*Baseline*" configuration, the piston starts the masking of the windows of the valve pockets at the correct angular position. On the other hand, the 2D throat section *t* increases, not being anymore consistent with the ratio between the actual throat area and the piston surface of the 3D geometry.

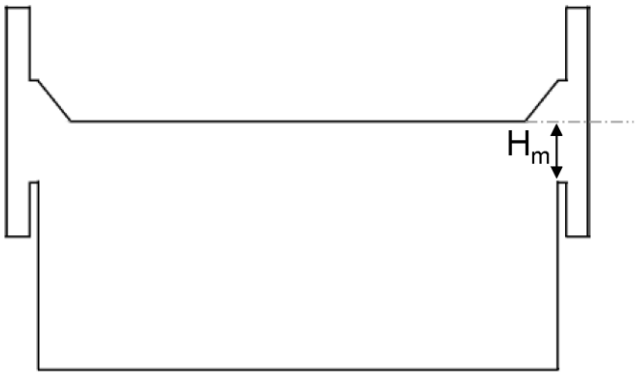

Figure 6.15 - Computational domain of the "*Configuration 3*" with corrected masking height

On these bases, a comparative analysis was carried out between the selected configurations with the goal of establishing the sensitivity of the compression cycle to the modified characteristics.

Figure 6.16 reports the comparison of the experimental in-cylinder pressure with the results of all of the four 2D CFD numerical configurations.

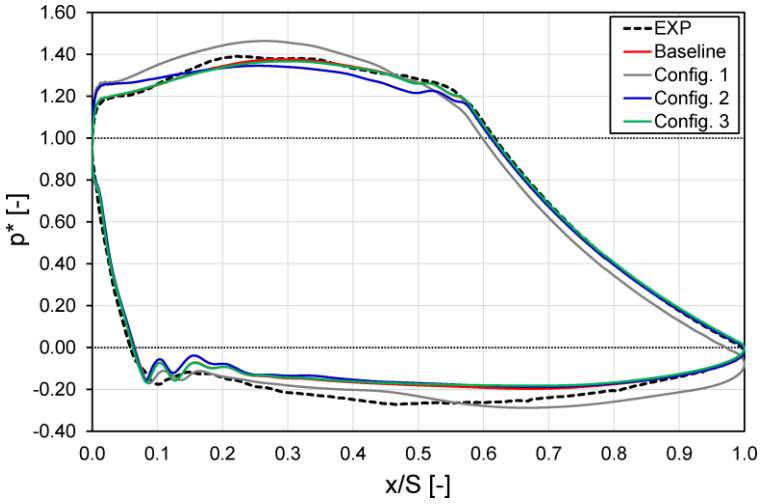

Figure 6.16 - In-cylinder pressure: comparison between measurements and results of four numerical models

From the results of Figure 6.16 the following observations can be made:

- The results of "*Configuration 1*" reveal a substantial modification of the working cycle with respect to the "*Baseline*". In particular, a large increase of pressure drops during both the suction and discharge phases can be observed. As a consequence, the pressure trend during the compression phase is not matching

anymore with the experiments. Therefore, the model is not able to predict the correct elaborated mass of gas per cycle;

- The results of "*Configuration 2"* reveal a slight modification of the dynamic response, in particular during the discharge phase. Globally, the working cycle is not significantly affected when considering a single "combined" porous medium, although the in-cylinder pressure is moderately underestimated in the first part of the discharge and overestimated when getting closer to the TDC;
- The results of "*Configuration 3"* reveal an almost equivalent behavior with respect to the "*Baseline"* configuration.

Within these considerations, the analysis was further examined in depth by focusing on a more detailed evaluation of the pressure trends during the suction and discharge processes.

Figure 6.17 and Figure 6.18 report the same comparisons of Figure 6.16 showing the zooms of the high pressure and low pressure phases of the cycle, respectively. In this way, the small-scale differences can be appreciated, especially for "*Configuration 2"* and "*Configuration 3"*, which were still in good agreement with the experimental data.

Starting from "*Configuration 2"*, the change in the porosity distribution along the suction and discharge lines affects the outflow of gas at the time of valve opening. Indeed, the phenomenon of pressure increase with discharge valves already open, observed experimentally and also numerically with the "*Baseline"* model, is interrupted in advance. This leads to a subsequent lower pressure during the largest part of the discharge phase.

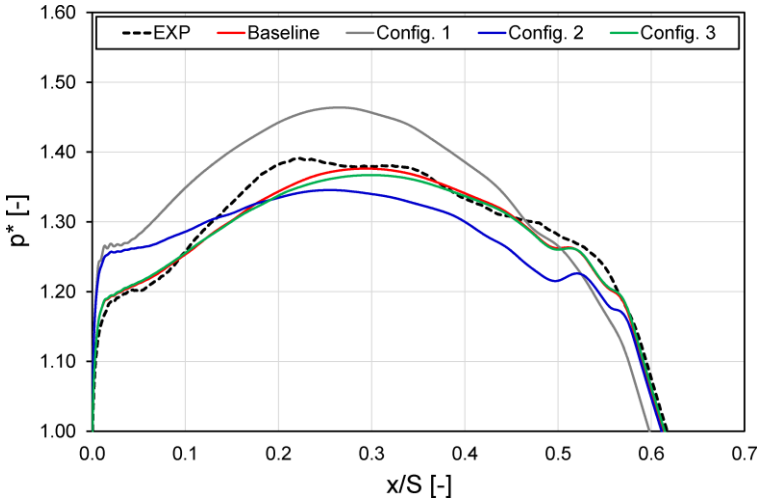

Figure 6.17 - In-cylinder pressure during the discharge phase

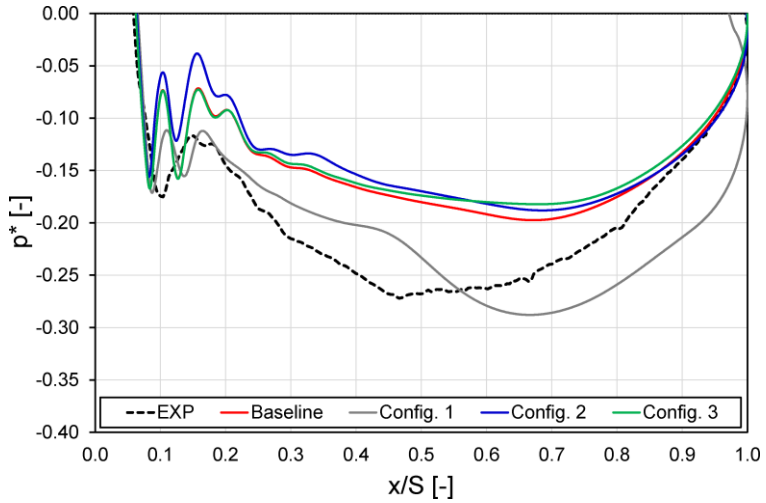

Figure 6.18 - In-cylinder pressure during the suction phase

To analyze this inconsistency, Figure 6.19 reports the pressure contours and the flow streamlines in the cylinder and the discharge line at ϑ=300°CA. The whole porous medium representing both valve and plenum is characterized by an almost linear decrease of pressure, conversely to Figure 6.10 for the "*Baseline*" configuration, in which a strong decrease of pressure is concentrated in a short length corresponding to the valve. Although the global resistance of the two modeling approaches is analogous, the splitting of the two contributions is necessary to provide the correct resistance to the flow in correspondence of the exact distance from the cylinder.

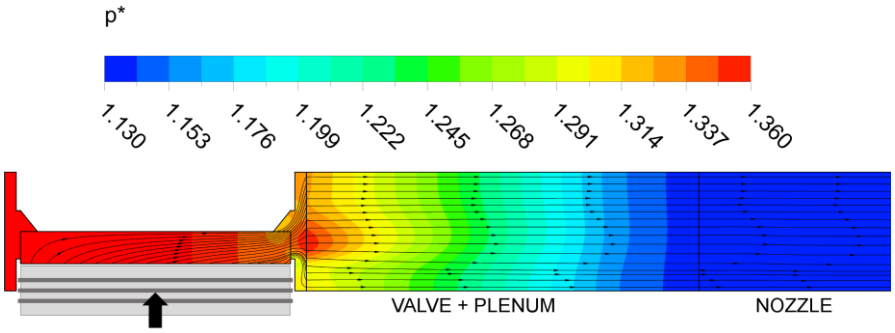

Figure 6.19 - Pressure contours and flow streamlines for the "*Configuration 2*": discharge phase @300°CA

Moving to "*Configuration 3*", an almost negligible variation of pressure levels reached during the suction and discharge phases can be detected.

This is related to the minimal increase of the throat section when changing the masking height, which leads to a reduction of the pocket losses. With particular reference to the suction phase, the prediction is slightly worsened.

The attention was then focused on the comparison between the propagation of pressure waves in the suction and discharge lines.

Figure 6.20 and Figure 6.21 show the experimental and numerical pressure oscillations in correspondence to valve heads and nozzles for the discharge system and suction system, respectively.

From a perusal of both figures, it can be easily seen that the effect of the modeling strategy of cylinder and porous mediums has a minor impact of the fluid-dynamic response of the ambient external to the cylinder. In particular, the pressure at both discharge and suction nozzles (Pictures b) is almost unaffected, since the curves for all of the tested configurations are almost superimposed.

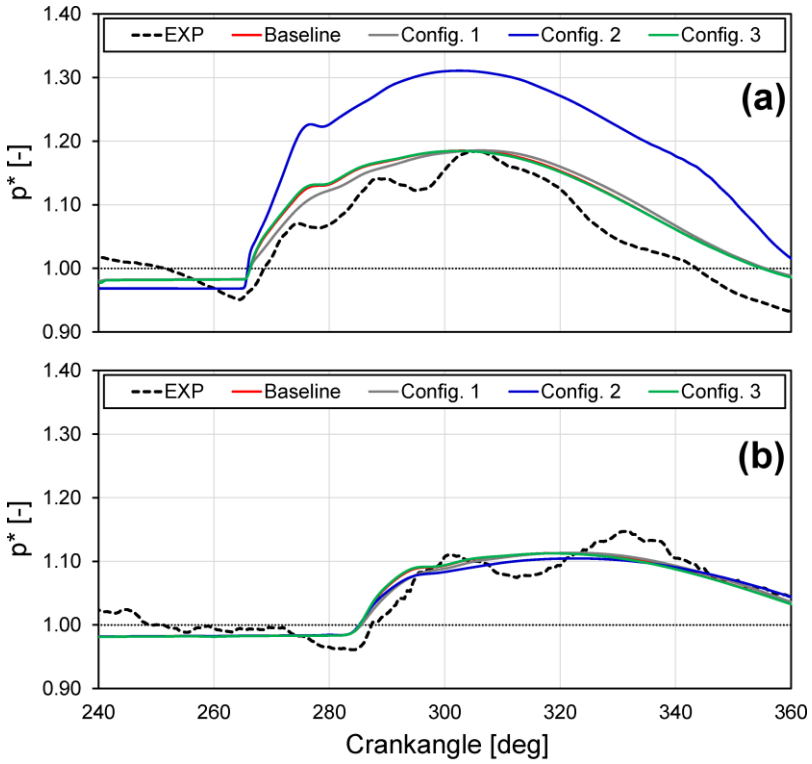

Figure 6.20 - Comparison between computed and measured pressure during the discharge phase at two locations: discharge valve head (Picture a) and discharge nozzle (Picture b)

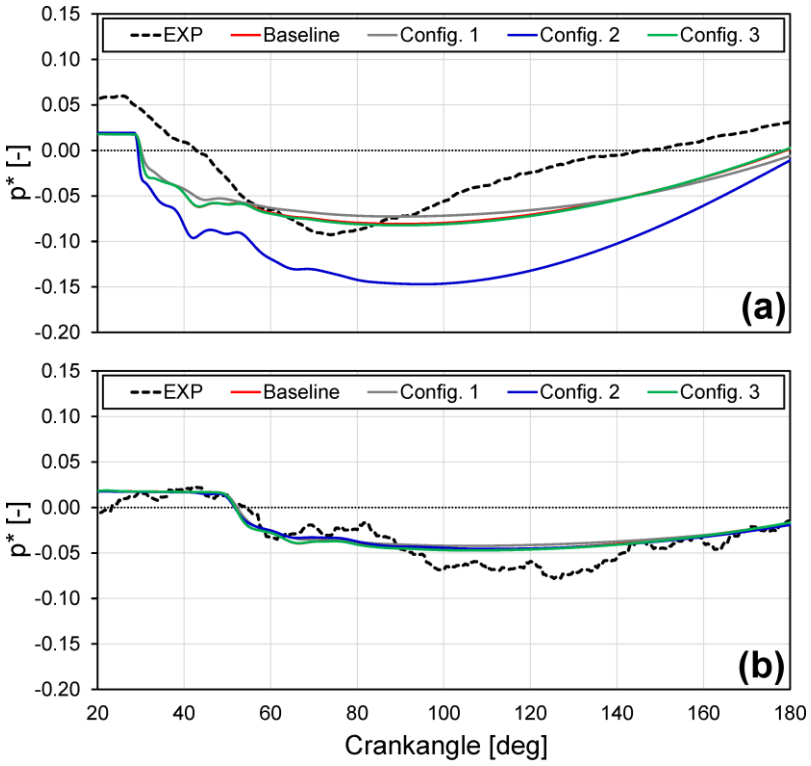

Figure 6.21 - Comparison between computed and measured pressure during the suction phase at two locations: suction valve head (Picture a) and suction nozzle (Picture b)

Moreover, also the pressure at both discharge and suction valve heads (Pictures a) is almost unaffected, with the exception of "*Configuration 2*". This behavior is simply related to the fact that with the combined porous medium there is no distinction between valve and plenum, therefore is not possible to define a location where placing the sensor for the valve head. In other words, the difference is due to an intrinsic limitation of such porous modeling and it does not affect the results of the simulation.

The last analysis was addressed to quantify the different prediction capability of the tested configurations by the evaluation of the matching with the experimental *p-V* cycle. The results in terms of coefficient of determination are illustrated in Figure 6.22.

As expected, "*Configuration 1"* is characterized by the lowest similarity with the measured data. Based on this evidence, it is clear that a suitable 2D model must include some critical features of the valve pocket in order to define an equivalent geometry. This requirement is due to the substantial influence of pocket losses on the compressor performance.

A better estimate of the trend of the pressure profile is provided by "*Configuration 2"*, although the matching is still worse than the "*Baseline"*. The correct distribution of sources of loss is pivotal to properly simulate the resistance offered to the flow and, therefore, the mass transport.

Only "*Configuration 3"* shows a R^2 almost analogous to the "*Baseline"* configuration. This implies that the level of geometrical detail reached is sufficient and such a small modification does not affect the model response.

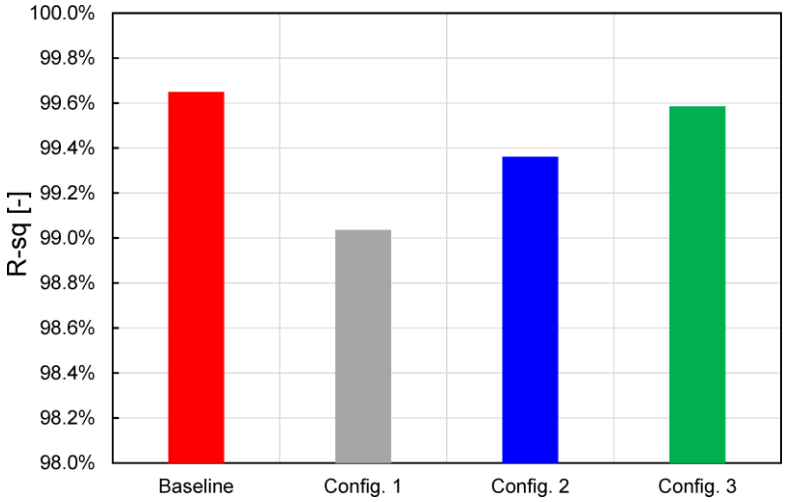

Figure 6.22 - Coefficient of determination: comparison between different geometrical configurations

7 CHT approach for the analysis of the cylinder cooling system

7.1 Introduction

Another important aspect that is typically taken into account in a reciprocating compressor is the analysis of the cylinder cooling system. In fact, the working cycle of a reciprocating compressor is characterized by heat generation, mainly due to compression transformation and friction phenomena. The main consequences are a reduction of the volumetric efficiency and an increase in the gas discharge temperature; current regulations require then a cylinder cooling system. A proper design of the cooling circuit is needed in order to achieve the best balance between refrigerating potential and system capacity.

A systematic methodology for the evaluation of the heat transfer process is essential and since experimental characterization of the circuit is complex and case-dependent, the use of numerical techniques is the most favorable and generalizable approach.

Within this scenario, 3D analysis shows a great potential, although several phenomena must be accounted for in order to accurately model the system.

For this reason, a conjugate heat transfer (CHT) approach for the analysis of the double-acting water-cooled reciprocating compressor cylinders was developed by the

REASE GROUP of the Industrial Department of the University of Florence jointly with Baker Hughes, a GE company [4].

Using this approach, the flow field of the water circuit and the thermal conduction inside the solid metal are solved simultaneously.

In this paragraph, a brief description of the numerical approach is given (Paragraph Figure 7.3); in particular, the possibility to use the numerical CFD routine of Chapter 3 for the forced convection modeling inside suction and discharge gas ducts is highlighted.

Moreover, the capability of the CHT approach to accurately predict both the thermal state and the temperature field of the cooling water of a double acting reciprocating compressor is shown (Paragraph 7.5). Therefore, the results of the three-dimensional simulations of the water-circuit flow field and the thermal conduction inside the solid metal were compared to temperature measurements collected on a dedicated test bench for both the coolant and the metal structure. Satisfactory agreement was obtained between the experimental data and the numerical computations.

7.2 State of the art

Large reciprocating compressor cylinders require the presence of a cooling system. The goals are to avoid the presence of cold and hot spots, to reduce the fresh gas heating due to hot cylinder body and to limit the thermal expansion of the metal parts, thus reducing the thermal stresses on the cylinder. On the other hand, the production costs increase due to the need of a cooling console and to the more complex shape, which complicates casting. Moreover the presence of the cooling circuit imposes undesired constraints and restrictions to the gas ducts' shape. The consequence is a deterioration of the fluid-dynamic performance due to the increased pressure loss of the working fluid.

Accurate numerical models for the prediction of the fluid-dynamics and heat generation of reciprocating compressor cylinders could represent a valuable step towards a more robust and effective design of the machines, with subsequent power and costs savings.

Most design tools used in the analysis of the performance are based on analytical models of compressors [43] and [44] but they introduce several simplifications that limit the applicability of these techniques. In particular, the possibility of replicating the actual

geometric shape of the fluid systems becomes crucial to ensure accurate predictions of the real behavior of the machine.

Examples of higher-level studies on full 3D simulations for the evaluation of the heat transfer in reciprocating compressors can be found in literature. Aigner [45] and Disconzi [46] simulated the heating process of the working gas only, without accounting for thermal conduction inside the solid metal. Abidin [47] considered also the metal structure, but fluid and metal domain were solved separately and their results are iteratively coupled.

A further improvement on the prediction of the cylinder thermal state was carried on in a previous work of the REASE GROUP of the Industrial Department of the University of Florence [4]. In this work, the simultaneous solution of the water-circuit flow field and the thermal conduction inside the solid metal (conjugate heat transfer) was proposed.

Though 3D simulations are deemed to provide accurate results, validation practices through experimental data are often not available, reducing the reliability of the numerical predictions.

This chapter addresses this latter aspect; in fact, the most important objective is the validation of the results of the conjugate heat transfer (CHT) simulation on a double-acting reciprocating compressor cylinder against measurements collected in a dedicated test campaign.

7.3 Conjugate heat transfer approach

In this paragraph, a brief description of the defined approach for the simulation of the heat transfer in a double-acting water-cooled reciprocating compressor cylinder is given. The simultaneous solution of the water-circuit flow field and the thermal conduction inside the solid metal (conjugate heat transfer) can be suitably achieved by performing a steady-state analysis, considering a constant mass flow rate through the cooling circuit [4].

A more accurate investigation would also require the simultaneous simulation of the flow of the working fluid (i.e. gas) being responsible for the heat generation. Complete consideration of the compression cycle does not allow a steady state approach since the increase in gas temperature occurring inside the compression chamber could be obtained only with the execution of a transient simulation of the working cycle [47]. However, the complexity of the 3D domain and the grid requirements would lead to an excessively large calculation time, making the steady-state analysis the most favorable approach.

Therefore, in the CFD method described in this paragraph, the heat transfer from the gas compression cycle is modeled as a boundary condition applied on the solid walls of the metal body, whose half section is shown in Figure 7.1 together with the water body.

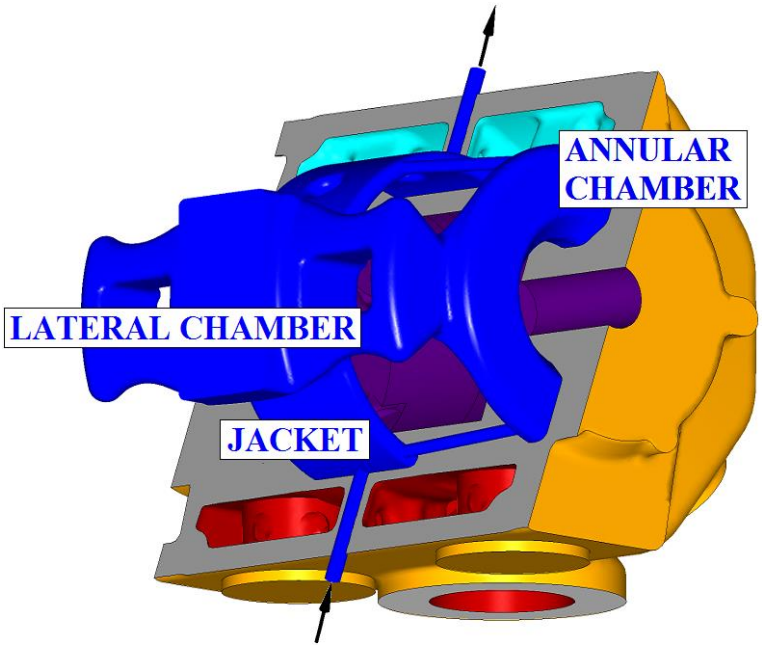

Figure 7.1 – Domain for the CHT analysis: water body in blue and surfaces of the metal body in orange (external), violet (compression chamber), red (discharge ducts) and light blue (suction ducts)

The cooling circuit is oriented such as the water enters from an inlet pipe, which is the side where the pressurized hot gas is discharged. At the end of the inlet duct, the water flows into the water jacket surrounding the cylinder walls; two lateral horizontal chambers are then addressed to the isolation of the hot side of the cylinder from the cold side. Both the jacket and the lateral chambers are connected to an annular chamber, on the crank-end side, for the cooling of the connecting rod packing.

Velocity-inlet and pressure-outlet boundary conditions were supplied for the simulation of the water flow.

The conservation of the heat flux between the water body and the metal body was ensured by a fluid-solid interface, whereas thermal boundary conditions were imposed for all other metal surfaces, in order to account for the various heat transfer phenomena:

- natural convection on the external cylinder surface;
- forced convection inside suction and discharge ducts;
- forced convection and heat generated by friction inside the compression chamber.

In the matter of heat transfer related to friction between piston and liner, the heat flux q through the boundary surfaces was known from experimental data.

Regarding the heat transfer related to a generic convective process, the metal temperature can be calculated by evaluating the heat flux q through the boundary surfaces, defined as:

$$q = HTC(T_w - T_{Bulk})$$

where T_w is the unknown wall temperature, HTC is the heat transfer coefficient between fluid and metal and T_{bulk} is the undisturbed fluid temperature.

The values of HTC and T_{bulk} were evaluated through a proper modelling of all the convection processes.

For the external natural convection, the heat transfer coefficients were determined with a simplified method.

McAdams correlations available in literature [48] were used, which provide the Nusselt-number (*Nu*) as a function of the Rayleigh-number (*Ra*) for vertical plates and horizontal plates having upper surface hot and lower surface hot respectively as:

$$Nu = 0.13(Ra)^{1/3}$$

$$Nu = 0.15\ Ra^{1/3}$$

$$Nu = 0.27\ Ra^{1/4}$$

In a first approximation, this simplification can be considered suitable since the amount of heat transfer with the ambient represents roughly 5-7% of the total heat exchange.

Concerning the convection inside the compression chamber, Fagotti [49] showed that best results are provided by Annand correlation for the Nusselt-number [50], expressed as a function of the average piston speed (v_p) and the piston bore (B) by means of the following relationship:

$$Nu = A\left(\frac{\rho v_p B}{\mu}\right)^b$$

Since the gas properties are notably variable inside the cylinder during a complete revolution, a 0D modeling of the compression cycle is required.

The correlation was used inside the 0D model in order to obtain the trend of the in-cylinder quantities as a function of the displacement (Figure 7.2).

In this thesis, the values of *HTC* are reported in a dimensionless form, normalized by the maximum in-cylinder value ($HTC^* \equiv HTC/HTC_{max}$).

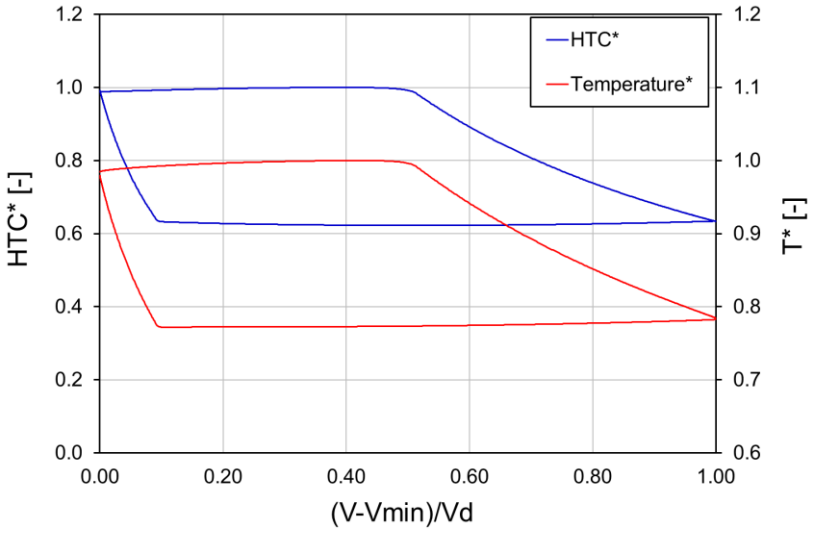

Figure 7.2 – Output of the 0D model: trends of HTC^* and T^*

An average effective value of both HTC^* and T^* was computed from the time-dependent functions to be imposed on the surfaces of the valve pocket, the cylinder head and the liner for the steady-state CHT simulations.

On the contrary, for the internal forced convection inside suction and discharge gas ducts, specific 3D CFD simulations were used in order to guarantee a more accurate estimation of the actual distributions of *HTC* and T_{bulk}.

At this scope, the parametric approach described in Chapter 3 can be used in order to reduce both the set-up and computational times with respect to the common approach used for the realization of CFD steady state simulations in a reciprocating compressor (Paragraph 3.3.1). For this reason, the *HTC* and T_{bulk} distributions can be extracted by the simulations of the suction and discharge domains making use of the *Master models* defined in Chapter 3 and patched as a boundary condition for the CHT simulations.

Figure 7.3 shows an example of the results of a steady-state simulation for the suction geometry of a 3+3 nodular cast iron cylinder.

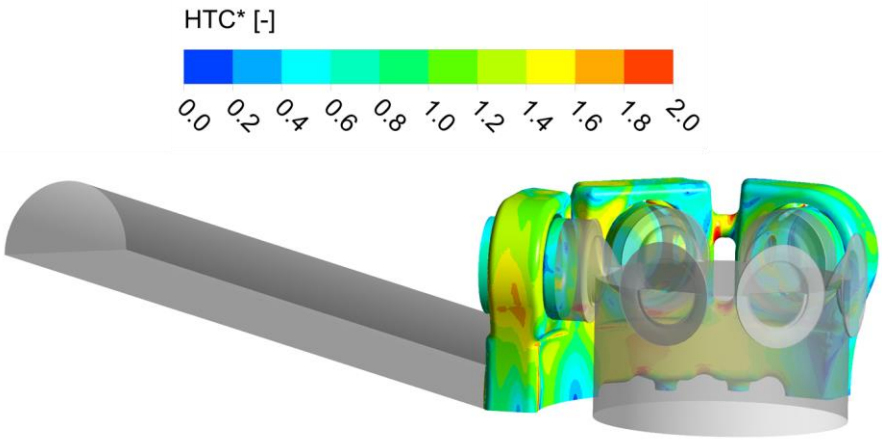

Figure 7.3 – Results of the 3D CFD simulation of the suction duct: Distribution of the HTC^* on the walls

The approach described is summarized in Figure 7.4, where all the boundary conditions for the simulation of the conjugate heat transfer between the solid cylinder body and the fluid cooling circuit are indicated.

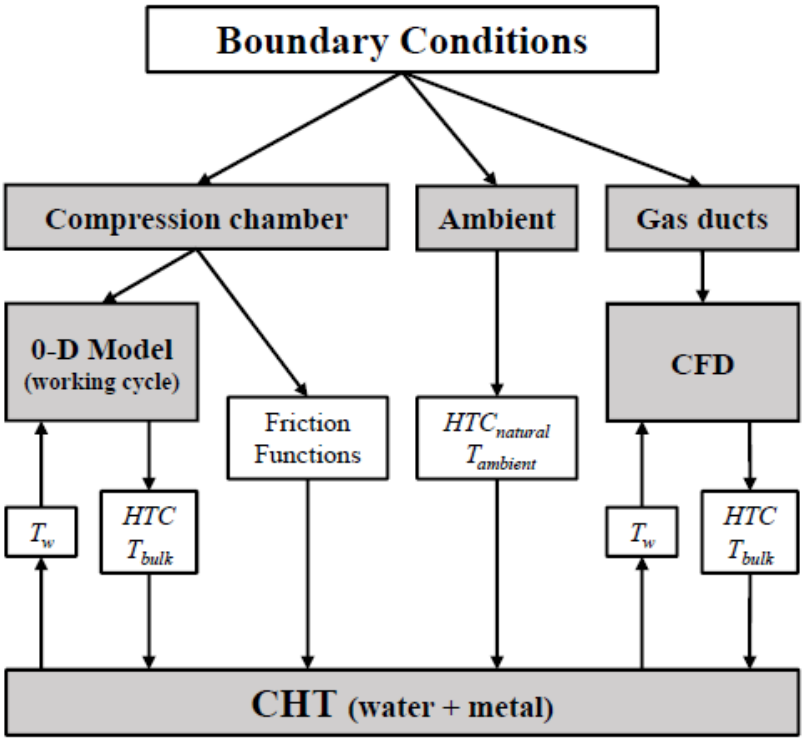

Figure 7.4 – Boundary conditions for the CHT simulation approach

The assessment and validation of the numerical settings for the 3D CHT simulations was treated in detail in previous works of the REASE GROUP of the Industrial Department of the University of Florence [4], [51] and [52]. For this reason, the details on the choice of simulation settings and on the mesh sensitivity analysis are not given in this thesis: however, a brief description of the most important CFD solutions adopted is shown below.

The simulations were performed with the ANSYS CFX software package by means of a 3D steady state Reynolds-Averaged Navier-Stokes (RANS) analysis. With this approach, all conservation equations are solved for the water fluid region, while for the solid region only the equation for heat transfer is solved, but with no flow.

The standard k-ω closure model was adopted to predict the complex turbulent structure of the confined flow, along with the automatic treatment in the near-wall region.

The effect of gravity was accounted for by activating the buoyancy model since the low fluid velocity and the large volumes are responsible of the free convection onset.

A tetrahedral unstructured grid was generated for the computational mesh of both the metal (Figure 7.5) and the water body (Figure 7.6). In addition, in the latter case, an extrusion of 16 prism layers was placed adjacent to the viscous wall, with an expansion ratio of adjacent cells below 1.1, in order to resolve the thermal boundary layer. The first cell at any surface point was sized such that y^+~1.

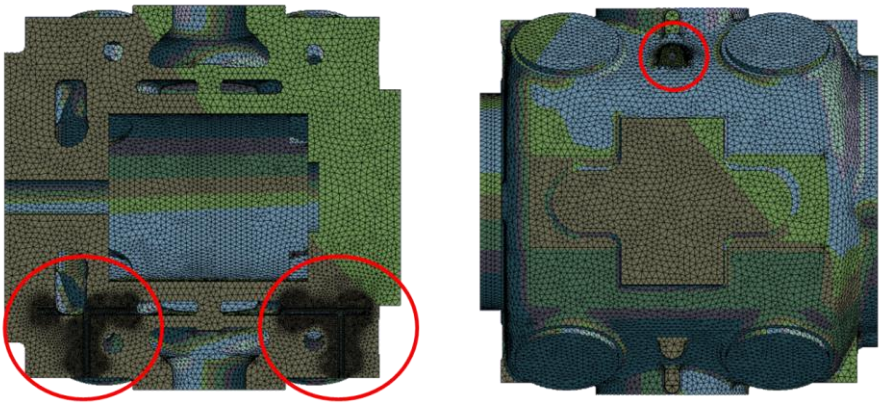

Figure 7.5 – Detail of the mesh used for the metal domain discretization

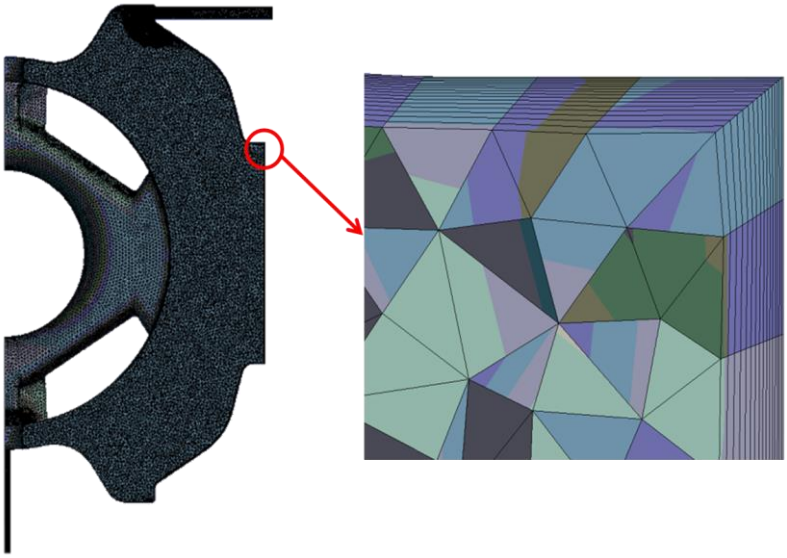

Figure 7.6 – Detail of the mesh used for the water body domain discretization

7.4 Case study: experimental apparatus

Experiments have been conducted on the 3+3 water-cooled double-acting cast iron cylinder of Figure 5.1 at full load conditions. The cylinder was equipped with multiple sensors for monitoring the working conditions.

The heating of the cooling water was measured using thermocouples located at the inlet and outlet sections of the cooling circuit.

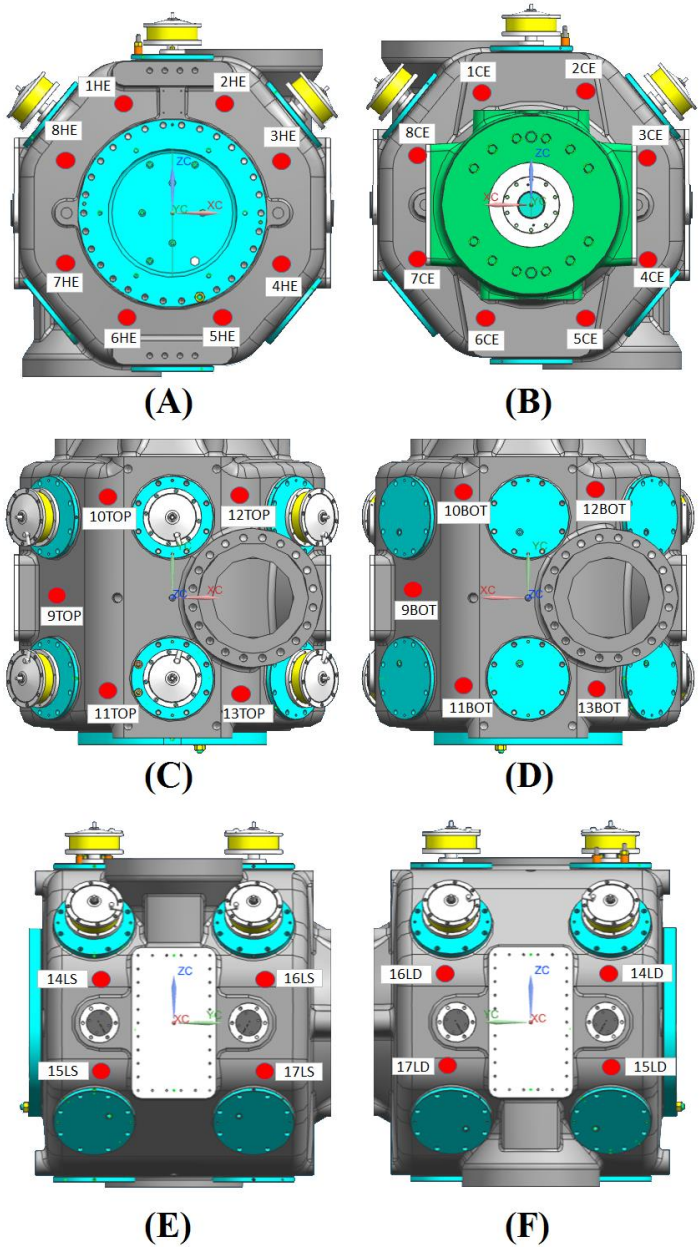

Figure 7.7 – Measuring locations on the cylinder surface: (A) Head-End view, (B) Crank-End view, (C) Top view, (D) Bottom view, (E) Lateral-Suction view, (F) Lateral-Discharge view

The thermal state of the cylinder body was also monitored. A discrete map of the external surface temperature was obtained by capturing the metal temperature using a radiation pyrometer.

Figure 7.7 shows the set of 34 acquisition points covering the whole cylinder wall:

- 16 locations on the cylinder ends, 8 on the head-end side (Picture A) and 8 on the crank-end side (Picture B);
- 10 locations in proximity of the suction and discharge flanges, 5 on the top side (Picture C) and 5 on the bottom side (Picture D);
- 8 locations on the lateral vertical surfaces, 4 on the side of the suction flange (Picture E) and 4 on the side of the discharge flange (Picture F).

7.5 Results

In order to evaluate the predictive capabilities of the CHT simulation and also investigate the thermo-fluid dynamics of the considered compressor, the thermal state resulting from the simulation with the CHT approach is reported below [53].

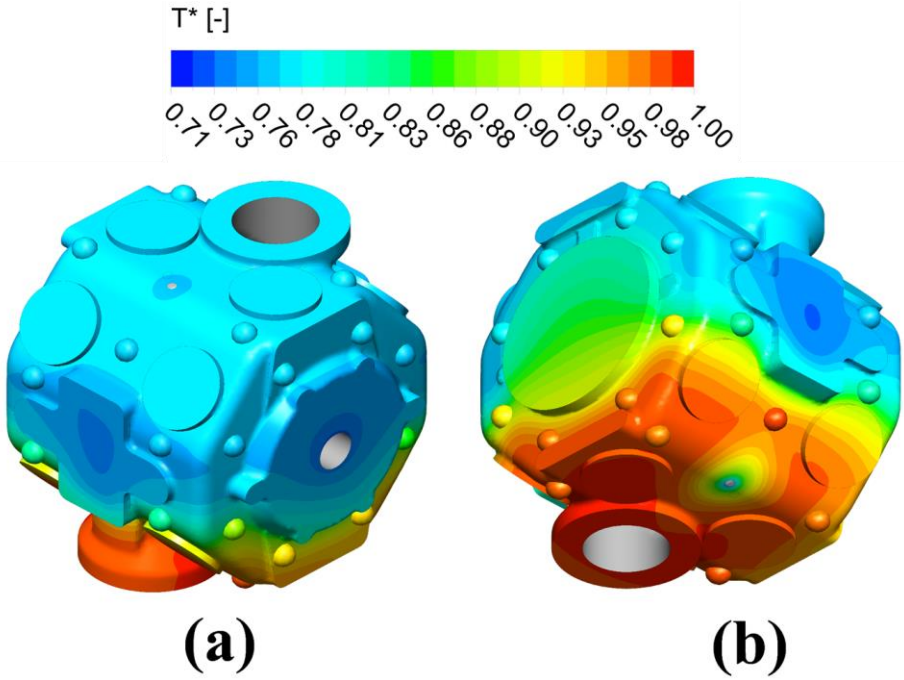

Figure 7.8 – Comparison between numerical (contours) and experimental (point cloud) temperature distributions on the external walls: Suction side (Picture a) and Discharge side (Picture b)

Figure 7.8 provides a snapshot of the temperature contours on the cylinder walls computed by the numerical code.

Moreover, a point cloud has been placed on the external boundary in correspondence to the measuring locations. The "experimental points" are colored by the actual temperature values.

Upon examination of the figure, it is first worth noticing that results for both the suction side (Picture a) and the discharge side (Picture b) compare favorably, showing a good agreement between the contour maps and the measurements.

In order to better highlight this good matching between the numerical results and the experimental measurements, three different zones were considered, corresponding to the regions of the external metal wall at different temperatures [53]. In more detail, the attention was alternatively focused on the hot zone, the cold zone and the transition zone.

Starting from the hot zone, Figure 7.9 reports the comparison between measured and computed T^*.

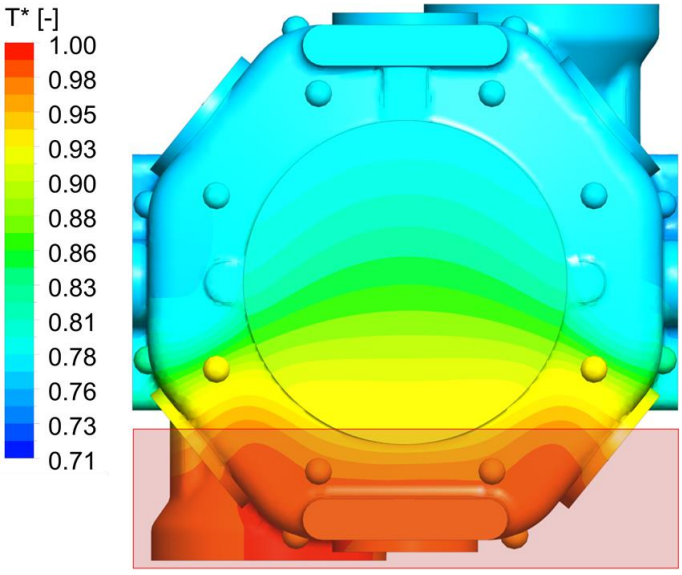

Figure 7.9 – Comparison between numerical (contours) and experimental (point cloud) T^* distributions: hot zone highlighted in red

The consistency of the results was also confirmed by Figure 7.10, where the values of normalized temperature are reported as a function of the location of the measuring points. In the figure, the reference values of discharge, suction and water temperature are also reported.

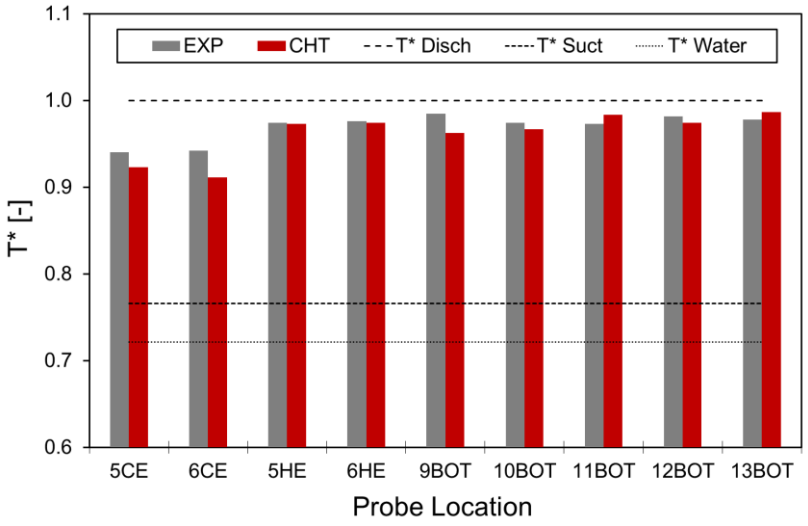

Figure 7.10 – Comparison between measured and computed T^* values: hot zone

Focusing the attention on the zone of transition between the hot and the cold part of the machine, the comparison between measured and computed T^* is reported in Figure 7.11 and Figure 7.12. Again, the numerical results appear in good agreement with the experimental ones, with the only exception of the points on the head-end side (probes 4HE and 7HE).

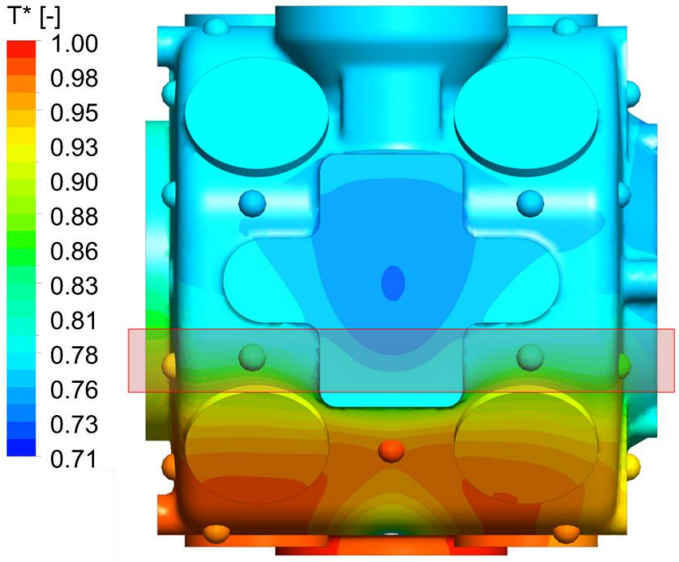

Figure 7.11 – Comparison between numerical (contours) and experimental (point cloud) T^* distributions: transition zone highlighted in red

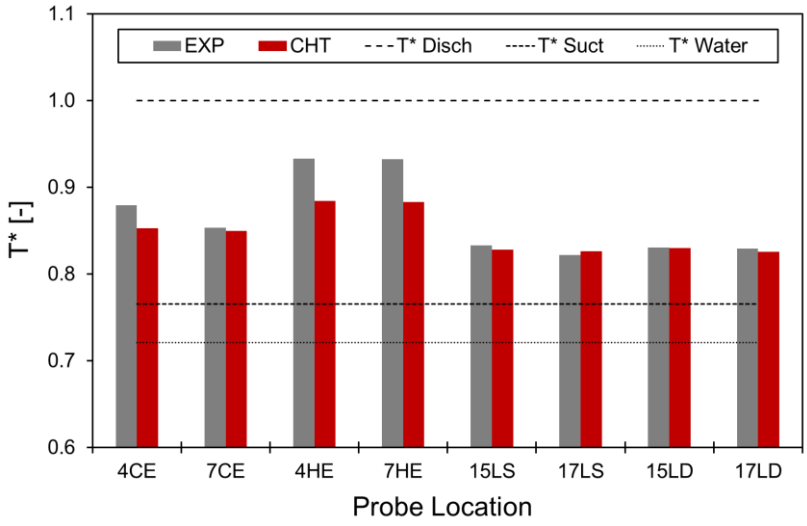

Figure 7.12 – Comparison between measured and computed T^* values: transition zone

These particular probes, as can be clearly seen in Figure 7.9 above the highlighted zone, are located in proximity of temperature gradients that are very significant. Within a distance of few centimeters the temperature variation is almost corresponding to the 50% of the entire range. Results in this region are particularly unreliable since the correct location of the measurement points plays a relevant role for the comparability of the predictions. The observed differences between experimental and computed values are expected to be in the uncertainty range associated with this factor.

The last comparison is reported in Figure 7.13 and Figure 7.14 for the cold zone of the compressor. It is apparent that the temperature is approximately uniform for almost half of the external surface of the cylinder. The temperature values vary within a range that is very close to the temperature of the suction gas. This behavior confirms the role of the two lateral chambers of the cooling circuit for the isolation of the cold side from the hot side of the cylinder. The lowest values of temperature found in the lateral surfaces (14LS, 16 LS, 14LD and 16LD) and in the crank-end side (3CE and 8CE) were correctly predicted.

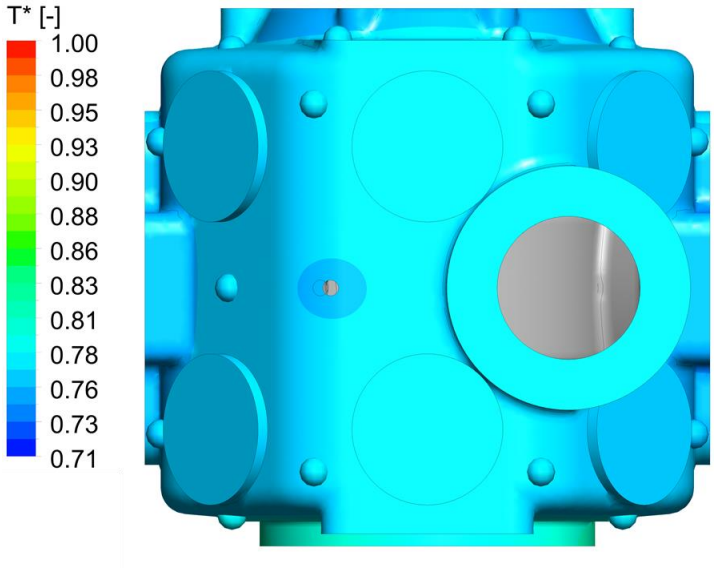

Figure 7.13 – Comparison between numerical (contours) and experimental (point cloud) T^* distributions: cold zone

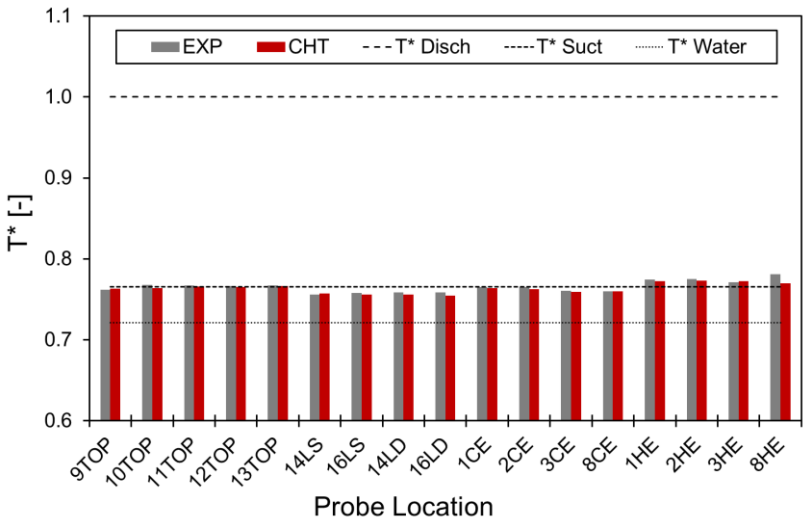

Figure 7.14 – Comparison between measured and computed T^* values: cold zone

It is apparent that the CFD and the experimental trends exhibit the same behavior. The thermal state of the cylinder has been correctly reproduced since the temperature levels and gradients effectively match.

Moreover, the difference between the two data sets was quantified by calculating the coefficient of determination R^2 between the measured and computed values (Paragraph 5.4), expressed as:

$$R^2 = 1 - \frac{\sum_i \left(T_{EXP,i} - T_{NUM,i}\right)^2}{\sum_i \left(T_{EXP,i} - T_{EXP,AVE}\right)^2}$$

This value is equal to 96.8% and confirms the accuracy achieved by means of the proposed approach on the cylinder thermal state evaluation.

Finally, the response in terms of total heat absorbed by the water was also quantified. The global heating of the water (ΔT^*_w) was found to be equal to 2.14%, while the results of the present test campaign showed a global heating equal to 2.64%. Considering the level of approximation of the approach, due to the large number of unknown input data, a 19% error on the estimation of the water ΔT can be considered admissible.

As a general remark, the present numerical results showed a good agreement with experimental data since all the small temperature variation from point to point were accurately replicated. Moreover, the error in the total heat absorbed by the water allows affirming that the order of magnitude of the heat provided by the hot gas flowing through the discharge duct, which is the main driver of the overall heat transfer phenomena, is correctly predicted.

In conclusion, although very computationally expensive, the 3D numerical simulation can provide a valuable tool for thermal state predictions. In particular, the design of the machine would benefit from an appropriately validated tool thanks to the possibility of optimizing the fluid-dynamics with great time and cost savings. Deep analyses can be performed in order to assess the proper sizing of the cooling circuit to minimize its occupancy volume, thus avoiding unnecessary restrictions of the gas chambers and improving the global performance.

Conclusions

The large diffusion of reciprocating compressors together with the increasing worldwide demand for higher efficiency in every energy conversion process caused a strong increase of the research in these machines with the goal to enhance the performance predictability and to reduce the global pressure losses. In particular, numerical simulations represent an useful tool in order to obtain accurate results and meet the demands of engineers for usability and short computation times.

In this scenario, the research activity presented in this work was focused on the development of CFD modeling with the objective to evaluate both the global pressure losses during the working cycle and the thermal state of the cylinder.

In particular, an original parametric CFD routine for the evaluation of the pressure losses occurring along the overall gas path was developed with the purpose of introducing a new methodology that allows obtaining accurate results with an important reduction of the set-up and computational times. Nowadays, the possibility of performing steady state CFD simulations for similar systems in a common industrial application is remarkably limited by the high number of configurations that should be simulated. In fact, the common strategy to realize this kind of simulations for a reciprocating compressor starts by the extraction of the fluid domains of the compression chamber and of the suction and discharge ducts by the solid CAD models. A similar approach could be used for the simulation of a small number of cylinders but does not allow obtaining a reliable database in a common industrial application for the extremely high computational and set-up times.

The idea of the CFD routine described in this thesis is then to use parametric CAD models for the simulations of a large number of cylinders in order to reduce the global computational times. Indeed, the parameterization comprises also the mesh definition and

the simulation setup phases, thus leading to a fully automatable approach. Therefore, in this work, the strategy used for the realization of parametric CAD models was described, as well as the solutions used in order to obtain a reliable and fully automated mesh.

Experimental measurements were not available for a direct validation of the CFD parametric models. However, the comparison between the results obtained using the parametric approach and the common one allowed the parametric approach to be validated. Multiple cylinders were compared obtaining an error always lower than 5% for both the global pressure losses and the global flow coefficients along the overall suction and discharge gas path.

At the same time, different analyses were carried on in order to reduce the number of simulations needed for the evaluation of the overall configurations in a typical industrial application.

The linear dependence between the bore diameters and the global flow coefficients for a same machine allowed the number of configurations simulated to be halved.

At the same time, the analytical procedure defined in order to take the effect of the valve change into account was useful to obtain another strong reduction of the simulated configurations maintaining the results accuracy. In fact, the comparison between the global flow coefficients calculated with different cylinders by means of the analytical procedure instead of specific CFD simulations showed a maximum error equal to 3.2%.

The piston masking effect was considered using three simulations at different piston positions for each phase and for each effect: this solution allowed the *p*-*V* cycle trend at the end of the discharge phase to be accurately reproduced.

Finally, the flow coefficients calculated for different working fluids and in different operating conditions allowed understanding the effect of the Reynolds number on the results.

Globally, the evaluation of all the possible operating conditions of the large size reciprocating compressors analyzed in this thesis was achieved by means of 48 simulations for each machine.

The utility of the proposed approach was proved by means of the application of the defined procedure to an industrial case. In fact, the whole fleet of cylinders of Baker Hughes was simulated making use of simplified CFD parametric models together with the solutions proposed for the reduction of the number of configurations to simulate.

A reliable database was obtained in 10 months with a strong reduction of the global computational and set-up times with respect to the corresponding needed using the common approach for the realization of steady state CFD simulations. Some considerations on the global efficiency in a reciprocating compressor were made, starting by the results of the database.

At the same time, the utilization of these results for some different applications and the comparison with experimental measurements allowed confirming the accuracy of the parametric routine to correct predict the thermodynamic behavior in a reciprocating compressor.

In more detail, the comparison between the *p-V* cycles obtained with an in-house one dimensional model using different flow coefficients and the experimental measurements collected on a dedicated test bench for different cylinders models confirmed the importance to correct evaluate the global flow coefficient in order to obtain an accurate prediction of the working cycles of these machines. Three different compressor sizes and three different working gases were analyzed; the results showed that the requirements in terms of flow coefficient accuracy depend on the specific case. However, a good agreement between numerical and experimental results were obtained for all the tested configurations when the flow coefficients calculated with the parametric approach were used. At the same time, the quite perfect overlapping between the *p-V* cycles calculated using the *K*s of the parametric approach and the corresponding achieved with the common strategy for the realization of CFD steady state simulations proved the potential of the proposed routine in order to maintain the results accuracy with a strong reduction of the global computation times.

Moreover, an original CFD two-dimensional approach aimed to predict the working cycle of a large-bore reciprocating compressor has been presented in this work. The method is based on a two-dimensional simplification of the computational domain and on the replacement of the valve and plenum geometries by equivalent porous regions. The goal of both simplifications is to allow a remarkable reduction of the computational resources required for the transient simulation of the machine. In this context, the parametric CFD routine is useful to extract the flow coefficients for the evaluation of the global pressure losses in the suction and discharge plenum geometries. This method has been applied to the simulation of a real-world application (double-acting cast iron

cylinder) in order to verify its prediction capability. The comparison of the results of the unsteady CFD simulation of the compressor cycle demonstrated the accuracy of the proposed tool in predicting the compressor performance, showing a significant reduction of the error in the cycle estimation with respect to corresponding 0D and 1D numerical models. Due to the cost-efficiency of the process, compared to the fully 3D unsteady CFD simulation of the compressor cycle, and to the possibility of an easy implementation of the model in a general purpose CFD code without any programming effort, this approach is an accurate and practical tool that can be used during all phases of the system development. Indeed, this method allows the simulation of the compressor within timescales consistent with the necessity of the design stage, similar to low order models, though guaranteeing the accuracy of a high-fidelity simulation.

Finally, a numerical methodology for the simulation of conjugate heat transfer (CHT) of a water-cooled reciprocating compressor was described. The CHT analysis aims at accurately predicting both the thermal state of the compressor cylinder and the temperature field of the cooling water. The assessment of appropriate thermal boundary conditions for the metal body in the water-metal coupled simulations was addressed; in particular, the importance to accurately predict the *HTC* distribution in the suction and discharge gas ducts was highlighted. In this context, the parametric CFD routine can be used with the goal to obtain an accurate modeling of the forced convection inside the suction and discharge gas domains. Moreover, a comparison between the experimental data and the numerical results of the CHT simulation for a double-acting reciprocating compressor was proposed. The agreement between the results was extremely promising, confirming the validity of the CHT approach in the prediction of the thermal state of the compressor cylinder and the temperature field of the cooling water.

In conclusion, in this work, different approaches were proposed in order to enhance the predictability for both the global pressure losses during the working cycle and the thermal state of the cylinder. All these approaches were validated by means of the comparison with experimental measurements obtained in different experimental campaigns on dedicated test benches. The good agreement between the numerical and experimental results allowed confirming the potential of the proposed approaches in order to guarantee a good compromise between the accuracy on the evaluation of the compressors performance and the global computational times.

References

[1] F.C. Possamai and M.L. Todescat, «A review of household compressor energy performance», Int. Compressor Engineering Conference, Purdue University, Indiana, 2004.

[2] I. Stiaccini, N. Fiorini, F. Balduzzi, G. Ferrara, A. Babbini, G. Orsi, «Large size reciprocating compressor analysis with a Finite Volume 1D model», 3rd International Rotating Equipment Conference (IREC) Pumps, Compressors and Vacuum Technology, Dusseldorf, 14-15 September 2016.

[3] F. Balduzzi, «Development of a CFD approach for the performance prediction of reciprocating compressors», University of Florence, Florence, 2010-2012.

[4] F. Balduzzi, G. Ferrara, A. Babbini and R. Maleci, «Reciprocating compressor cylinder's cooling: a numerical approach using CFD with conjugate heat transfer», Proc. of the ASME 2014 PVP Conference, Anaheim, California, 2014.

[5] I. Stiaccini, «A hybrid model for reciprocating compressor with FEM acoustic characterization», University of Florence, Florence, 2011-2014.

[6] W. A. Griffith and E. B. Flanagan, «Online continuous monitoring of mechanical condition and performance for critical reciprocating compressors», Int. Proceeding of the 30th Turbo-machinery Symposium, Texas A&M University, Houston, 2001.

[7] A. Bosio, «Sistemi energetici», Università degli studi di Genova e di Firenze.

[8] Nuovo Pignone, "Cylinder valve training".

[9] M. Costagliola, «Theory of spring loaded valves for reciprocating compressors,» The Journal of Applied Mechanics, 1950.

[10] McLaren et al., «The institute of refrigeration: modelling of compressors and valves,» University of Strathclyde, Glasgow, 1974.

[11] J. Heywood, «Internal combustion engines fundamentals», McGraw-Hill, 1998.

[12] F. Bauer, "Valve losses in Reciprocating Compressors", Int. Compressor Engineering Conf.,Purdue University, Indiana, 1988.

[13] E. H. Machu, "Increased Power Consumption of High-Speed, Short -Stroke Reciprocating Compressors Caused by Pocket Losses and Gas Inertia Effects",Compressor Tech, pp. 107-111, March-April, , 1999.

[14] L. Boeswirth e V. Milovanova, "Simple but Efficient Methods for Estimation of Value Loss, Capacity Loss Due to Suction Valve Throttling and Heat Transfer in Cylinder", Int. Compressor Engineering Conf., Purdue University, Indiana, 1998.

[15] F. Balduzzi, G. Ferrara, R. Maleci, A. Babbini, G. Pratelli, «A parametric CFD analyses of the valve pocket losses in reciprocating compressors», Proceedings of the ASME 2013 Pressure Vessels & Piping Division Conference, PVP2013, Paris, July 14-18.

[16] H.P. Bloch and J.J. Hoefner, «Reciprocating Compressors, Operation & Maintenance», Butterworth-Heinemann, USA, 1996.

[17] P.A. O'Neill, «Industrial Compressors», Butterworth-Heinemann, 1993.

[18] H.K. Versteeg and W. Malalasekera, «An introduction to Computational Fluid Dynamics. The finite volume method», Longman Group, England, 1995.

[19] J. Ferziger and M. Peric, «Computational Methods for Fluid Dynamics», 3rd rev, Berlin: Springer, 2002.

[20] R. Fox, A. McDonald and P. Pritchard, «Introduction to fluid mechanics», John Wiley & Sons.

[21] D. C. Wilcox, «Turbulence Modeling for CFD», California: DCW Industries Inc., 1998.

[22] S. Majumdar, «Role of underrelaxation in Momentum Interpolation for Calculation of Flows with Non-Staggered Grids», Numerical Heat Transfer, vol. 13, pp. 125-132, 1988.

[23] S.V. Patankar, «Numerical Heat Transfer and Fluid Flow», Hemisphere Pub. Corp., 1980.

[24] B.E. Launder and D.B. Spalding, «The Numerical Computation of Turbulent Flows», Comput. Methods Appl.Mech. Eng., vol. 3, pp. 269-289, 1974.

[25] D.C. Wilcox, «Reassessment of the Scale-Determining Equation for Advanced Turbulence Models», AIAA J., vol. 11, pp. 1299-1310, 1988.

[26] A. Neale, D. Derome, B. Blocken and J. Carmeliet, «Determination of surface convective heat transfer coefficients by CFD», 11th Canadian Conference on Building Science and Technology Banff, Alberta, 2007.

[27] H. Schlitching, «Boundary-layer theory», 7th Ed. McGraw-Hill, New York, NY, 1979.

[28] Ansys, Inc., «ANSYS-CFX Solver Theory Guide», release 13.0.

[29] C.E. Fothergill, S. Chynoweth, P. Roberts e A. Packwood, «Evaluation of a CFD porous model for calculating ventilation in explosion hazard assesments», J. of Loss Prevention in the Process Ind., vol. 16, pp. 341-347, 2003.

[30] S.L. Lee and J.H. Yang, «Modeling of Darcy-Forchheimer Drag for Fluid Flow Across a Bank of Circular Cylinders», Int. J. Heat Mass Transfer, vol. 40, n. 13, pp. 3149-3155, 1997.

[31] M. Faretra, G. Barbanti, R. Traversari and M. Galbiati, «Multi-phase CFD study of a reciprocating gas compressor with liquid slug ingestion», EnginSoft International Conference, 2009.

[32] Y. V. Birari, S. S. Gosavi and P. P. Jorwekar, «Use of CFD in Design and Development ofR404A Reciprocating Compressor», Int. Compressor Engineering Conf., Purdue University, Indiana, 2006.

[33] F. Fagotti and F. C. Possamai, «Using Computational Fluid Dynamics as a Compressor Design Tool», Int. Compressor Engineering Conf., Purdue University, Indiana, 2000.

[34] F. Balduzzi, G.Ferrara, A. Babbini and G. Pratelli, «CFD evaluation of the pressure losses in a reciprocating compressor: a flexible approach», ASME 11th ESDA Conference, Nantes, France, 2012.

[35] G. Pratelli, A. Babbini, F. Balduzzi, G. Ferrara, R. Maleci and L. Romani, «CFD Evaluation of Pressure Losses on Reciprocating Compressor Components», 8th Conference of the EFRC, Dusseldorf, 2012.

[36] H. Schlichting, «Boundary Layer Theory», 7th Edition, McGraw-Hill, 1979.

[37] E. Machu, «Problems with modern high speed short stroke reciprocating compressors: increased power requirement due to pocket losses, piston masking and gas inertia, eccentric gas load on the piston», Proceedings of Gas machinery conference, USA, 1998.

[38] G. Machu, «Calculating reliable impact valve velocity by mapping instantaneous flow in a reciprocating compressor», Proceedings of gas machinery conference GMRC, USA, 2004.

[39] R. Aigner, «Internal flow and valve dynamics in a reciprocating compressor», PhD Thesis, Wien, 2007.

[40] H. Steinrück, R. Aigner and G. Machu, «Transversal waves in a reciprocating compressor», Acta Mechanica (eigenladent), 1-4, S. 231-248, 2008.

[41] J. Mandel, «The statistical analysis of experimental data», Dover Publications, New York, 1984.

[42] F. Balduzzi, A. Tanganelli, G. Ferrara and A. Babbini, «Two-dimensional approach for the numerical simulation of large bore reciprocating compressors thermodynamic cycle», Applied Thermal Engineering, 129, pp. 490-501, 2018.

[43] K.T. Ooi, «Heat transfer study of a hermetic refrigeration compressor», Applied Thermal Engineering, 23 (15), pp. 1931-1945, 2003.

[44] M. Elhaj, F. Gu, A.D. Ball, A. Albarbar, M. Al-Qattan, and A. Naid, «Numerical simulation and experimental study of a two-stage reciprocating compressor for condition monitoring», Mechanical Systems and Signal Processing, 22 (2), pp. 374-389, 2008.

[45] R. Aigner e H. Steinrück, «Modelling Fluid Dynamics, Heat Transfer and Valve Dynamics in a Reciprocating Compressor», Proc. of the 5th Conference of the EFRC, Praga, Repubblica Ceca, 2007.

[46] F.P. Disconzi, C.J. Deschamps and E.L.L. Pereira, «Development of an In-Cylinder Heat Transfer Correlation for Reciprocating Compressors», Int. Compressor Engineering Conference, Purdue University, Indiana. 2012.

[47] Z. Abidin, R. Almbauer, A. Burgstaller and D. Nagy, «Domain Decomposition Method for 3-Dimensional Simulation of the Piston Cylinder Section of a Hermetic Reciprocating Compressor», Int. Compressor Engineering Conf., Purdue University, Indiana. 2006.

[48] W.H. McAdams, «Heat Transmission», 3rd Ed. McGraw-Hill, New York, NY, 1954.

[49] F. Fagotti, M.L. Todescat, R.T.S. Ferreira e A.T. Prata, «Heat transfer modeling in a reciprocating compressor», Int. Compressor Engineering Conference, Purdue University, Indiana, 1994.

[50] W.J.D. Annand, «Heat Transfer in the Cylinders of Reciprocating Internal Combustion Engines», Proc. J.Mech. Engrs., 117 (36), pp. 973-996, 1963.

[51] F. Balduzzi, G. Ferrara, R. Maleci, A. Babbini, « Improvement of the cooling performance of a reciprocating compressor cylinder by a conjugate heat transfer and deformation analysis», Proc. of the 9th Conference of the EFRC, Vienna, 2014.

[52] A. Tanganelli, «Development of a combined CFD-CHT approach for the analysis of the cylinder cooling of reciprocating compressors», University of Florence, Florence, 2014.

[53] F. Balduzzi, A. Tanganelli, G. Ferrara, A. Babbini and R. Maleci, «Numerical analysis and experimental assessment of the cylinder temperature in a reciprocating compressor», Proc. of the ASME 2015 PVP Conference, Boston, Massachusetts, USA, 2015.